Study on structural control of hydrogenated amorphous carbon films using plasma-enhanced chemical vapor deposition

JIA Lingyun

2015

Nagoya University

Department of Electrical Engineering and Computer Science

Contents

Chapter 1 Introduction

1.1 Carbon materials ······ 1
1.1.1 sp^2 carbon: graphite ······ 4
1.1.2 sp^3 carbon: diamond ······ 7
1.1.3 sp^2 and sp^3 carbon: amorphous carbon (a-C) ······ 8
1.2 Synthesis of amorphous carbon films ······ 10
1.2.1 Growth methods ······ 10
1.2.2 Growth mechanism under PECVD ······ 17
1.3 Objective and composition of this thesis ······ 22
References ······ 27

Chapter 2 Experimental setup and characterization of a-C:H films

2.1 Synthesis of a-C films ······ 31
2.1.1 Radical injection plasma-enhanced chemical vapor deposition system ······ 33
2.1.2 Growth procedure ······ 36
2.2 Characterization of a-C films ······ 39
2.2.1 Thickness: stylus profiler ······ 39
2.2.2 Crystallographic properties: Raman spectroscopy ······ 42
2.2.3 C-H vibration: Fourier Transform Infrared Spectroscopy (FT-IR) ······ 45
2.2.4 Band gap: E_g and E_{04} (Spectrophotometer) ······ 47
References ······ 50

Chapter 3 Deposition characteristics

3.1 Introduction ······ 51
3.2 Residence time of radicals in the chamber ······ 54
3.3 Radical species in plasma ······ 56
3.3.1 Actinometery ······ 56

3.3.2 Variation in CH, Hα, C_2 ··· 57
3.4 Growth rate ··· 60
3.5 Hardness ··· 62
3.6 Summary ··· 66
References ··· 67

Chapter 4 Effect of radical species on film properties

4.1 Introduction ··· 71
4.2 Electronic structure and electrical properties ··· 72
4.2.1 E_g and E_{04} ··· 72
4.2.2 Conductivity ··· 75
4.2.3 Correlation between radical species and optical bandgap ··· 77
4.3 H concentration ··· 80
4.3.1 Qualitative analysis of H content by FT-IR ··· 80
4.3.2 Quantitative calculation of H concentration by SIMS ··· 83
4.3.3 Correlation between variation in H concentration and optical bandgap ··· 87
4.4 Crystallographic properties ··· 83
4.4.1 Raman scattering ··· 88
4.4.2 Effect of crystallographic properties on the optical bandgap ··· 92
4.5 Summary ··· 94
References ··· 95

Chapter 5 Effect of radical species on bonding configuration

5.1 Introduction ··· 97
5.2 Variation in sp^2-C fraction ··· 99
5.2.1 Qualitative analysis of π bond fraction ··· 99
5.2.2 Quantifying of sp^2-C fraction ··· 104
5.3 Variation in C-H bond ··· 113
5.4 Discussion model ··· 114
5.4 Summary ··· 116
References ··· 117

Chapter 6 Conclusions and future works

6.1 Summary of this thesis ········ 119
6.2 Scopes for future works ········ 123

Acknowledgements ········ 125
List of papers ········ 127

Contents

Chapter 1

Introduction

1.1. Carbon materials

Recent years, carbon materials have attracted much attention, because of their low cost and various characteristics. It is well known of their applications as environmental, thermal and biomedical applications. Another important field is the electrical applications, which include electrodes, electronic devices, and so on.

Carbon, a chemical element with atomic number of 6 and expressed as symbol “C”, is abundant in the Earth’s crust. Thus, it is possible to apply carbon materials for a large-scale of industrial application. On the other band, various characteristics of carbon materials are originated from the diverse structure. As shown in Figure.1.1, the electron configuration of carbon consists of two electrons in the $1s^2$ orbit of the K-shell and four electrons in the $2s^2$ and $2p^2$ orbits of the L-shell. (two in the so called 2s orbital and two in the so called 2p orbital) There are many types of carbon allotropes depending on various covalent chemical bonds with the neighboring carbon-atoms. When carbon atoms move close to other adjacent atoms, a phenomenon called hybridizations occurs. As shown in Figure.1.2, Four obits in L-shell, two 2s orbits and two sp orbits will hybridize into four hybridized orbits, which could appear as two different types of orbits, π and σ orbits. And a carbon atoms consisting of four σ orbits are called a sp^3 carbon

atom. Similarly, a sp^2 carbon atom consists of three σ and one π orbits, and a sp carbon atom consists of two σ and two π orbits [1]. The difference in the electron orbits will cause different chemical bond between carbon atoms and other atoms and thus different macro properties. It can be understood easily from the totally different characteristics of diamonds, graphene sheet, and carbyne, which consist of 100% sp^3-C, sp^2-C, and sp-C, respectively [2,3].

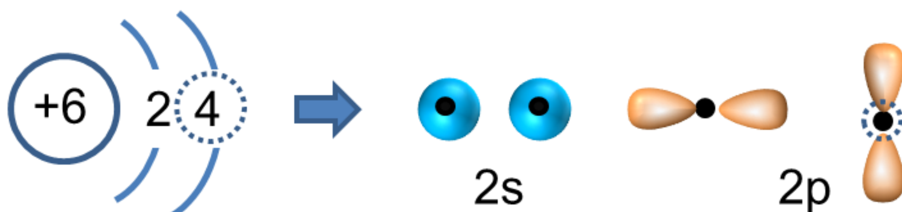

Figure 1.1 Schematic illustration of electrons orbits of carbon atoms.

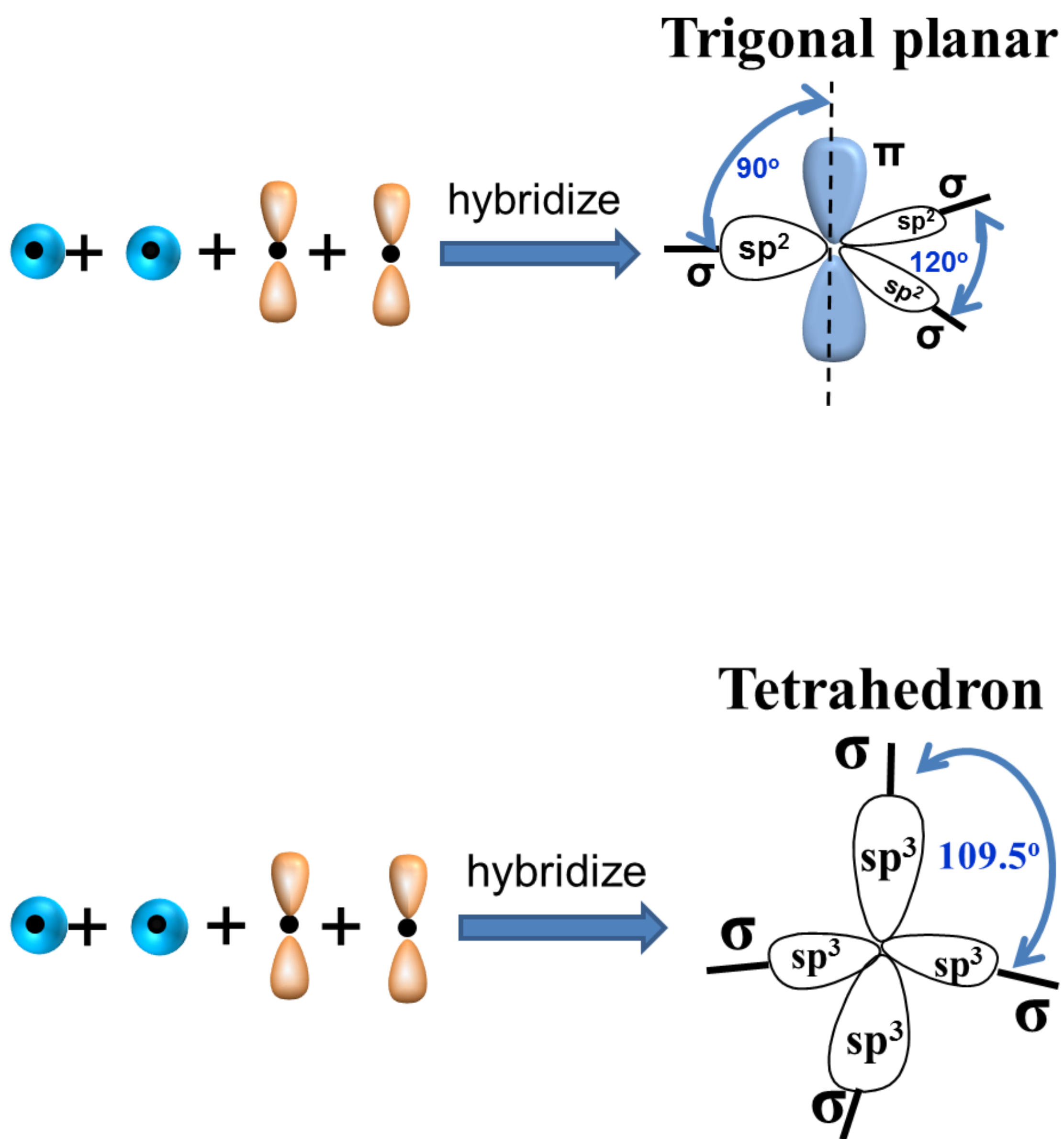

Figure 1.2 Schematic illustration of sp^3, sp^2 hybridization.

1.1.1. sp^2 carbon: graphite

Graphite is composed of stacked graphene sheets, which is a two-dimensional honeycomb lattice as shown in Figure 1.3. In the graphene, every carbon atom is covalently bonded to three other carbon atoms in the plate with the sp^2 bonding configuration (with a bond angle of 120 °, and bond length of 0.142 nm). The basic unit of graphene is a hexagonal ring composed of six sp^2 carbon atoms. In the graphite, every layers of graphene sheet is bonded to each other by weak forces of Van der Waals. This stacked structure of graphite causes sliding movement of the parallel graphene plates. Weak bonding between the plates would affect the softness and self-lubricating properties of graphite.

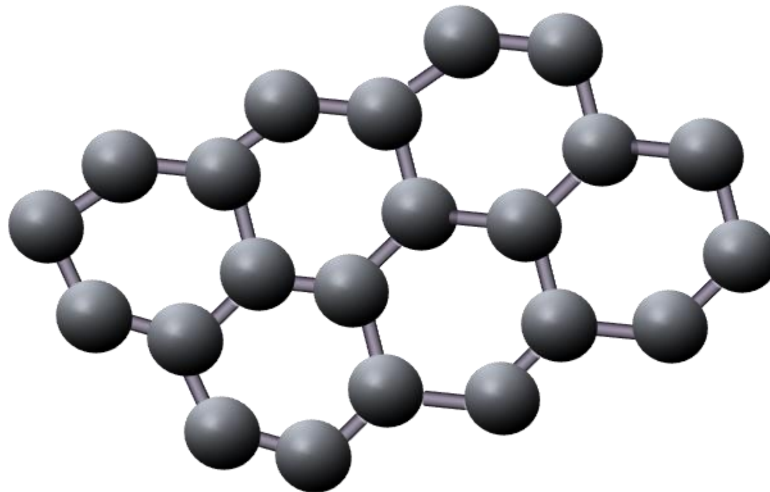

Fig 1.3 The sp^2 structure of graphene.

In graphite, L shell of a carbon atom has four valence electrons, three of which form the covalent bonds. The fourth valence electron does not involve into covalent bonds and may be easily escape from the electron shell. These electrons promise graphite an excellent electrical conductivity. And this was supported by the experimental results of transport measurements operated by Novoselov group [3]. It was reported that, even at room temperature, graphene has an extremely-high electron mobility of more than 15 000 $cm^2V^{-1}s^{-1}$, which is less dependent from the temperature but and still affected by scattering on defects. Besides, the carriers in graphene could be always tuned between holes and electrons and with a concentration about 10^{13} cm^{-2} [3-5].

There are also some other types of materials with other dimensionalities of this basic unit, like CNWs shown in Figure 1.4, which consisting of stacks of nanometer-scaled graphene sheets which are vertically aligned on a substrate. The height of each wall depends on growth time and generally can be up to several micrometers. And this kind of structure provides CNWs a high aspect ratio and large surface area. Besides, CNWs also show unique electronic states different from that of other carbon nanomaterials. For example, it has been found that CNWs have similar but not identical electronic structures as the HOPG. [6,7]. According to the Hall measurements CNWs also possess semiconducting properties caused by structural fluctuations [8,9].

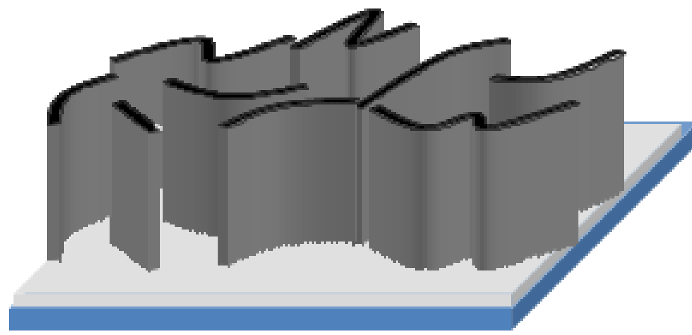

Fig. 1.4. Schematics of structures of CNWs.

1.1.2. sp^3 carbon: Diamond

Diamond is made completely of carbon atoms with typical tetrahedron sp^3 bonding configuration. As shown in Figure.1.5, diamond is composed of carbon atoms which are arranged in a form of face-center cubic crystal structure. Diamond is composed of many basic units which are a lot of carbon atoms arranged in a long-term order of tetrahedron composed of four triangular faces. And these units are periodically repeated in three dimensions within diamond lattice. The lattice constant and bond length are very short, with a value approximately 3.567 Å and 1.54 Å, respectively. That promises diamond the hardest material in the nature and many special properties. The electrical and electronic structure of diamond are also attracted much attention, which generally shows a variable conductivity from 10-106 Ω·cm, and wide bandgap of about 5.45 eV.

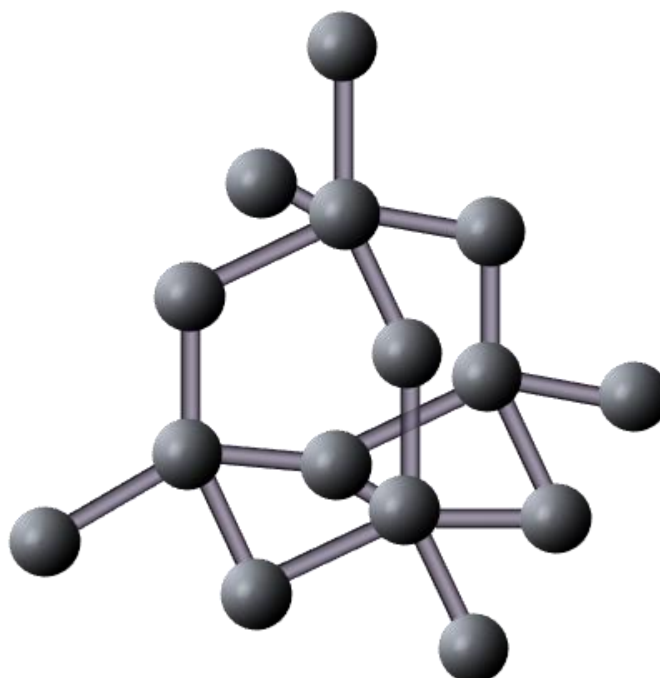

Fig1.5. The sp^3 structure in diamond.

1.1.3. sp^2 and sp^3 carbon: amorphous carbon

Amorphous carbon, has attracted much attention, because of both scientific interest and promising industrial applications, owing to their excellent, wide-ranging physical and chemical characteristics.[10,11] As shown in Figure.1.6, these kinds of materials have a highly disordered structure with hybridized bonding configuration of sp^3 carbon (C), sp^3-C. [12,13] which results in lack of structural integrity. The disorder of this structure promises it many available bonds, and thus to generate many more complex carbon based molecules. And this kind of carbon structure probably appears at the edges or exists as the residue of other elemental compounds.

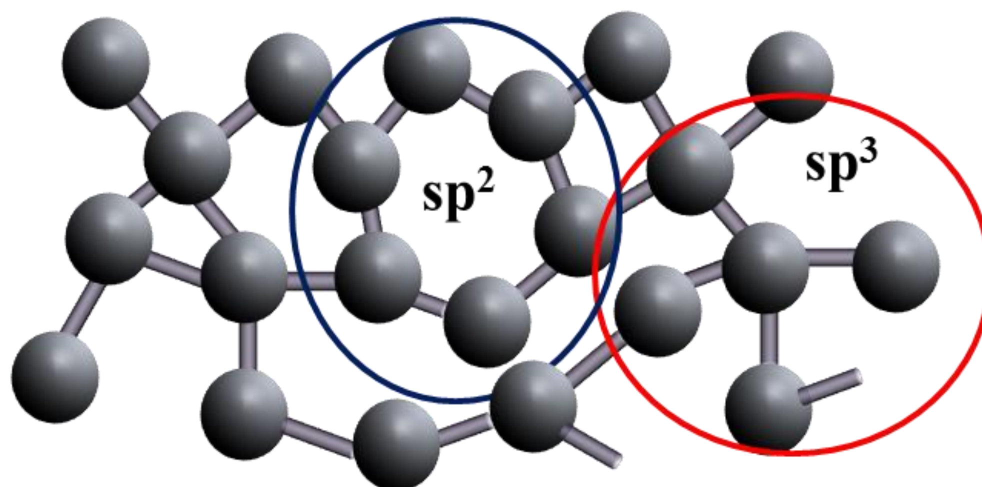

Fig 1.6 The structure of amorphous carbon.

Fig 1.7 shows the well-known ternary phase diagram of carbon materials proposed by Jacob and Moller, the structures and properties of a-C films are basically determined by composition ratios of sp^2-C, sp^3-C and H. Then sp^3 bond and sp^2 bonds will form an area like diamond and graphite.

This special structure promises amorphous carbon materials diverse properties, running from electrically conductive to insulating, from exceptionally hard to soft and from optically transparent to opaque, can be attributed to variations in the relative ratios of sp^2-C, sp^3-C and H. As an example, films that are relatively well crystallized, representing so-called diamond-like carbon (DLC), are applied as protective coatings in applications such as optical windows, car parts, and so forth, because they are harder than sapphire and exhibit optical transparency in the infrared.

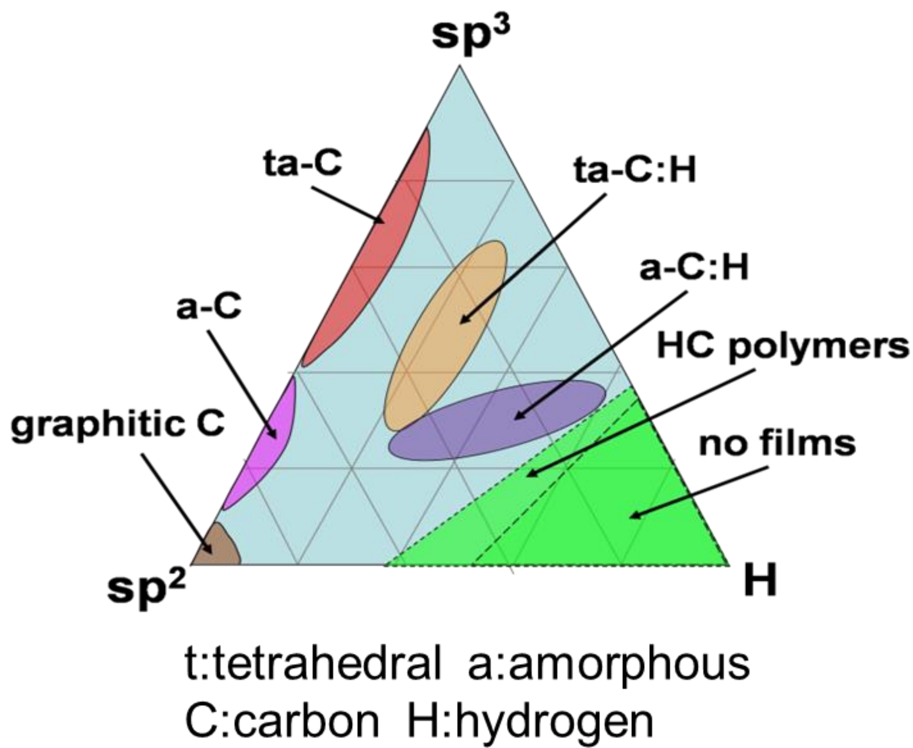

Fig 1.7 Ternary phase diagram of bonding in amorphous carbon-hydrogen alloys[14].

1.2. Synthesis of amorphous carbon films

1.2.1. Growth methods

Recently, there has been a very fast progress in the synthesis technology of carbon materials, for example, chemical vapor deposition of diamond, and there have also been an advance in the deposition of a-C films, which could be fabricated in many different ways both for laboratory research and industrial production. Essentially, all of these depiction methods share a common key point that a-C films are deposited based on a beam of carbon or hydrocarbon ions. In another word, it is generally determined by a physical process, the impact of ions on the a-C films. For example, many experiment results show that the most optimized condition for deposition of a-C films with a high sp^3-C fraction, may be obtained by producing a carbon ion flux with a centralized energy distribution around 100 eV

Ion beam

In Figure.1.8, it shows the initial deposition method of a-C films, which is called ion beam deposition operated by Aisenberg Chabot.[15] By this system, carbon ions can be generated based on the sputtering of graphite cathode. As mentioned above, hydrocarbon ions can also be used instead of carbon ions. In that case, usually some hydrocarbon source gas like CH_4 should be ionized for the generation of hydrocarbon ions. Finally, the generated ions flux will be accelerated by a bias voltage to the substrate. Sometimes it is also desirable that the deposition process was controlled by some specially appointed species with fixed energy. Lifshitz group[16] proposed that

mass selected of ion species before incident on the growing films can provide a well-defined ion species and energy. By this so called mass selected ion beam deposition, we can achieve a precisely controlled deposition process. However, relatively low deposition rate makes this approach limited only for laboratory research. Another disadvantage of this approach is that a-C films with high fraction of sp^3-C are hard to be deposited, due to a relative low ratio of energetic ions to neutral species.

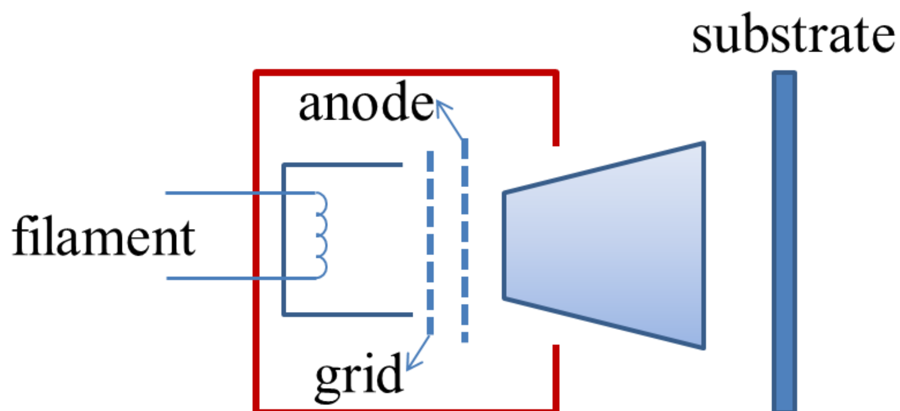

Fig 1.8 A schematics of ion beam deposition system for synthesis of a-C.

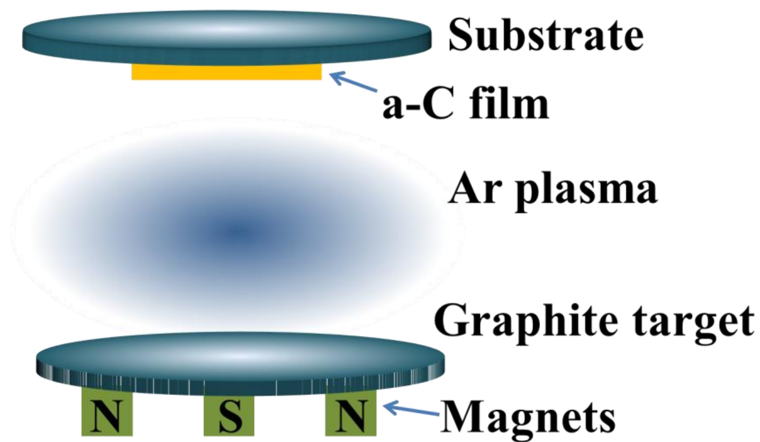

Fig 1.9 A schematic of sputtering system for synthesis of a-C.

Sputtering

Figure 1.9 shows a sputtering system, which is the most popular industrial approach for synthesis of a-C films. Generally Ar plasma is produced by a DC or RF power source. Then carbon radical species are generated based on the bombardment of Ar ions with a graphite target, which also acts as the cathode electrode. Usually magnetron sputtering is often used for more sputter yield, with magnets mounted below the target. Finally, a-C film would be generated on the surface of the substrate. A dc bias power can also be connected to the substrate for the control of the ion energy. In addition, a-C:H films can be achieved by using Ar and H_2 plasma. Similarly, a-C:N film can be synthesized by producing Ar - N plasma.

By this kind of sputtering system, density and sp^3-C fraction can be modified by increasing the bombardment of ions with the film on the surface of substrate. And this can be achieved by configuring the magnetic field to cover the substrate, which thus can make the Ar ions bombard not only the lower target but also the upper substrate. The other way to increase the bombardment with substrate is introducing one more assisted Ar ion beam.

Generally, sputtering is popular for industrial application, because it is flexible to fabricate many different kinds of thin films by applying corresponding target source. However, the problem of relative low density and sp^3-C still exist in sputtering

Plasma enhanced chemical vapor deposition (PECVD)

Figure 1.10 shows plasma enhanced chemical vapor deposition system, which is the most popular synthesis method of a-C films for laboratory research. Capacitively coupled plasma is generated between two parallel electrodes. Generally an RF power supply is applied to the lower electrode where the substrate is mounted, and the upper one is grounded. Since the wall of the chamber is also usually earthed, so the area of the earthed electrode is larger than that of the RF coupled one. When the RF power is induced, both electrons and ions will move and follow the change of electrical field. And electrons will move faster than ions due to much less mass than ions. Thus, this will cause an excess of ions near the electrodes, which is called plasma sheath. Generally this sheath works as a diode, so that the RF voltage between electrodes can be considered as a DC self - bias voltage. And the lower, RF coupled electrode will be negative with respect to the upper earthed electrode. And the potential difference is mainly concentrated between two sides of plasma sheath. When the ions flow into the sheath region, they will be accelerated and bombard to the substrate.

Since the ion energy is important for deposition of a-C films, so the collision of ions with other species should be avoided, because this would cause an energy loss of ions. And for this purpose, mean free path of ions should be larger than the sheath thickness. From the formula (1) and (2), [17] we can see that the ratio of mean free path and plasma sheath thickness, λ/d scales as $P^{-1/2}$, thus relative lower pressure is necessary for the ratio of λ/d larger than 1.

Another important factor in PECVD is the source gas used for synthesis of a-C films. Benzene is a good choice for high growth rate, since the ionization potential of Benzene is relative low. [18] The mechanical properties of a-C:H films are strongly

affected by the ratio of C and H of the source gas, which is correlation with the incorporation of hydrogen into the films. The number of carbon atoms in source gas in also very important. As mentioned above, the ion energy per carbon atom strongly affects the macro properties of a-C films. And 100 V per carbon atom is claimed to be the most suitable for high sp^3-C fraction. Thus, Benzene is not a good choice for synthesis of hard a-C films, since C_6Hn^+ requires high bias voltage to reach 100 V per carbon atom. Instead, C_2H_2 is a common choice for mechanical application However, when it is applied for electronic application which need a source gas with high purity, C_2H_2 cannot be used because of its substantial nitrogen impurity. In that case, CH_4 is preferred because can be used in very high purity. But too high a hydrogen content in the film becomes another new problem.

$$d = \mathrm{k}P^{-1/2} \qquad (1)$$

where d represents sheath thickness, and P is process pressure

$$\lambda = \mathrm{k}'/P \qquad (2)$$

where λ represents mean free path.

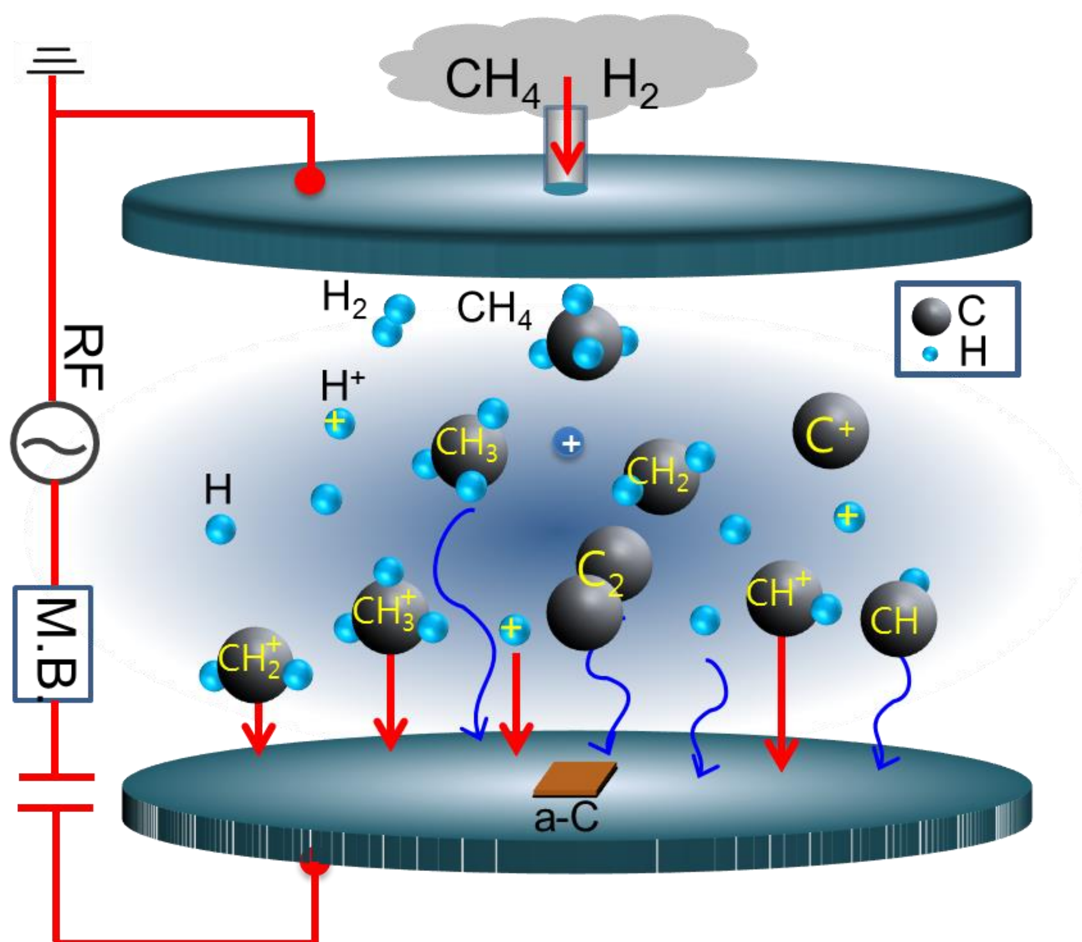

Fig 1.10 Plasma enhanced chemical vapor deposition system.

1.2.2. Growth mechanism under PECVD

As shown in Figure.1.7, sp^2-C, sp^3-C, and H are three basic factors that determine the properties of a-C films. As noted above, ion bombardment can promote generation of sp^3-C, and it is essentially a physical process. Thus it is crucial for us to clarify this physical process.

To see from the obvious research, Spencer group [19] proposed that sp^3 sites originated from a mixture of sp^2-C and sp^3-C, by a preferential sputtering of sp^2-C. But this speculation was queried by Lifshitz group.[20] They stated that the sputtering mainly determined by the cohesive energy, which does not show a pronounced difference between sp^2-C, sp^3-C. Besides, They proposed that the growth is sub-surface, based on their investigation on depth profile of C ions incident on Ni substrate. And the generation of sp^3-C is correlated to preferential displacement of sp^2-C. In the model they proposed, both sp^2-C and sp^3-C will be displaced into interstitial sites, then fall back at similar rates. During this process, a preferential displacement of sp^2-C will lead to an increase in sp^3-C. We can see that there is an important premise that displacement energy in sp^2-C and sp^3-C are different. Although some obvious literature reported an estimated data, about 25 and 80 eV for sp^2-C and sp^3-C respectively, recent direct measurement data [21] did not confirmed an obvious difference between that of diamond and graphite. Actually the displacement of graphite should be investigated for more details, because graphite shows an anisotropic structure.

Weissmantel [22] reported a presumption that sp^3-C is caused by a shock wave of displacement spike of ions. But the problem is the shock wave is more appropriate to higher ion energy. Robertson group[23] supported the model of sub-plantation proposed by Lifshitz group. In addition, they stated that sub-plantation cause a metastable

increase in the density of films, which then lead to the change of local bonding into sp^3-C. In this view, the preferential displacement of sp^2-C is not necessary, but a limited volume is important for generation of sp^3-C.

By now, the model of sub-plantation is widely accepted. However, there are still some details need to be clarified. For example, the reason why sp^3-C will be inhibited and even transformed into sp^2-C, when the ion energy is too high. A model [24] proposed by Robertson group gave a lot of details about the generation of sp^3-C, and transform of sp^3-C to sp^2-C.

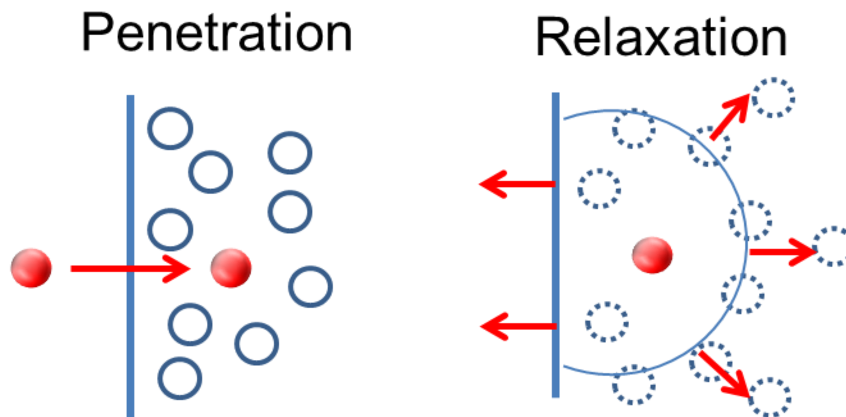

Fig 1.11 Basic processes in sub-plantation: Penetration and Relaxation.

In this model, it is stated that when the carbon ions do have enough energy to penetrate into the surface of film, they will remain on the surface as outward growing sp^2-C layer. On the other hand, if the energy of carbon ions is larger than the penetrate threshold, they will incident into the sub-surface of film. As shown in Figure.1.11, these penetrated carbon ions thus increase the local density and cause a variation of local bonding configuration. Generally, the local density will determine the local configuration. Higher density encourages the formation of sp^3-C. Usually, the ion energy is increased for high density or higher fraction of sp^3-C. But when the ion energy rises over a threshold, a special phenomenon called relaxation will occur. After penetrating into the sub-surface of film, there is still some excess energy in these high energy ions, which then have to be dissipated the as phonons And this process will cause a decrease in the local density, thus a corresponding decrease in local sp^3-C fraction..

Deposition mechanism of a-C:H films

The a-C:H films can be synthesized by using many different kinds of source gas, like CH_4, C_2H_2, C_2H_4, C_6H_6. And it is found that no matter which kind of source gas was used, the maxima in density appeared at the same bias voltage per carbon atom. It indicates that during deposition of a-C:H, ion energy still play an important role, and the growth model is still sub-plantation.

From the literature, we can see many deposition models of a-C:H have been proposed, including chemical and physical processes. Generally, the deposition process can be divided into three basic aspects, (1) Dissociation and ionization in plasma, (2) interaction between precursors and surface of growing film, (3) reaction in sub-surface of film.

In the first aspect, the composition of ions, radicals is very complex, and strongly affected by plasma condition, such as electron temperature, electron energy distribution (EED) and so on. And the data derived from Mass Spectrometer tells that undissociated source gas molecules are still the main species in the plasma.

In the second part, the species incident to the surface of a-C:H film consist of ions and neutrals. The action of ions has been described above. On the other hand, neutrals also play an important role during deposition, especially for the growth rate. Generally, there are four kinds of neutrals existing in the plasma, (1) undissociated source gas molecules, like CH_4, H_2, (2) mono-radicals like CH_n, (3) di-radicals and other unsaturated radicals, like C_2H_2, C_2H_4 (4) atomic hydrogen, H. And these four kinds of neutrals show completely different sticking coefficient. Di-radicals and other unsaturated radicals show highest sticking coefficient nearly 1, since they can insert directly into the C-C or C-H bonds in the surface of films. The second one is the

mono-radicals. And whether they can insert into the films depends on whether there are dangling bonds existing on the surface. Corresponding, the dangling bond can be created by two methods, (1) abstracting H from C-H bond by H atom or CH_n radicals, and the efficiency of former is about 30 times higher than that of latter.[25] (2) ion displacing H from C-H bond. It is reported that presence of H atom will promote the sticking coefficient of CH_3 radials. The source gas molecules like CH_4 have a very low sticking coefficient which could be negligible.

Hydrogen atoms can penetrate the film like ions, about 2 nm.[26] So they can abstract H from C-H bond in sub-surface, which then create the dangling bonds and H_2 there. Of course penetrated H can also saturate the dangling bonds in sub-surface of film.

1.3. Objective and composition of this thesis

Amorphous carbon (a-C) films have attracted much attention, because of both scientific interest and promising industrial applications, owing to their excellent, wide-ranging physical and chemical characteristics.[27,28] These films are composed of sp^3 carbon (C), sp^2-C and hydrogen (H).[29,30] It is believed that their diverse properties, running from electrically conductive to insulating, from exceptionally hard to soft and from optically transparent to opaque, can be attributed to variations in the relative ratios of these species. As an example, films that are relatively well crystallized, representing so-called diamond-like carbon (DLC), are applied as protective coatings in applications such as optical windows, car parts, and so forth, because they are harder than sapphire and exhibit optical transparency in the infrared. [31-35] In contrast, the applications of these films as device materials, such as electrodes and channels, are less advanced. In particular, there has been almost no significant progress in the field of semiconductor devices using a-C films as channels, such as a-C solar cells, even though a-C films exhibit a wide range of optical and energy band gaps.[36-39] Although there have been many reports concerning solar cells using a-C films, the solar cell operation has been observed only in the case of a-C/Si stack structures and is attributable to photovoltaic effects on the Si surfaces.[40,41] There have been no reports with regard to the photovoltaic effect in the a-C film itself, or of solar cells operating with junction structures consisting solely of a-C layers.

Many fundamental researches about a-C films have been done at the viewpoints of not only plasma physics but also material science. For example, according to the

well-known ternary phase diagram of carbon materials proposed by Jacob and Moller, the structures and properties of a-C films are basically determined by composition ratios of sp^2-C, sp^3-C and H[42]. On the other hand, there are also many studies regarding the deposition mechanisms of a-C films.[43-46] Dissociation processes of hydrocarbon and fluorocarbon molecules, and the formation of individual radicals in plasmas have been investigated.[47,48] Effects of generated radicals on the formation of sp^2 and sp^3 bonding states, and film growth have been also discussed.[49,50] Generally, highly-dissociated species, such as C_2, tend to induce sp^2 bonds, while CH_3 radicals induce sp^3 ones. Furthermore, in the so-called sub-plantation model, ion bombardment is considered to be the primary factor determining the bonding configuration and thus the resulting properties of the a-C.[51-53] However, electronic properties of a-C films, especially semiconducting characteristics, have not been sufficiently optimized and controlled. In the energy band structure of a-C film, a huge number of electronic levels corresponding to sp^2-C bonds are present in the energy band gap region formed by sp^3-C atoms. They induce metallic features or pronounced current leakage.[54,55] On the other hand, clustering of the sp^2 phase and their effects on macroscopic properties of a-C films have also been suggested.[56-61] Therefore, it is deduced that the electronic properties of a-C films cannot be predicted only by the composition ratios of sp^2-C, sp^3-C and H in the film, so there may be other factors that affect the electronic properties of these films.

As mentioned above, concerning the radical species, the dissociation of hydrocarbon or fluorocarbon gases, and the generation of various types of C-containing radicals such as C_2, CH_x and CF_x in the plasma, and their effects on formation of bonding configuration (sp^2 and sp^3) have also been discussed in previous papers.

However, the mechanism how such the radicals induce electronic structures of a-C films, such as energy band gap, is not clarified yet. In terms of experimental studies, there are few reports about how the change of radical species generated in the plasma affects the electronic properties of a-C films. It is crucial to elucidate the manner in which individual radical species influence the electronic and electrical properties of a-C films.

Therefore, in the present study, the anthor studied changes of radical species present in the plasma during the deposition of a-C films. The effects of the variation of the total gas flow rate from 50 to 400 sccm, and the associated changes in the residence times of radical species and molecules, on the deposition characteristics and crystallographic, bonding configuration and electronic structure of the resulting a-C films were investigated.

In Chapter 1, it is an introduction of the background of this thesis, carbon material. The structures and properties of carbon nanomaterials are described in Section 1.1. He gave a detailed description of a-C materials, composed of a hybridization configuration of sp^2-C and sp^3-C. This kind of materials has characteristic structural features and exhibit unique macro and micro properties. In Section 1.2, previous studies on growth methods of a-C films are concluded. Especially, he focused on the growth mechanism under plasma enhanced chemical vapor deposition (PECVD), which is the most popular synthesis method of a-C films for laboratory research. Section 1.3 refers to various applications of a-C films, including mechanical application, such as protective coatings, and medical application, and so on. And also he bridged a correlation between the application and the corresponding desirable properties of a-C films.

In Chapter 2, experimental setup and characterization of a-C films were described for details. In section 2.1, the synthesis system of a-C:H films used in this research are

described, which is called radical injection plasma-enhanced chemical vapor deposition system. The design concept, difference with conventional PECVD and many details of this custom system are all stated. Besides, to improve the reproducibility and stability of deposition process, growth procedure of a-C:H films are strictly operated. He also gave many details of the growth procedure for deposition of a-C:H films in this section. Section 2.2 is mainly about the characterization of a-C films, including thickness derived from stylus profiler, crystallographic properties by Raman spectroscopy, C-H vibration by Fourier Transform Infrared Spectroscopy (FT-IR), bonding configuration by Electron energy loss spectroscopy (EELS) and Near edge X-ray absorption fine structure (NEXAFS), Tauc gap E_g and optical gap E_{04} by Spectrophotometer, and H concentration by Secondary ion mass spectrometry (SIMS). In this section, he introduced not only the basic measurement mechanism of these characterization approaches but also some practical details and important points during measurement in this research.

In Chapter 3, he did an investigation of the plasma condition and basic film properties. The radical species in plasma were monitored by OES, and according to method of actinometory, revolution of observed radical species were investigated. Then the growth process of a-C:H films was evaluated by calculating the deposition rate. At last, with the purpose to give a general describe of resulting samples, hardness was evaluated by nano-indenter. That will be helpful to make a rough positioning of resulting samples.

In Chapter 4, effects of radical species on film properties are investigated. Firstly, resulting a-C:H samples deposited under different total flow rate are evaluated in terms of the optical bandgap, conductivity, crystallographic structure and H content. Then he

also tried to bridge a correlation between the variation in H content, crystallographic structure and optical bandgap.

In Chapter 5, effects of radical species on bonding configuration are investigated. With the change of the residence time of radicals in the chamber, both qualitative and quantitative analysis of the variation in π bond fraction, and sp^2-C fraction was operated. Besides, the information some other bonding configuration was also clarified by FT-IR. Similarly, he tried to find the correlation between the variation in bonding configuration and optical bandgap.

In Chapter 6, firstly all the results in the present study are summarized, and a discussion about the effect of radical species on the structural and electronic structure is stated. According to this, he proposed that electronic structure of a-C:H can be controlled through modification of the bonding configuration via the optimization of radical species and their densities throughout the deposition process. In addition, the prospect of application of resulting a-C:H films is also described in this section. The last part of this thesis is the future scopes.

References

[1] Tanso zairyou gakkai "Shin Tansozairyou Nyumon, [New carbon materials introductory book]" Realize Science & Engineering, Tokyo, 1996. [in Japanese]

[2] 2007 International Technology Roadmap for Semiconductors, Executive Summary.

[3] K. S. Novoselov, A. K. Geim, S. V. Morozov, D. Jiang, Y. Zhang, S. V. Dubonos, I. V. Grigorieva, and A. A. Firsov: Science **306** (2004) 666.

[4] K. S. Novoselov, A. K. Geim, S. V. Morozov, D. Jiang, M. I. Katsnelson, I. V. Grigorieva, S. V. Dubonos, and A. A. Firsov: Nature **438** (2005) 197.

[5] Y. Zhang, Y.-W Tan, H. L. Stormer, and P. Kim: Nature **438** (2005) 201.

[6] J. A. Carlisle, S. R. Blankenship, L. J. Terminello, J. J. Jia, T. A. Callcott, D. L. Ederer, R. C. C. Perera, and F. J. Himpsel: J. Electron Spectrosc. Relat. Phenom. **110-111** (2000) 323.

[7] H. Kondo, W. Takeuchi, M. Hori, S. Kimura, Y. Kato, T. Muro, T. Kinoshita, O. Sakata, H. Tajiri, and M. Hiramatsu: Appl. Phys. Lett. **99** (2011) 213110.

[8] W. Takeuchi, K. Takeda, M. Hiramatsu, Y. Tokuda, H. Kano, S. Kimura, O. Sakata, H. Tajiri, and M. Hori: Phys. Status Solidi **207** (2010) 139.

[9] S. Kawai, S. Kondo, W. Takeuchi, H. Kondo, M. Hiramatsu, and M. Hori: Jpn. J. Appl. Phys. **49** (2010) 060220.

[10] N. Ohtake, T. Uchi, T. Yasuhara and M.Takashima: Jpn. J. Appl. Phys. **051**(2012) 090128-1.

[11] Y. Ohsone, H. Nishi, M. Saito, M.Suzuki, H. Murakami, N. Ohtake: J. Solid Mech. Mater. Eng, **3**(2009) 691.

[12] J. Robertson: Adv.Phys. **35**(1986) 317.

[13] A. Bubenzer, B. Dischler, G. Brandt, P. Koidl: J. Appl. Phys, **54**(1983) 8.

[14] W. Jacob and W. Moller: Appl. Phys. Lett., **63**(1993) 1771.

[15] S. Aisenberg and R. Chabot: J. Appl. Phys. **42**(1971) 2953

[16] Y.Lifshitz: Diamond Rel.Mater. **5**(1996) 388.

[17] M.A.Lieberman, A.J.Lichtenberg, Principle of Plasma Discharge and Material Processing, Wiley, NewYork, (1994).

[18] P. Koidl, C. Wagner, B. Dischler, J. Wagner, and M. Ramsteiner: Mater. Sci. Forum. **52**(1990)41.

[19] E.G. Spencer, P.H. Schmidt, D.C. Joy, F.J. Sansalone: Appl. Phys. Lett. **29**(1976)118.

[20] Y. Lifshitz, S.R.Kasi, J.W. Rabalais, W.Eckstein: Phys.Rev.B. **41**(1990) 10468.

[21] J.C.Bourgoin, B.Masarini: Phys. Rev.B. **14**(1976)2690.

[22] C.Weissmantel: Thin Solid Films, **92**(1982)55.

[23] J.Robertson: Pure. Appl. Chem. **66**(1994)1789

[24] J.Robertson: Diamond. Rel. Mater. **3**(1994)361

[25] A. von Keudell, T. Schwarz-Selinger, and W. Jacob: J.Appl.Phys. **87**(2001)2719.

[26] A. von Keudell, T. Schwarz-Selinger, and W. Jacob: J. Vac. Sci. Technol. A **19**(2001)101.

[27] N. Ohtake, T. Uchi, T. Yasuhara and M.Takashima: Jpn. J. Appl. Phys. **051**(2012) 090128-1.

[28] Y. Ohsone, H. Nishi, M. Saito, M.Suzuki, H. Murakami, N. Ohtake: J. Solid Mech. Mater. Eng., **3**(2009) 691.

[29] J. Robertson: Adv.Phys. **35**(1986) 317.

[30] A. Bubenzer, B. Dischler, G. Brandt, P. Koidl: J. Appl. Phys., **54**(1983) 8.

[31] L. P. Andersson, S. Berg, H. Norstrom, R.Olaison, S. Towta: Thin Solid Films.,

63(1979) 155.

[32] Y.Catherine, P. Couderc: Thin Solid Films. **144**(1986)265.

[33] K. Kobayashi, N. Mutsukura, and Y. Machi: Thin Solid Films. **158** (1988) 233.

[34] M. Alaluf, J. Appelbaum, L. Klibanov, D. Brinker, D. Scheiman, and N. Croitoru: Thin Solid Films. **256**(1995) 1.

[35] M. Alaluf, J. Appelbaum, M. Maharizi, A. Seidman, and N. Croitoru: Thin Solid Films., **303**(1997) 273.

[36] J. Robertson: Prog. Solid. State Chem., **21**(1991) 199.

[37] P. Koidl, C. Wagner, B. Dischler, J. Wagner, and M. Ramsteiner: Mater. Sci. Forum. **52**(1990)41.

[38] D.R. McKenzie,Rep: Prog. Phys., **59**(1996) 1611.

[39] Y. Lifshitz: Diamond Rel. Mater., **8**(1999) 1659.

[40] H. Zhu, J. Wei, K. Wang, D. Wuet: Solar Energy Materials & Solar Cells. **93**(2000) 1461.

[41] K. M. Krishna, M.Umeno, Y.Nukaya, T.Soga, T.Jimbo: Appl. Phys. Lett., **77**(2000)1472.

[42] W. Jacob and W. Moller: Appl. Phys. Lett., **63**(1993) 1771.

[43] C. Weissmantel: Thin Solid Films., **92**(1982) 55.

[44] Y. Lifshitz, S.R. Kasi, J.W. Rabalais, W. Eckstein: Phys. Rev. B., **41**(1990) 10468.

[45] E.G. Spencer, P.H. Schmidt, D.C. Joy, F.J. Sansalone: Appl. Phys. Lett. **29**(1976)118.

[46] W. Moller: Appl. Phys. Lett., **59**(1991) 2391.

[47] N.Mutsukura, S. Inoue, Y.Machi: J. Appl. Phys., **72**(1992) 43.

[48] P. J. M. van der Burgt, J. W. McConkey: J. Phys. B: At .Mol .Opt .Phys. **24**(1991)

4821.

[49] Yasuo Murakami, Seishi Horiguchi, Satoshi Hamaguchi: Phys. Rev. E, **81**(2010) 041602-1.

[50] A.A. Voevodin, J.G. Jones, J.S. Zabinsk: J. Appl. Phys. **92**(2002) 724.

[51] J.W. Zou, K. Schmidt, K. Reichelt, D. Dischler: J. Appl. Phys. **67**(1989) 487.

[52] M.A. Tamor, W.C. Vassell, K.R. Carduner: Appl. Phys. Lett. **58**(1991) 592.

[53] J. Ristein, R.T. Stief, L. Ley, W. Beyer: J. Appl. Phys. **84**(1998) 3836.

[54] J. Robertson: Philos. Mag. B., **76**(1997) 335.

[55] C.W. Chen, J. Robertson: J. Non Cryst. Solids. **227/228** (1998) 602.

[56] J. Robertson: Pure. Appl. Chem., **66**(1994)1789.

[57] N.M.J. Conway, A.C. Ferrari, A.J. Flewitt, J. Robertson, W.I. Milne, A. Tagliaferro, W. Beyer: Diamond Rel. Mater. **9**(2000) 765.

[58] R.H. Jarman, G.J. Ray, R.W. Stadley: Appl. Phys. Lett. **49**(1986)1065.

[59] M.A. Tamor, W.C. Vassell, K.R. Carduner: Appl. Phys. Lett., **58**(1991) 592.

[60] M.A. Tamor, W.C. Vassel: J. Appl. Phys, **76**(1994) 3823.

[61] M. Weiler, S. Sattel, T. Giessen, K. Jung, H. Ehrhardt, V.S. Veerasamy, J. Robertson: Phys. Rev. B, **53** (1996) 1594.

Chapter 2

Experimental setup and characterization of a-C films

2.1. Synthesis of a-C films

Plasma-enhanced chemical vapor deposition (PECVD) has been widely applied to fabricate various kinds of material including carbon materials such as amorphous carbon (a-C) film, graphene, carbon nanotubes (CNTs), and carbon nanowalls (CNWs) as well as various silicon (Si) films such as hydrogenated amorphous Si (a-Si:H) films. These materials are synthesized by surface reactions with ions and radicals at relatively low temperature.

In typical plasma, free electrons are accelerated by an electric field and have high energies. Chemically-reactive and energetic species are usually generated under low pressure by collisions between the energetic electrons and molecules. These active species chemically and physically interact or react with the surface atoms of the substrate. Continuous cycle of such surface reactions deposits materials on a substrate. To control the surface reactions, we should determine to control the plasma state by changing the gas flow rates, total gas pressure, frequency of the power source, the input power, etc as parameters. The typical process carbon gases are methane (CH_4), ethylene (C_2H_4), acetylene (C_2H_2), CF_4, and C_2F_6 for fabrication of carbon nanomaterials.

Hydrogen (H_2) and argon (Ar) gases are used as additional gases to alter the plasma states and directly or indirectly the reactions. Various electrical power sources with different frequencies including direct current (DC) and 13.56 MHz-2.45 GHz and pressures ranging between 1 Pa and 10 kPa (atmospheric pressure) are widely used.

Remote plasma sources are widely used for effective plasma processes such as CVD deposition, etchings, and surface treatments of films due to extraction of target species, in general, neutral species such as radicals. Furthermore, such a remote plasma is also applied as a radical source (or ion source with extraction and acceleration electrodes) to clarify surface reactions in detail. As localized and partially-limited plasmas with a relatively-high density are needed to make the remote plasma sources, inductively-coupled rf plasmas (rf-ICP) and surface-wave microwave excited plasma (SWP) are usually used.

2.1.1. Radical injection plasma-enhanced chemical vapor deposition (RI-PECVD) system

In this research, amorphous carbon film (a-C:H) was fabricated by an custom experimental system called radical injection plasma-enhanced chemical vapor deposition (RI-PECVD) system, as shown in Figure. 2.1.

This RI-PECVD has been designed based on a concept of precisely-controlling internal parameters of plasma such as an electron density, an electron temperature, etc., which are critical factors in PECVD.

The advantage of this system is individual control of H and CH radicals during the deposition. For this purpose, two separate chamber and power source were applied, one is the surface wave plasma (SWP) for generating high density of H radicals in the top chamber, and the other one is the capacitively coupled plasma (CCP) for CH_n radicals in the bottom chamber. With the purpose of independent control of ion flux and ion energy, double high frequency power source was applied.

From Figure 2.1, we can see that this system has a tandem structure, in which two different types of plasma sources are vertically stacked and connected through a showerhead electrode. The upper source is a surface wave plasma (SWP) obtained by injecting 2.45 GHz microwaves through a quartz window, while the lower is a parallel-plate capacitively-coupled plasma (CCP) source based on very high frequency (VHF) power. H_2 gas is introduced to the SWP region, generating H radicals and undissociated H_2 molecules that flow through the shower head into the lower region. Concurrently, CH_4 gas is introduced into the CCP chamber and the resulting CH_n radicals and ions mix with the H radicals diffusing from the upper SWP. In this

apparatus, 100 MHz VHF power and 13.56 MHz radio-frequency (RF) power are applied to the upper (showerhead) and lower (substrate stage) electrodes, respectively. As a result, a-C films are deposited on synthetic quartz substrates placed on a substrate stage heated by a carbon heater. Employing this tandem PECVD system, the H to CH_n radical density ratio can be controlled precisely, and the tailored synthesis of various carbon nanomaterials can be realized.[1] The total pressure was maintained at 1 Pa during the deposition process. The SWP, CCP and RF power values were 400, 100 and 50 W, respectively, and the substrate stage temperature was set at 550 ℃. In these trials, the total gas flow rates (the sum of H_2 and CH_4) were varied in the range from 50 to 400 sccm in order to control the residence time of gas molecules in the plasma regions.

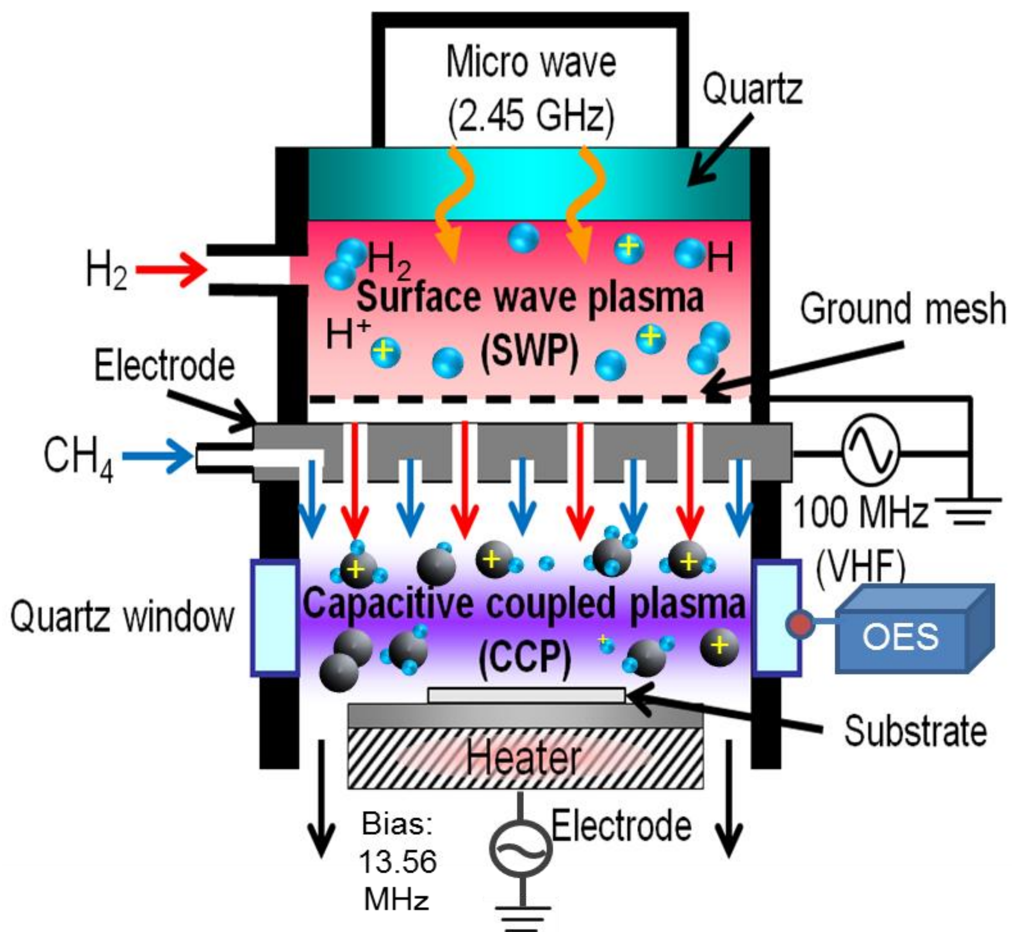

Fig. 2.1 Schematic diagram of the RI-PECVD system.

2.1.2. Growth procedure

The substrate used is synthetic quartz which was fixed by a custom sapphire mask showing in the Figure 2.2. This kind of mask was designed for improving the reproducibility and uniformity of deposited film by enhancing the heating uniformity and stability of substrate during progress.

From Figure 2.2, it can be seen that there are 4 square holes in the mask, under which the 16×16 mm synthetic quartz substrates can be fixed and the upper hole size is 14 mm×14 mm opened to the upper plasma bulk. Generally, the author employed 4 pieces of synthetic quartz substrates in one generation circle. As described above, the plasma bulk was created in the reaction chamber and the various radicals like H, CH_n bombard with the surface of the substrate under the applied electric magnetic field and finally the film was generated on the substrates.

The detail of the deposition process was shown in the process plot in Figure 2.3. Before 20 minutes film deposition, the pre-discharge was carried out with no substrate for 5 minutes for steady chamber condition during the whole process.

Both in the preparation for the pre-discharge and the deposition process, it cost several minutes for the substrate temperature rising from the room temperature to the target temperature, e.g 550 ^oC. After the target temperature of 550 ^oC was reached, the stock gas of H_2/CH_4, at the flow rate ratio 1/2 was introduced into the main chamber. After the pressure was set steady at 1Pa, SWP and CCP power was then fixed at 400 W and 100 W respectively, and once the plasma appears, the bias power was immediately turned on and fixed at 50 W. Because the initial discharge is not so steady, so the start deposition time was accounted after steady plasma was confirmed.

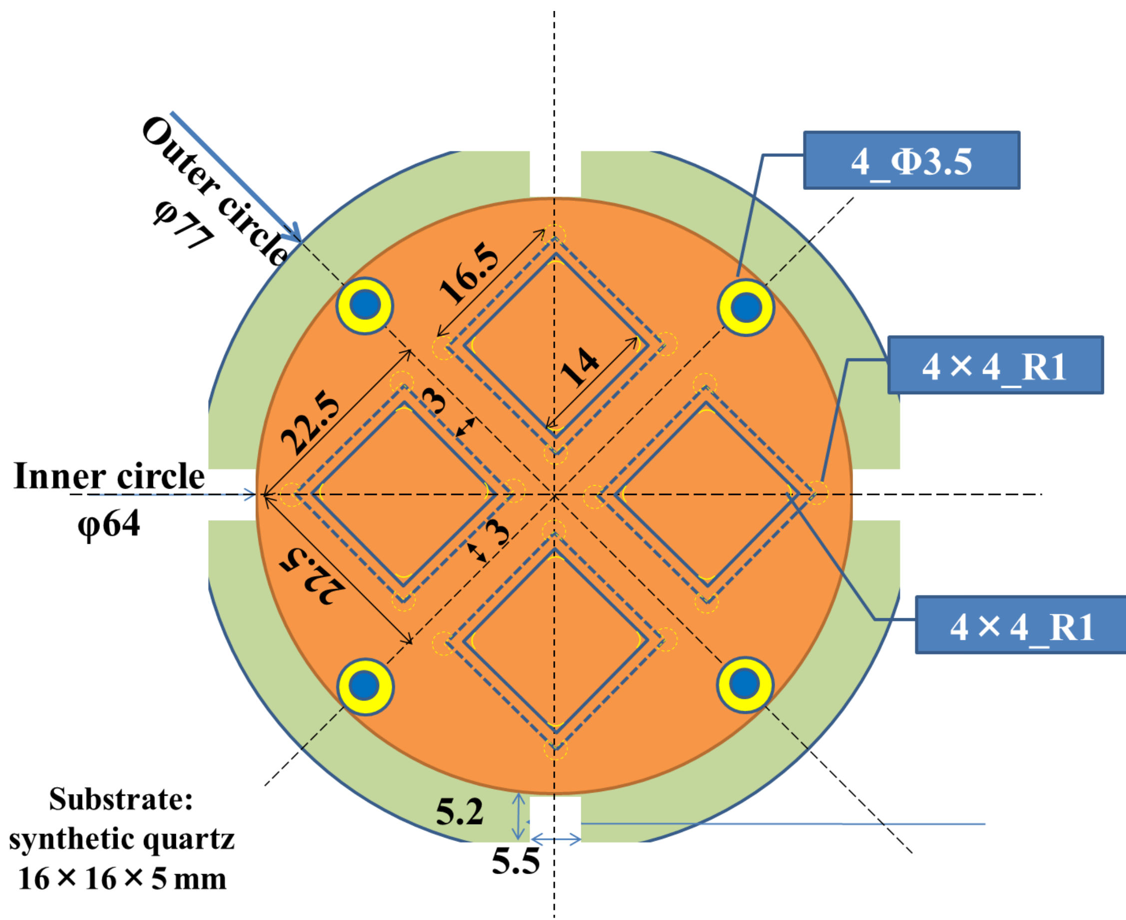

(a) Top view

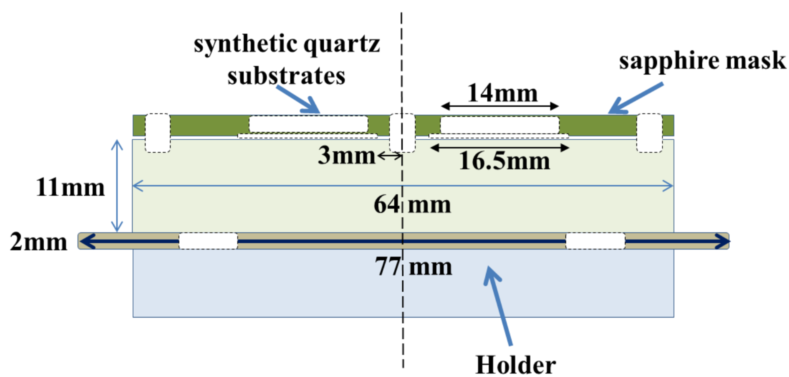

(b) Side view

Fig 2.2 Schematics of the sapphire mask and the substrate.

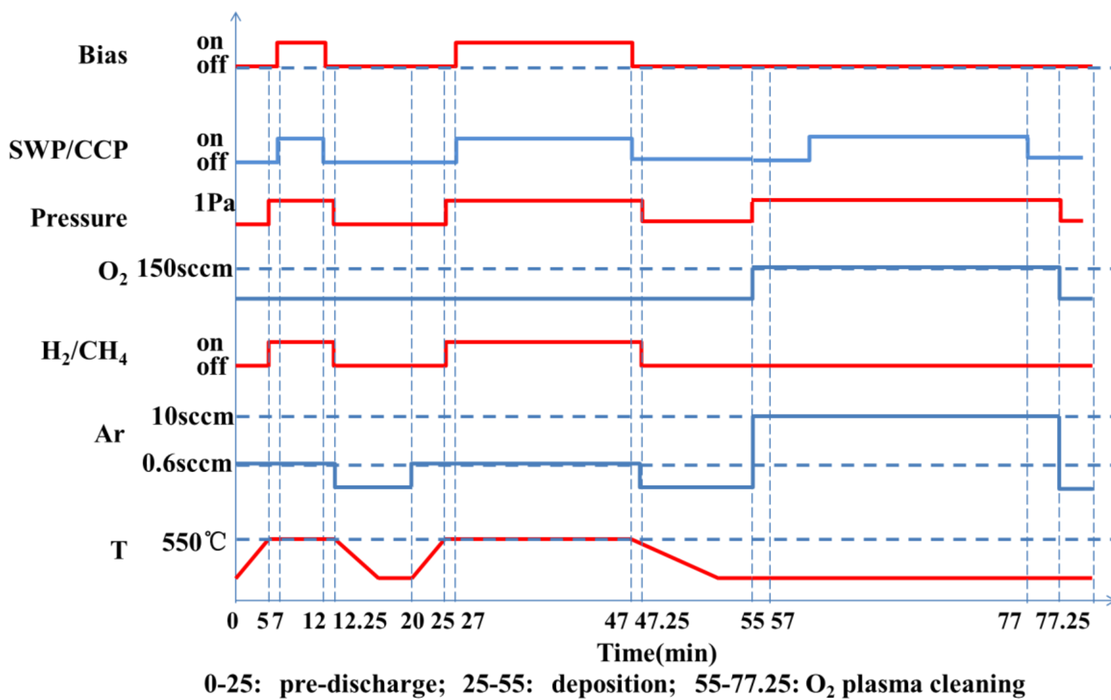

Fig.2.3. The sequence of all parameters during the whole generation process.

2.2. Characterization of a-C films

After generation, the macro and micro properties of resulting a-C:H films were systemically evaluated, including thickness derived from stylus profiler, crystallographic properties by Raman spectroscopy, C-H vibration by Fourier Transform Infrared Spectroscopy (FT-IR), bonding configuration by Electron energy loss spectroscopy (EELS) and Near edge X-ray absorption fine structure (NEXAFS), Tauc gap E_g and optical gap E_{04} by Spectrophotometer, and H concentration by Secondary ion mass spectrometry (SIMS). And the detailed method of the mentioned measurement will be discussed as below.

2.2.1. Thickness (stylus profiler)

In this research, the thickness of a-C:H films are determined by stylus profiler. A stylus scans on the surface of solid material, and the value we derived is actually a height difference between two steps. In our case, the height difference between synthetic quartz substrate and bulk film considered as the thickness of a-C:H films as shown in Figure.2.4. During this measurement, the scanning length was fixed as long as possible, so that the value we get can reflect a mean thickness of the whole piece of film, or it only can represent the thickness of edge region of measured film.

In addition, to decrease the error occurring during the measurement, as it is shown in Figure 2.5, 2 points were chosed at every side of the film edge for calculating the

average value of thickness. And the scan range was set at 2 mm, 1.5 mm away from the edge of the film towards the center.

Figure.2.4 shows an idealized result of curve, from which the height difference is easy to be confirmed. In practical, usually the curve in the right region is not parallel with that of left region. For accurate calculation of thickness, firstly the baseline of substrate area has to be subtracted, and then a fixed range has to be defined for calculating the average thickness of film. The fixed range in this experiment is 1.4 mm from edge of film towards the center.

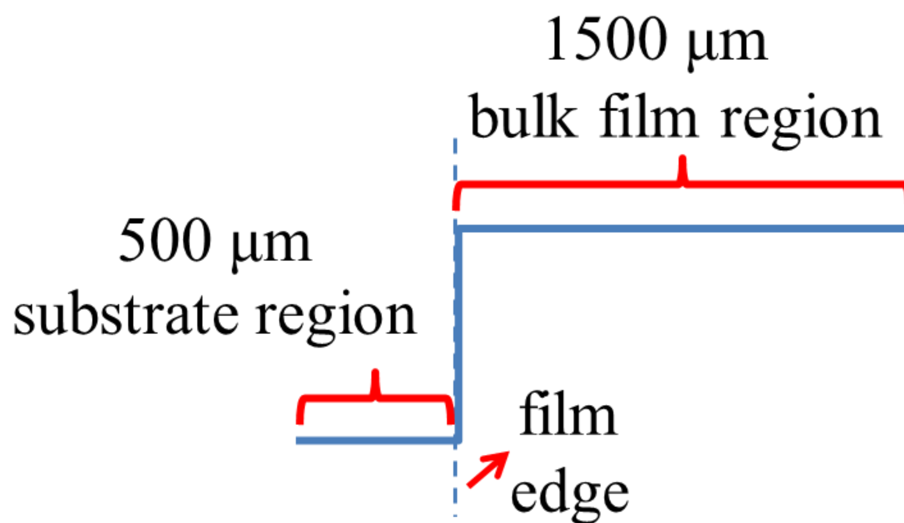

Fig 2.4. A schematic of the measurement mechanism of stylus profiler.

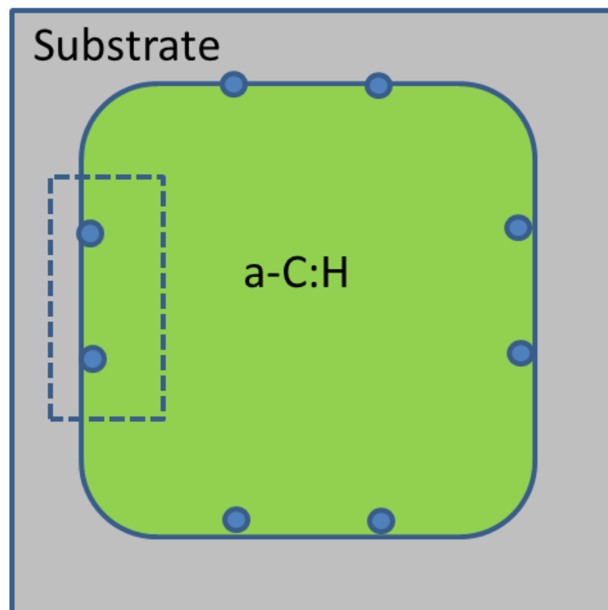

Fig 2.5. A schematic of the measurement procedure of thickness by stylus profiler. (top view of film deposited on the substrate)

2.2.2. Crystallographic properties (Raman spectroscopy)

Raman spectroscopy is usually used to observe vibrational modes of many different kinds of materials. And it is also a useful tool for analyses of graphitic structures in graphene or graphite, graphite fiber, amorphous carbon, diamond, carbon nanotubes, and CNWs [2-12]. Thus, in present research, it is applied for evaluation of the crystallographic properties of a-C:H films.

Essentially, the mechanism of Raman spectroscopy is correlated to the Raman scattering. Photons irradiated to materials are scattered and then loss or gain some amounts of energy.[13-15] And thus this would cause a variation in frequency of photons, from which the structural properties of molecular bonds within the irradiated materials can be characterized. Therefore, Raman scattering is very sensitive to the crystalline structures of many materials.

In this study, Raman spectra for a-C:H were measured by Raman microscope, Renishaw. In practical during measurement, a-C:H samples are illuminated under a laser beam. A 532 nm line of Ar^{+} laser with a focal spot size of approximately 10 μm was used and the laser power was 1 mW.

In Figure.2.6, it shows a typical Raman spectrum of resulting a-C:H films in present research. From this spectrum, we can see two obvious peaks at about 1580 cm^{-1} and 1450 cm^{-1}. The slope of background is relative low, indicating that resulting a-C:H films are different from polymeric material.

In practical, the real measurements were operated as shown in the Figure 2.7. Generally spectra were derived from five points of the sample films to check the uniformity within the whole piece of film. And also precise coordinate was applied,

with the left lower corner of the 16×16 mm quartz glass substrate as the origin point (0, 0). Then we took the spectra from the Point 1 to 5. The distance between points is 4 mm.

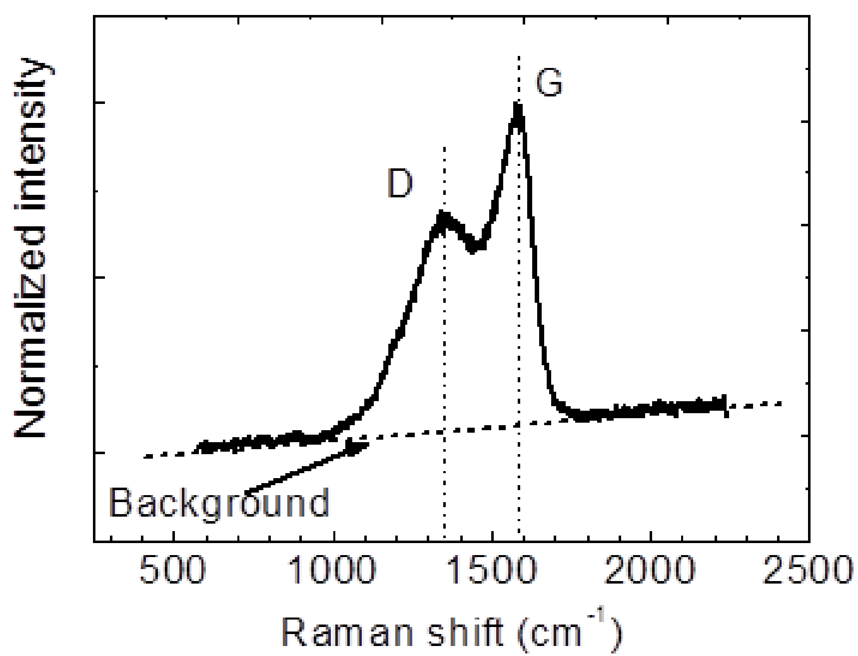

Fig. 2.6. Typical Raman spectrum of resulting a-C:H films in this research.

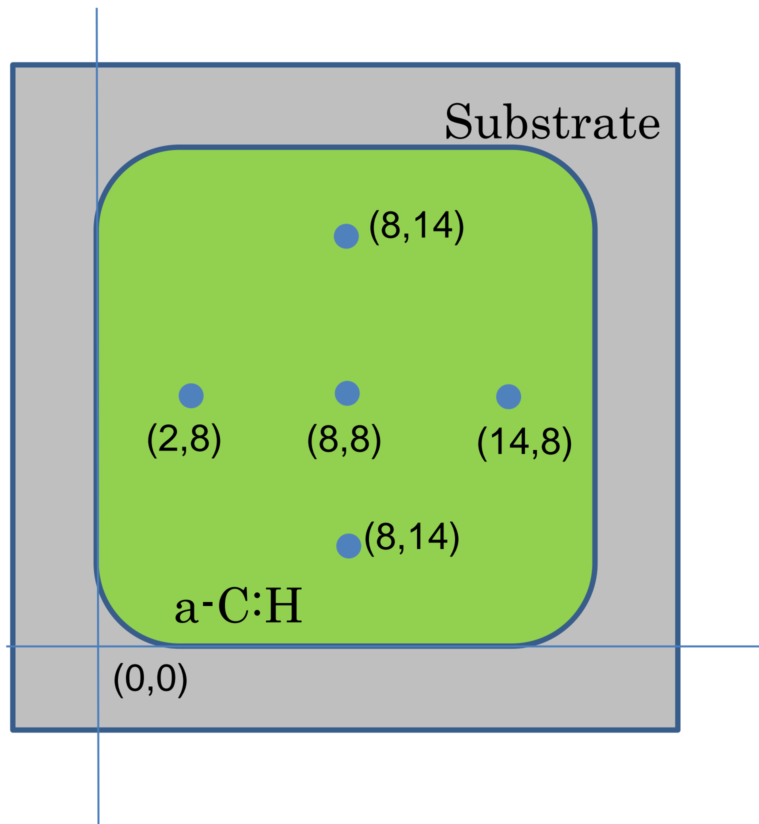

Fig. 2.7. A schematic of practical Raman measurement approach in this research.

2.2.3. C-H vibration: Fourier Transform Infrared Spectroscopy (FT-IR)

Fourier transform infrared spectroscopy (FT-IR) is a common used method for analysis of C-H bonding in the a-C:H films. In the FT-IR spectra of a-C:H films, C-H stretching mode appears at 2800-3300 cm^{-1}, and C-H bending mode is below 2000 cm^{-1}.

The features of C-H mode have a close relation with CH molecules. And generally C-H mode can be divided into three parts for analysis, sp^1 CH mode centered at 3300 cm^{-1}, sp^2 CH_n mode between 2975-3085 cm^{-1}, sp^3 CH_n mode between 2850-2955 cm^{-1}.[16,17] Table 1 shows a conclusion of the assignments of IR vibrational frequency in the case of a-C:H films. Figure 2.8 shows a typical FT-IR spectrum of resulting a-CH film in this research.

Although it is popular to obtain the sp^3 fraction by fitting FT-IR spectrum with Gaussians, the decomposition result is not unique because of the broad band. Thus it is not reliable to derive sp^3 fraction from FT-IR spectrum

On the other hand, FT-IR spectrum can also be used for qualitative analysis of H content in the a-C:H films. Generally it is derived by calculating the ratio of all the C-H modes. However, there remains only one question that whether all hydrogen bonded in C-H mode in the case a-C:H films. Actually H_2 molecules have already been confirmed in the a-C:H films.[18] But there are also some other groups[19] claimed that H_2 molecules only account for a little fraction. Thus, for the analysis of H content in the a-C:H films, FT-IR spectra should be analyzed together with some other characterization method.

Table 1 Assignments of IR vibrational frequency in a-C:H.[16,17]

Wavenumber (cm^{-1})	Configuration	Olefinic or aromatic	Symmetric or antisymmetric
3085	sp^2 CH_2	Olefinic	A
3035	sp^2 CH	Aromatic	
2990-3000	sp^2 CH	Olefinic	S
2975[a]	sp^2 CH_2	Olefinic	S
2955[a]	sp^3 CH_3		A
2920	sp^3 CH_2		A
2920	sp^3 CH		
2885	sp^3 CH_3		S
2855	sp^3 CH_2		S

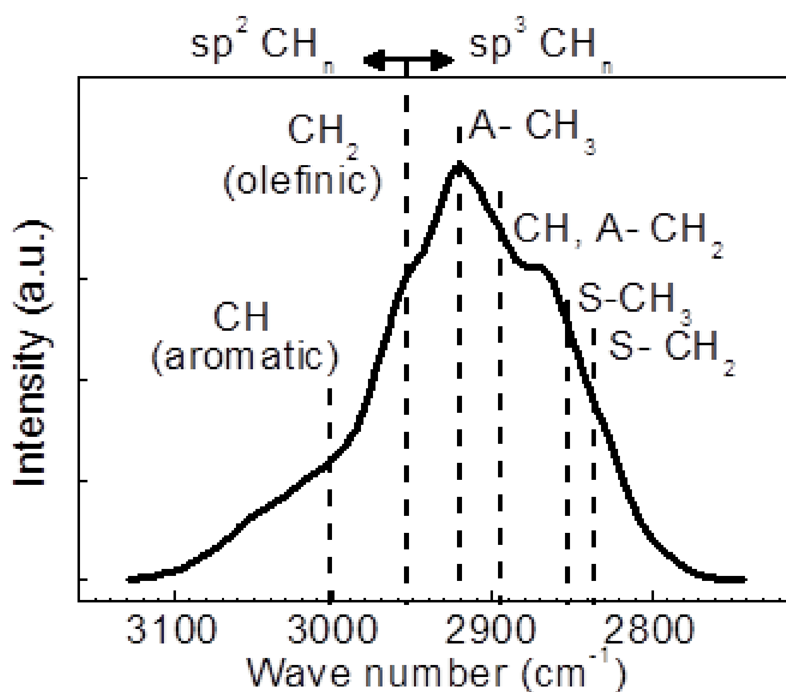

Fig 2.8. Typical FT-IR spectrum of resulting a-CH film in this research

2.2.4. Tauc gap E_g and optical gap E_{04} (Spectrophotometer)

A spectrophotometer is a photometer commonly used for measuring transmittance or reflectance of transparent or opaque solids, such as polished glass, or gases as a function of the light source wavelength.

When exposed in a light source of ultraviolet, electronic energy transition in molecules occur as a result of absorption of energy from the light source. And then from the relation between the absorbance and the wavelength of light source, it is possible to distinguish some special characteristic and composition of materials.

In our experiments, we used a spectrophotometer to obtain the optical band gap, light source can be operated at a large range about (200～2500nm). By this device, absorbance can be measured directly, then according to the formula 2.1, absorption coefficient α can be derived.

$$A = \log_{10}\left(\frac{I_0}{I}\right) = 0.43\alpha \cdot \mathrm{L} \qquad (2.1)$$

where A represents absorbance, α is the absorption coefficient, I_0 is the intensity of the incident light, I is the intensity of the transmitted light, L is the path length through the sample.

Generally optical bandgap E_g can be calculated from the absorption coefficient (α). But in the case of amorphous material, as our a-C:H samples, the arrangement of atomics shows a lack of short and long-range order. So it is rare to see a sharp absorption edge, as that usually appeared in a well crystalline material.

Actually in the case of amorphous materials, there is no true gap. Therefore, we have to give a definition for the optical gap. The most common one is Tauc gap, defined as the intercept E_g derived from a Tauc plotting, which has the quantity hν (the energy

of the incident light) on the abscissa and the quantity $(\alpha h\nu)^r$ on the ordinate. The constant r denotes the nature of the transition. As shown in formula 2.2, r = ½ which represents indirect transitions, is usually adopted in the case of amorphous material,

$$\sqrt{\alpha h v} = C(hv - E_g) \tag{2.2}$$

As shown in Figure.2.9, which is typical Tauc plot of resulting a-C:H film in present research, the plot has a distinct linear regime which denotes the onset of absorption. Thus, extrapolating this linear region to the abscissa will tell us the value of the optical band gap.

Experimentally, Although Tauc gap is a common method for evaluation of gap, some other characterization method should be used for reliable analysis of optical bandgap, like E_{04}, which is defined as the energy at which the optical absorption coefficient α is 10^4 cm^{-1}.

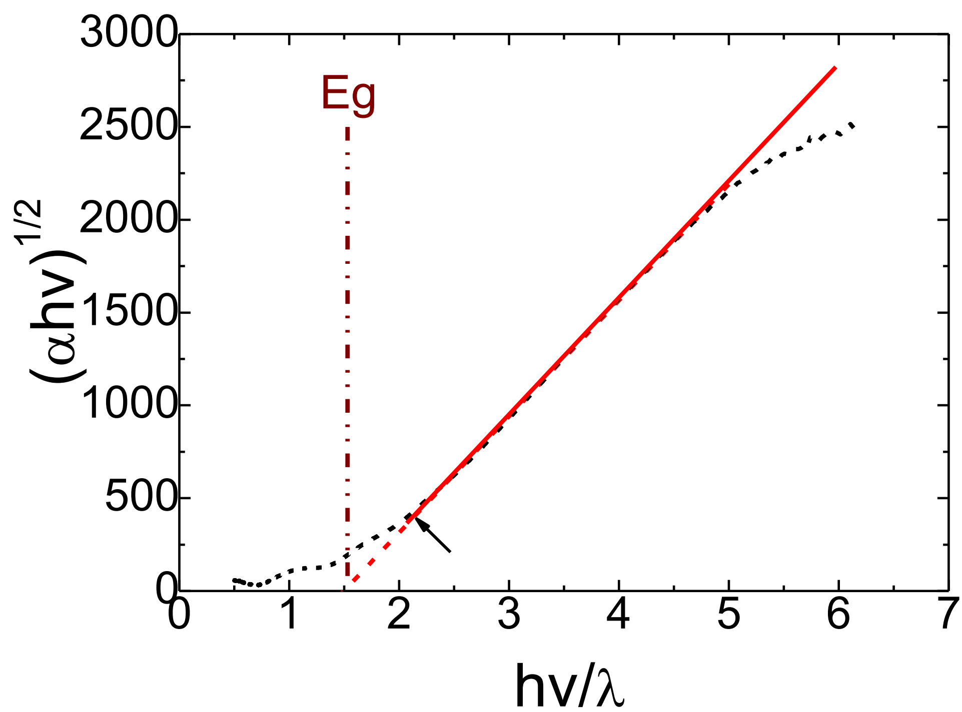

Fig 2.9. Typical Tauc plot of a-C:H films.

References

[1] J.W. Coburn, M.J.Chen: J. Appl. Phys, **51**(1980)3134–6.

[2] R. J. Nemanich and S. A. Solin: Phys. Rev. B **20** (1979) 392.

[3] G. Katagiri, H. Ishida, and A. Ishitani: Carbon **26** (1988) 565.

[4] M. Nakamizo, R. Kammereck, P.L. Walker Jr.: Carbon **12** (1974) 259.

[5] T. P. Mernagh, R. P. Cooney, and R. A. Johnson: Carbon **22** (1984) 39.

[6] T. C. Chieu, M. S. Dresselhaus, and M. Endo: Phys. Rev. B **26** (1982) 5867.

[7] H. Tsai and D. B. Bogy: J. Vac. Sci. Technol. A **5** (1987) 3287.

[8] J. Wagner, M. Ramsteiner, Ch. Wild, and P. Koidl: Phys. Rev. B **40** (1989) 1817

[9] A. C. Ferrari and J. Robertson: Phys. Rev. B **63** (2001) 12140

[10] A. M. Rao, E. Richter, S. Bandow, B. Chase, P. C. Eklund, K. A. Williams, S. Fang, K. R. Subbaswamy, M. Menon, A. Thess, R. E. Smalley, G. Dresselhaus, and M. S. Dresselhaus: Science **275** (1997) 187.

[11] S. Kurita, A. Yoshimura, H. Kawamoto, T. Uchida, K. Kojima, M. Tachibana, P. Molina-Morales, and H. Nakai: J. Appl. Phys. **97** (2005) 104320.

[12] Z. H. Ni, H. M. Fan, Y. P. Feng, Z. X. Shen, B. J. Yang, and Y. H. Wu: J. Chem. Phys. **124** (2006) 204703.

[13] C. V. Raman and K. S. Krishnan: Nature **121** (1928) 501.

[14] R. Singh: Physics in Perspective **4** (2002) 399.

[15] G. Landsberg and L. Mandelstam: Naturwissenschaften **16** (1928) 557.

[16] T. Heitz, B. Drévillon, C. Godet, and J. E. Bourée, Phys. Rev. B **58**(1998) 13957

[17] C. Thomsen and S. Reich, Phys. Rev. Lett. 85(2000)5214

[18] A.Grill, V.Pate: Appl. Phys.Lett. **60**(1992)2089.

[19] C.Donnet, J.Fontaine, F.Lefèbvre, A.Grill. V.Patel, J. Appl. Phys, **85**(1999)3264.

Chapter 3 Effect of radical species on electronic and electrical properties

3.1. Introduction

Amorphous carbon (a-C) films have diverse properties, running from electrically conductive to insulating, from exceptionally hard to soft and from optically transparent to opaque. As an example, films that are relatively well crystallized, representing so-called diamond-like carbon (DLC), are applied as protective coatings in applications such as optical windows, car parts, and so forth, because they are harder than sapphire and exhibit optical transparency in the infrared.[1-5] In contrast, the applications of these films as device materials, such as electrodes and channels, are less advanced. In particular, there has been almost no significant progress in the field of semiconductor devices using a-C films as channels, such as a-C solar cells, even though a-C films exhibit a wide range of optical and energy band gaps.[6-9] Although there have been many reports concerning solar cells using a-C films, solar cell operation has been observed only in the case of a-C/Si stack structures and is attributable to photovoltaic effects on the Si surfaces.[10,11] There have been no reports with regard to the photovoltaic effect in the a-C film itself, or of solar cells operating with junction structures consisting solely of a-C layers.

Many fundamental researches about a-C films have been done at the viewpoints of

not only plasma physics but also material science. For example, according to the well-known ternary phase diagram of carbon materials proposed by Jacob and Moller, the structures and properties of a-C films are basically determined by composition ratios of sp^2-C, sp^3-C and H.[12] On the other hand, there are also many studies regarding the deposition mechanisms of a-C films.[13-16] Dissociation processes of hydrocarbon and fluorocarbon molecules, and formation of individual radicals in plasmas have been investigated.[17,18] Effects of generated radicals on formation of sp^2 and sp^3 bonding states, and also film growth have been also discussed.[19,20] Generally, highly-dissociated species, such as C_2, tend to induce sp^2 bonds, while CH_3 radicals induce sp^3 ones. Furthermore, in the so-called sub-plantation model, ion bombardment is considered to be the primary factor determining the bonding configuration and thus the resulting properties of the a-C.[21-23] However, the electronic properties of a-C films, especially semiconducting characteristics, have not been sufficiently optimized and controlled. In the energy band structure of a-C film, a huge number of electronic levels corresponding to sp^2-C bonds are present in the energy band gap region formed by sp3-C atoms. They induce metallic features or pronounced current leakage.[24,25] On the other hand, clustering of the sp^2 phase and their effects on macroscopic properties of a-C films have also been suggested.[26-31] Therefore, it is deduced that the electronic properties of a-C films cannot be predicted only by the composition ratios of sp^2-C, sp^3-C and H in the film, so there may be other factors that affect the electronic properties of these films.

As mentioned above, concerning the radical species, the dissociation of hydrocarbon or fluorocarbon gases, and the generation of various types of C-containing radicals such as C_2, CHx and CFx in the plasma, and their effects on formation of

bonding configuration (sp^2 and sp^3) have also been discussed in previous papers.[32-33] However, the mechanism how such the radicals induce electronic structures of a-C films, such as energy band gap, is not clarified yet. In terms of experimental studies, there are few reports about how the change of radical species generated in the plasma affects the electronic properties of a-C films. It is crucial to elucidate the manner in which individual radical species influence the electronic and electrical properties of a-C films.

Therefore, in the present study, we studied changes of radical species present in the plasma during the deposition of a-C films. The effects of the variation of the total gas flow rate from 50 to 400 sccm, and the associated changes in the residence times of radical species and molecules, on the deposition characteristics and electronic structure of the resulting a-C films were investigated.

3.2. Residence time of radicals in the chamber

Residence time is a very important factor in plasma technology. As shown in Figure.3.1, we can see that with the change of total flow rate of source gas H_2 and CH_4, residence time of radicals and molecules existing in the plasma would change. And this has a predictable effect on the decomposition and ionization process in the plasma, thus radical species and density would also vary correspondingly. The residence time can be estimated using the following equation.[34]

$$\tau_{res} = \frac{V_{pl} \times \mathrm{P_{dep}}}{\mathrm{P_0} \times \mathrm{f_{total}}} \qquad \textbf{(3.1)}$$

Here, V_{pl} is the volume of the plasma region between the electrodes, P_{dep} is the total pressure, f_{total} is the total gas flow rate (the sum of CH_4 and H_2), and P_0 is the standard pressure. On increasing the total gas flow rate from 50 to 400 sccm, the residence time in the current apparatus was decreased from 17.7 to 2.2 ms. Hereafter, the experimental data variations with total flow rate are discussed with regard to the dependence on the residence time.

.

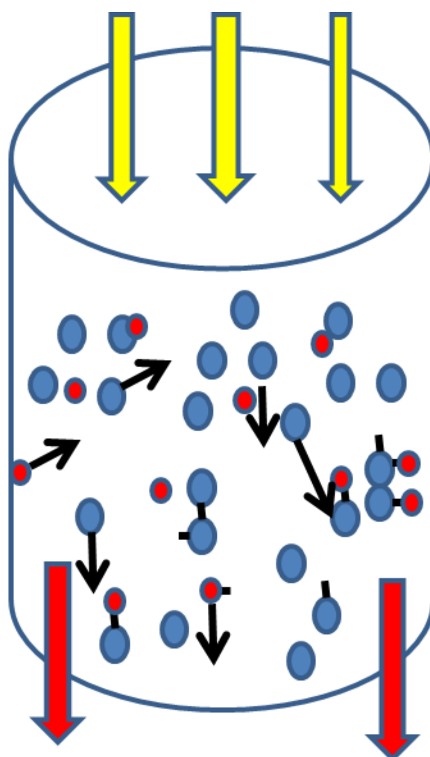

Fig. 3.1 A schematic of radical species in the chamber.

Table. 3.1 Variation of residence time with the change of total flow rate

F_{total} (sccm)	50	75	150	300	400
τ_{res} (ms)	17.52	11.68	5.84	2.92	2.19

3.3 Radical species in plasma

3.3.1 Actinometery

The characteristics of the VHF plasma with H radical injection were evaluated by actinometry using optical emission spectrometry. According to the actinometry method proposed by Coburn and Chen, introducing a trace amount of a noble gas such as Ar allows the evaluation of the relative density of radicals in the plasma.[35] In this study, Ar gas flows in the range of 0.4 to 3.2 sccm were added to the CCP region and the emission intensities of CH ($A_2\Delta \rightarrow X_2\Pi$ at approximately 430 nm), H (H_α:656.1 nm, H_β:486.1 nm), and Ar (811.5 nm) were subsequently recorded.

3.3.2 Variation in CH, H_α, C_2

Figure. 3.2 presents the optical emission spectrum of the CH_4/H_2 plasma at a total flow rate of 150 sccm, corresponding to a residence time of 6 ms. Emission lines of H_α (Balmer α, 656.2 nm), H_β (Balmer β, 486.1 nm), C_2 (Swan band, 516 nm), and CH ($A_2\Delta \rightarrow X_2\Pi$, 431.4 nm) are all clearly observed. A small amount of Ar (0.4-3.2 sccm), acting as an actinometry agent, was added to the CCP region. Since they have similar excitation energy, the intensity of the Ar emission line at 811.5 nm was used as a reference, for the calibration of the emission originated from H_α, H_β, C_2, and CH.[36,37] Figure 3.3 shows the intensity ratios of the H_α, C_2, and CH emission lines relative to the Ar line as functions of residence time, normalized by the values obtained at 50 sccm (residence time of 18 ms). As shown in Figure 3.3, [CH]/[Ar] decreased drastically with increasing residence time, while [H]/[Ar] and [C_2]/[Ar] were almost constant. During these trials, the CH_4 to H_2 flow rate ratio was maintained at 2, and therefore these results indicate that the dissociation of CH to C was suppressed by decreasing the residence time. Of course, other radicals such as CH_2 and CH_3 could have been present in the CH_4/H_2 plasma used in this study. It is therefore apparent that the dissociation of not only CH but also that of other reactive molecules, including CH_4, was suppressed by decreasing the residence time.

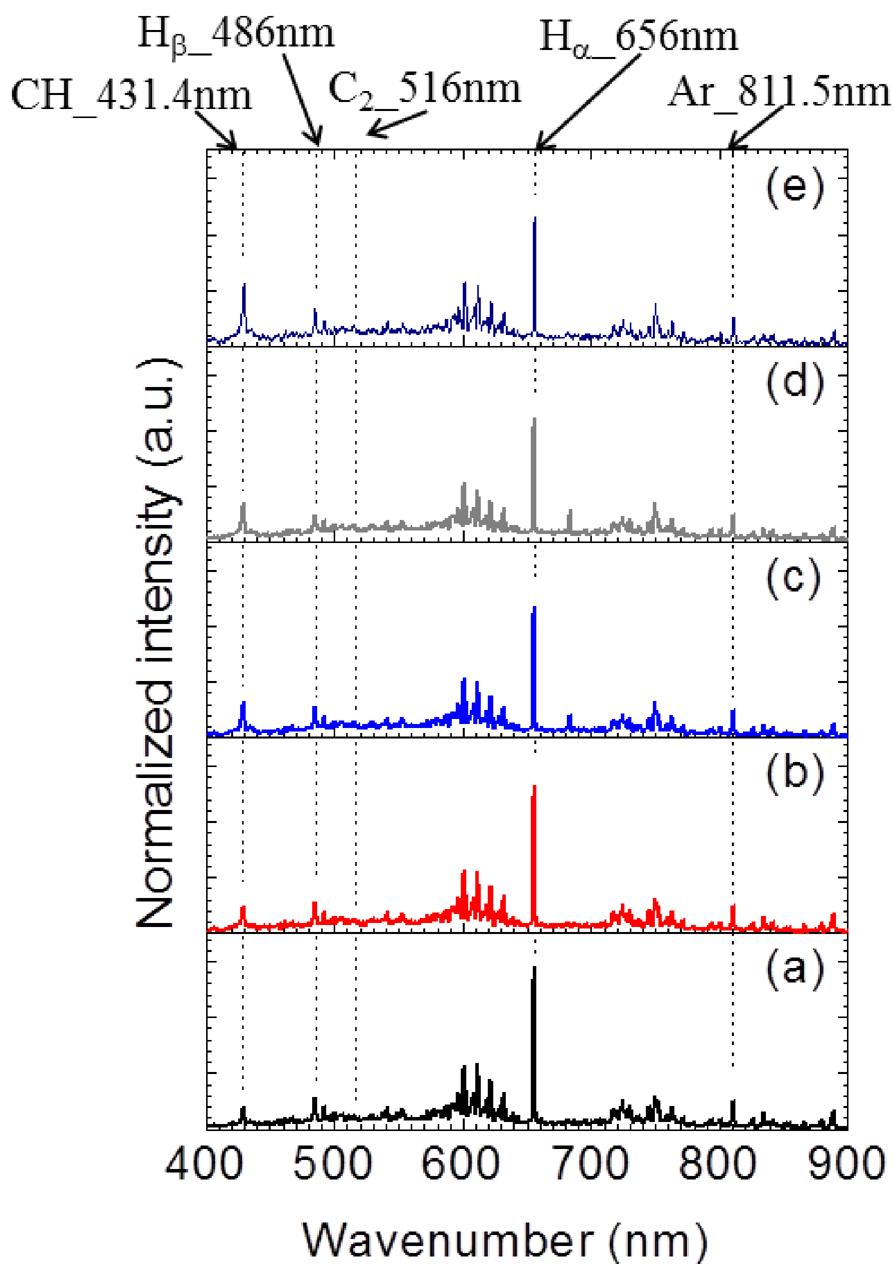

Fig.3.2. Optical emission spectra of the CH_4/H_2 CCP in the RI-PECVD system at different total flow rates, (a) 50sccm, (b) 75 sccm, (c) 150 sccm, (d) 300 sccm, (e) 400 sccm. Each spectrum was normalized using the Ar emission intensity.

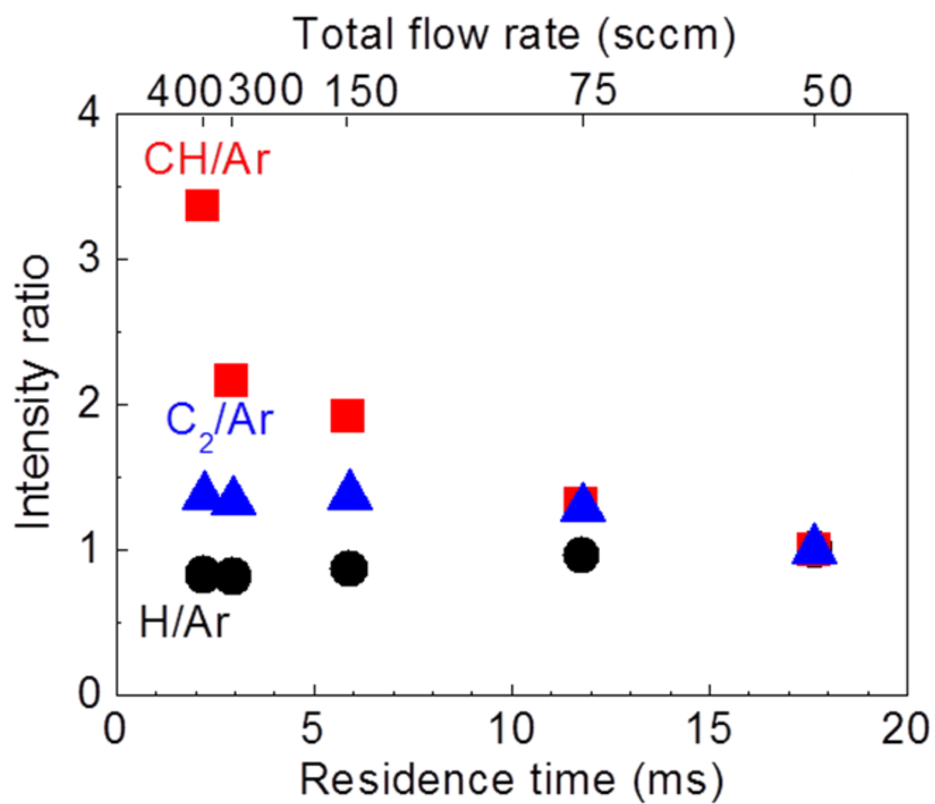

Fig.3.3 Normalized [CH]/[Ar], [C_2]/[Ar], and [H]/[Ar] intensity ratios as functions of residence time.

3.4 Growth rate

Figure 3.4 shows the growth rate of the a-C film as a function of residence time. As the residence time was increased, the deposition rate increased to a maximum value of 72 nm/min at a residence time of 6 ms, after which the rate decreased slightly. Doyle reported the changes in the dominant radical species during a-C film deposition using a 13.56 MHz acetylene (C_2H_2) glow discharge at 30 mTorr (4 Pa),[38] noting that C_2H was dominant at the lowest gas depletion, while C_4H_3 and C_6H_3 were dominant under higher depletion conditions. The important roles of CH radicals in the deposition of a-C films using a H_2/CH_4 plasma excited at 13.56 MHz have also been reported.[39,40] Based on these prior studies, the plot of deposition rate as a function of residence time in Figure 3.4 suggests that the dominant radical species contributing to the deposition of the a-C film undergo a compositional transition at a residence time of approximately 6 ms.

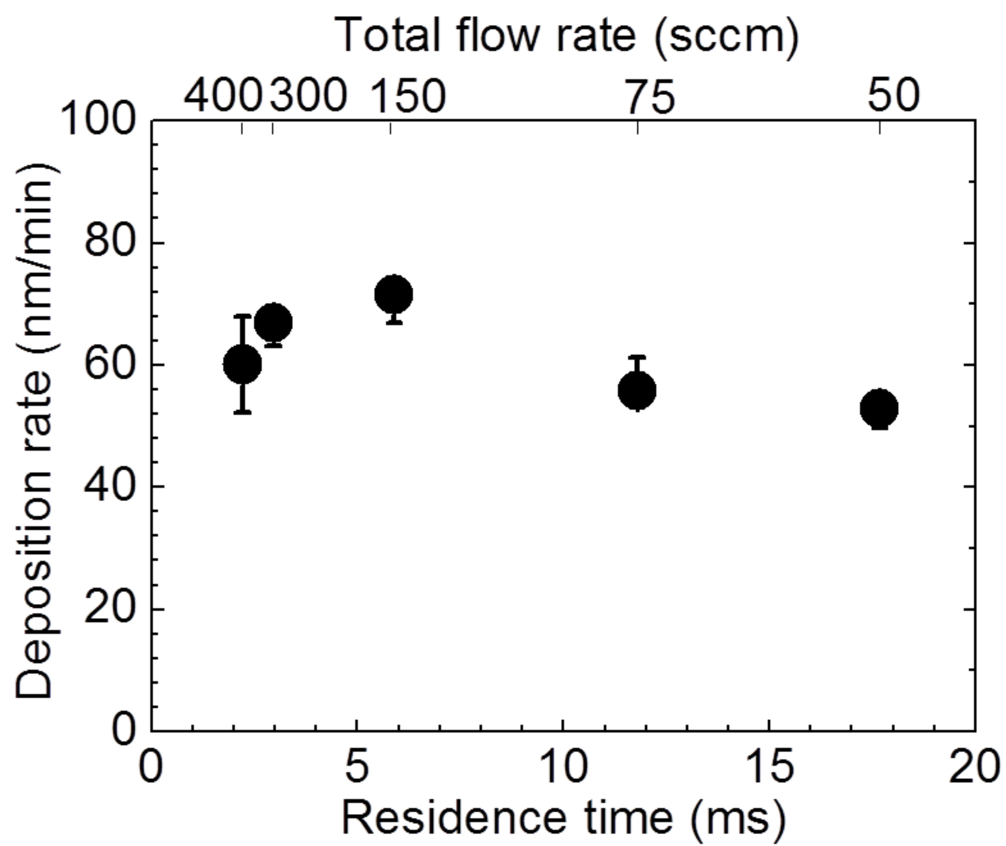

Fig. 3.4. Deposition rate of the a-C film as a function of residence time.

3.5 Hardness

As shown in Figure.1.7, there are many different kinds of amorphous carbon materials. And with different composition of sp^3 carbon (C), sp^2-C and hydrogen (H), they will show various properties, and thus for completely different application.

So it is very important to make clear of the status of resulting a-C:H films among all the different kinds of amorphous carbon materials. Investigation of the fraction of sp^3 carbon (C), sp^2-C and hydrogen (H) is an ideal approach to positioning our samples in Figure.1.7, but the quantitative analysis of sp^2-C, sp^3-C is very complicated.

Many research about the relation between sp^3-C fraction and Hardness have been reported.[41] Therefore, generally the information of hardness could provide a rough status of resulting a-C:H samples.

In this research, nano-indenter was used for investigating the hardness of resuling a-C:H samples. Figure 3.5 shows the hardness of a-C:H samples deposited under different residence time. And the results show that with decreasing residence time, hardness increased from about 12 to 18 GPa.

Figure.3.6 shows the hardness of a-C:H samples deposited under same condition but different deposition time, which means different thickness. And from the results, we can see that thickness did not display an obvious effect on the hardness. And according to the relation between hardness and sp^3-C fraction, to some extent, it indicates that sp^3-C fraction did not change a lot at different thickness, which also means a relative uniform property along the thickness orientation.

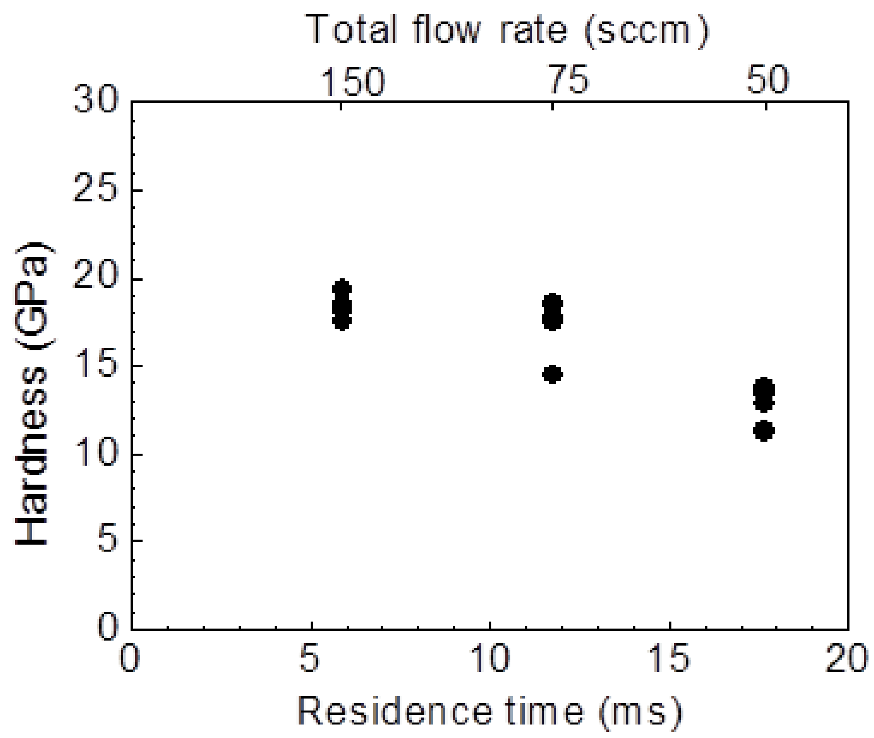

Fig. 3.5. Hardness of the a-C film as a function of residence time.

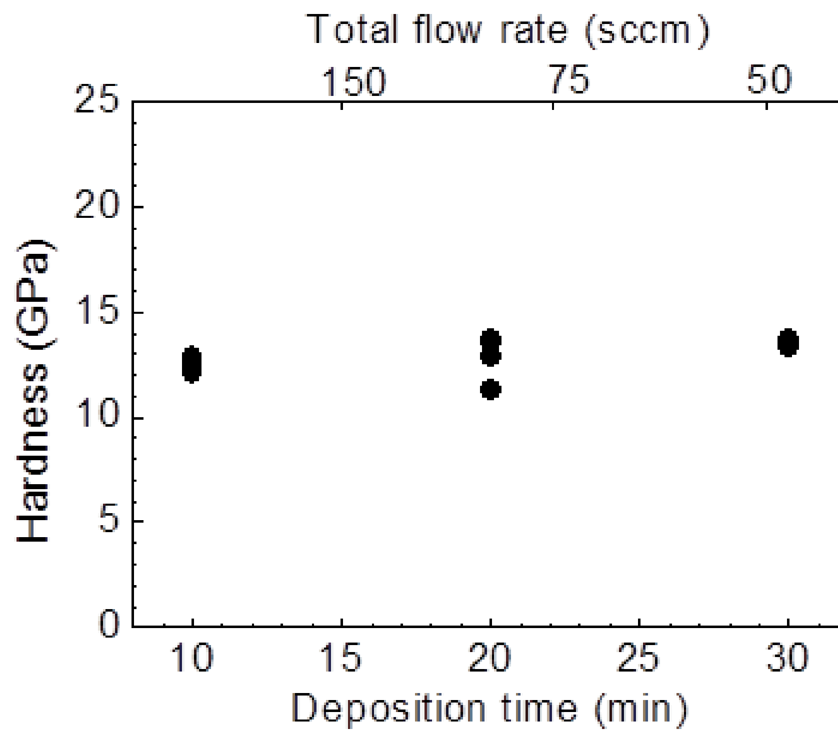

Fig.3.6. Hardness of the a-C film under different deposition time.

P.Koidle and C.Wagner. et.al reported a series of data about the hardness of a-C:H deposited by PECVD from methane and benzene.[42] In their case, the hardness is very low at lower bias voltage, indicating a polymeric a-C:H films. Then the hardness increased with increasing bias voltage, which is consistent with the reported revolution of sp3-C fraction under different bias voltage. [41]

Empirically the nano-hardness derived from nano-indenter is about three times lower than that from conventional micro-indenter. The maximum nano-hardness of a-C:H in literature [7] is about 17 GPa. which is very high in the case of a-C:H deposited by PECVD.

To compare our the hardness of our samples with that of literature, we found that the resulting a-C:H films possess a relative high degree of hardness, even higher than that in literature. This is very bare in the case of PECVD deposited a-C:H films. Besides, from the variation of hardness with the change of total flow rate, in another word, the residence time, it is speculated that sp^3-C fraction increased with decreasing residence time. It also provides a possible approach for well control of hardness and even the sp^3-C fraction in the film, which is extremely important for better application of amorphous carbon materials.

Therefore, as mentioned in the introduction, relative high degree of hardness would allow the resulting a-C:H films to be applied as protective coatings for the application in many area, such as optical windows, car parts, and so forth.

3.6 Summary

Amorphous carbon (a-C) films were deposited by radical-injection plasma-enhanced chemical vapor deposition (RI-PECVD) using a CH_4/H_2 gas mixture, and the deposition characteristics were investigated under different total flow rate. With increasing total gas flow rates, equivalent to a reduction in the residence time of radicals in the reaction chamber, the deposition rate reached its maximum value at a residence time of 6 ms. In addition, the optical emission spectral data also displayed a change in the relative intensity of the CH emission with variations in residence time. These two results indicate a transition in the dominant radical species with changing residence time. On the other hand, the nano-indenter measurement shows that the resulting a-C:H films possess a relative high degree of hardness. And it increased with the decreasing residence time, with a maximum about 18 GPa.

Generally the results in this chapter provide a description of the plasma condition and basic image of the film property. It acts as a fundament for the analysis of the effect from radical species variation in the rest chapters.

References

[1] L. P. Andersson, S. Berg, H. Norstrom, R.Olaison, S. Towta: Thin Solid Films., **63**(1979) 155.

[2] Y.Catherine, P. Couderc: Thin Solid Films. **144**(1986)265.

[3] K. Kobayashi, N. Mutsukura, and Y. Machi: Thin Solid Films. **158** (1988) 233.

[4] M. Alaluf, J. Appelbaum, L. Klibanov, D. Brinker, D. Scheiman, and N. Croitoru: Thin Solid Films. 256(1995) 1.

[5] M. Alaluf, J. Appelbaum, M. Maharizi, A. Seidman, and N. Croitoru: Thin Solid Films., **303**(1997) 273.

[6] J. Robertson: Prog. Solid State Chem., **21**(1991) 199.

[7] P. Koidl, C. Wagner, B. Dischler, J. Wagner, and M. Ramsteiner: Mater. Sci. Forum. **52**(1990)41.

[8] D.R. McKenzie,Rep: Prog. Phys., 59(1996) 1611.

[9] Y. Lifshitz: Diamond Rel. Mater., **8**(1999) 1659.

[10] H. Zhu, J. Wei, K. Wang, D. Wuet: Solar Energy Materials & Solar Cells. **93**(2000) 1461.

[11] K. M. Krishna, M.Umeno, Y.Nukaya, T.Soga, T.Jimbo: Appl. Phys. Lett., **77**(2000)1472.

[12] W. Jacob and W. Moller: Appl. Phys. Lett., **63**(1993) 1771.

[13] C. Weissmantel: Thin Solid Films., **92**(1982) 55.

[14] Y. Lifshitz, S.R. Kasi, J.W. Rabalais, W. Eckstein: Phys. Rev. B., **41**(1990) 10468.

[15] E.G. Spencer, P.H. Schmidt, D.C. Joy, F.J. Sansalone: Appl. Phys. Lett. 29(1976)118.

[16] W. Moller: Appl. Phys. Lett., **59**(1991) 2391.

[17] N.Mutsukura, S. Inoue, Y.Machi: J. Appl. Phys., **72**(1992) 43.
[18] P. J. M. van der Burgt, J. W. McConkey: J. Phys. B: At .Mol .Opt .Phys, , **24**(1991) 4821.
[19] Y. Murakami, S. Horiguchi, S. Hamaguchi: Phys. Rev. E, **81** (2010) 041602-1.
[20] A.A. Voevodin, J.G. Jones, J.S. Zabinsk: J. Appl. Phys., **92**(2002) 724.
[21] J.W. Zou, K. Schmidt, K. Reichelt, D. Dischler: J. Appl. Phys., 67(1989) 487.
[22] M.A. Tamor, W.C. Vassell, K.R. Carduner: Appl. Phys. Lett. **58**(1991) 592.
[23] J. Ristein, R.T. Stief, L. Ley, W. Beyer: J. Appl. Phys. **84**(1998) 3836.
[24] J. Robertson: Philos. Mag. B., **76**(1997) 335.
[25] C.W. Chen, J. Robertson: J. Non Cryst. Solids. **227/228** (1998) 602.
[26] J. Robertson: Pure. Appl. Chem. **66**(1994)1789.
[27] N.M.J. Conway, A.C. Ferrari, A.J. Flewitt, J. Robertson, W.I. Milne, A. Tagliaferro, W. Beyer: Diamond Rel. Mater. **9**(2000) 765.
[28] R.H. Jarman, G.J. Ray, R.W. Stadley: Appl. Phys. Lett. **49**(1986)1065.
[29] M.A. Tamor, W.C. Vassell, K.R. Carduner: Appl. Phys. Lett., **58**(1991) 592.
[30] M.A. Tamor, W.C. Vassel: J. Appl. Phys, **76**(1994) 3823.
[31] M. Weiler, S. Sattel, T. Giessen, K. Jung, H. Ehrhardt, V.S. Veerasamy, J. Robertson: Phys. Rev. B, **53** (1996) 1594.
[32] Yasuo Murakami, Seishi Horiguchi, Satoshi Hamaguchi: Phys. Rev. E . **81** (2010), 041602-1.
[33] A.A. Voevodin, J.G. Jones, J.S. Zabinski: J. Appl. Phys. **92**(2002)724.
[34] T. Roschek, B. Rech, J. Muller, R. Schmitz, H. Wagner: Thin Solid Films., **451-452**(2004) 466.
[35] J.W. Coburn, M.J.Chen: J. Appl. Phys, **51**(1980)3134–6.

[36]F. Liu, G. Huang, B. Ganguly: Plasma Sources Sci.Technol., **19**(2010)045017 (10pp).

[37]A. C. Ferrari, J. Robertson: Phys. Rev. B., **61**(2000) 14095.

[38]J.R. Doyle: J. Appl. Phys, **82**(1997) 4763.

[39]C. Gómez-Aleixandre, O. Sánchez, J. M. Albella: J. Vac. Sci. Technol, **A11**(1993) 143.

[40]A.Pastol, Y. Catherine: J. Phys. D., **23**(1990) 799.

[41]J. Ristein, R.T. Stief, L. Ley, and W. Beyer: J. Appl. Phys. **84**(1998)3836.

Chapter 4

Effect of radical species on film properties

4.1 Introduction

In the present study, we studied the effects of the variation of the total gas flow rate from 50 to 400 sccm, and the associated changes in the residence times of radical species and molecules, on the optical bandgap, conductivity, crystallographic, H content of the resulting a-C films were investigated.

Following the deposition, the film thicknesses were measured using a stylus profiler. and the crystalline structures were analyzed by Raman spectroscopy. The hydrogen (H) content was evaluated based on Fourier transform infrared (FT-IR) spectra. Besides, the film optical properties were determined by a spectrophotometer, in the ultraviolet – infrared spectral region (200-2500 nm). Then, an optical band gap value, so-called "Tauc gap", was determined using a Tauc plot. And for a better description of energy gap, E04 gap also was evaluated in this chapter.

4.2 Electronic structure and electrical properties

4.2.1 E_g and E_{04}

Tauc gap E_g of a-C:H under different residence time, was derived from the Tauc plot as shown in Figure 4.1. And the E_g values corresponding resulting a-C:H films under different residence time were also plotted in Figure. 4.2 as a function of residence time. Optical energy (E_{04}) values, defined as the energy at which the optical absorption coefficient is 10^{-4} cm-1, are also indicated in the figure.

Both E_g and E_{04} values are the common methods for analysis of energy band gap of some amorphous materials. The slopes in the Tauc plots of a-C films often are not as obvious as those of typical semiconducting materials, such as amorphous silicon, in the absorption region. Therefore, extrapolated values could have a margin of error. Therefore, the E_{04} values are supplementarily used for qualitative discussion. As shown in Figure 4.2, the E_g values evidently increase with decreasing residence time, such that the maximum E_g value around 0.9 eV is obtained at a residence time of 2 ms (400 sccm). It was also found that the E_{04} values also increased with decreasing the residence time.

Thus it is evident that variation in residence time is an efficient method to modify the electronic structure of a-C:H films.

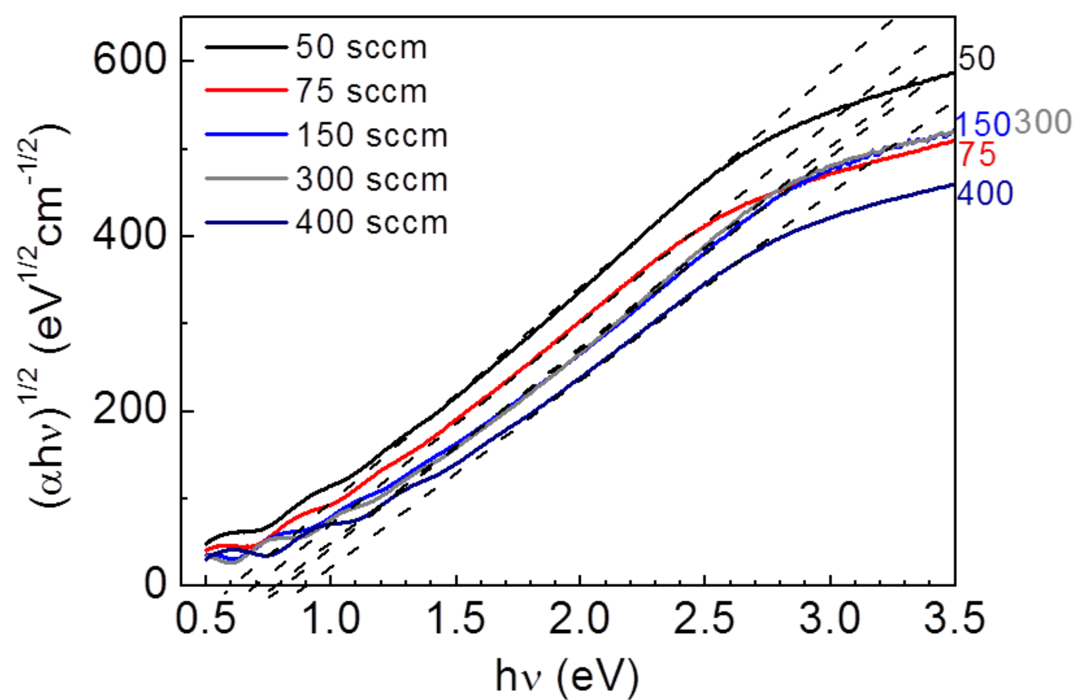

Fig.4.1 Tauc plot of a-C:H under different residence time.

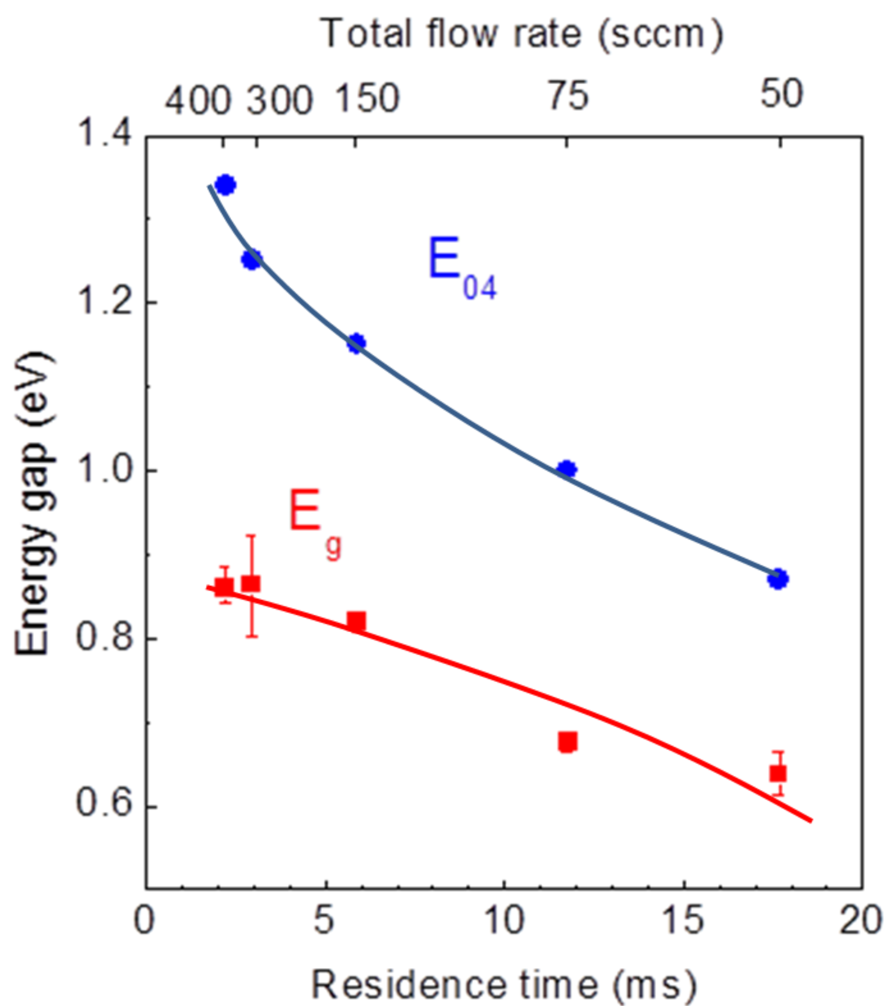

Fig. 4.2. Energy gap as a function of residence time.

4.2.2 Conductivity

Figure.4.3 shows the conductivity of the a-C films as a function of residence time. It can be seen that with the decrease in residence time, conductivity also decreased a lot. And the conductivity of resulting a-C:H film in this research shows that these deposited films have a good insulation.

Figure 4.4 shows the approach that we used for measuring the conductivity. Generally this method cannot provide a precise value of conductivity. Because by this method, the resistant between the interface of a-C:H films and substrate are also accounted.

However, the obvious variation in conductivity shown in Figure 4.3 can be used as a qualitative analysis of the conductivity with residence time.

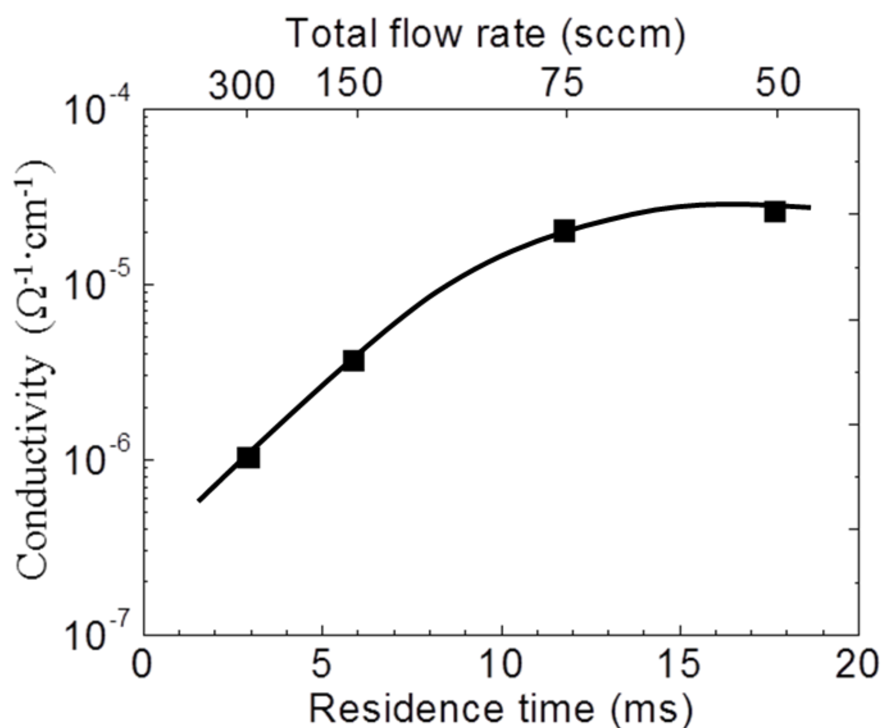

Fig. 4.3.Conductivity of a-C:H films as a function of residence time.

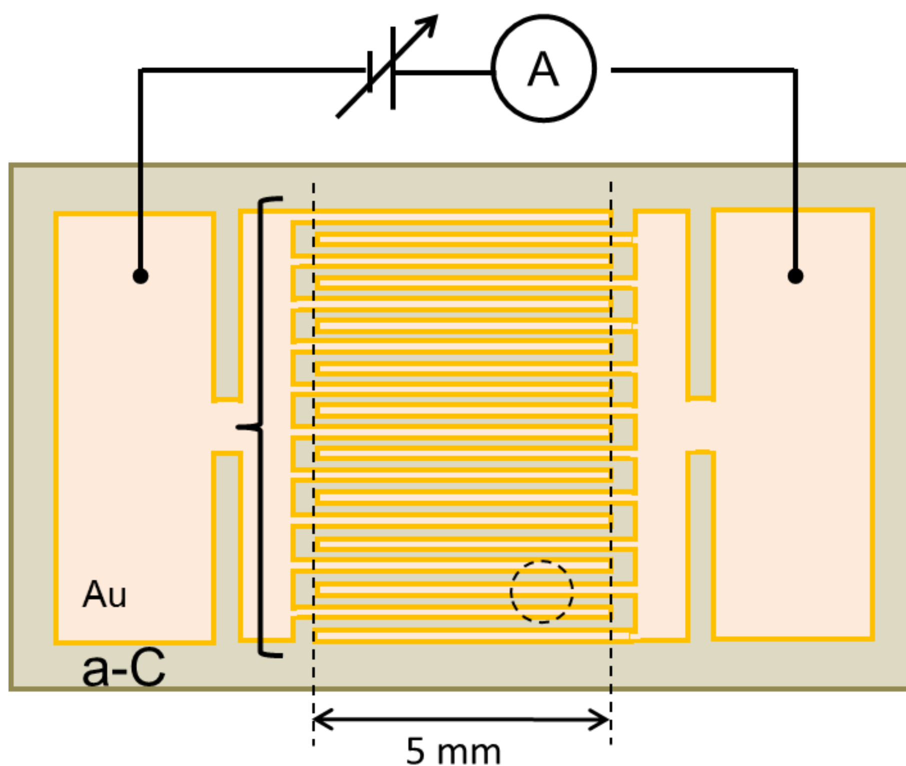

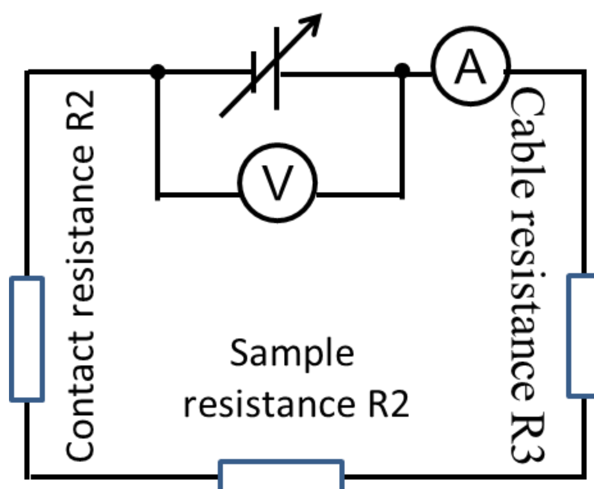

Fig. 4.4.Schematic and ba sic mechanism of the measurement of conductivity of a-C:H films in this research.

4.2.3 Correlation between radical species and optical bandgap

From Figure.3.3 and Figure.4.2, it can be seen that both radical species and optical bandgap varied with the decrease in residence time. So the author tried to find whether there is some relation between them.

And from Figure.4.5, it can be seen an almost linear increase in both E_{04} and E_g with the increase in the radical ratio of CH/H. So weaker decomposition of CH_4 gas, may encourage a wider energy gap. Because when decomposition of CH_4 gas gets weaker, CH_n radicals will increase.

But when the ratio is larger than 0.3, the linear relation between them vanished, which is very obvious in the case of E_g.

On the other hand, both E_{04} and E_g also increased with increasing radical ratio of C_2/H, and this trend does not change even at higher ratio of C_2/H. It indicates that the effect of C_2 in encouraging the formation of sp^2-C, maybe not the dominant mechanism with the change of residence time.

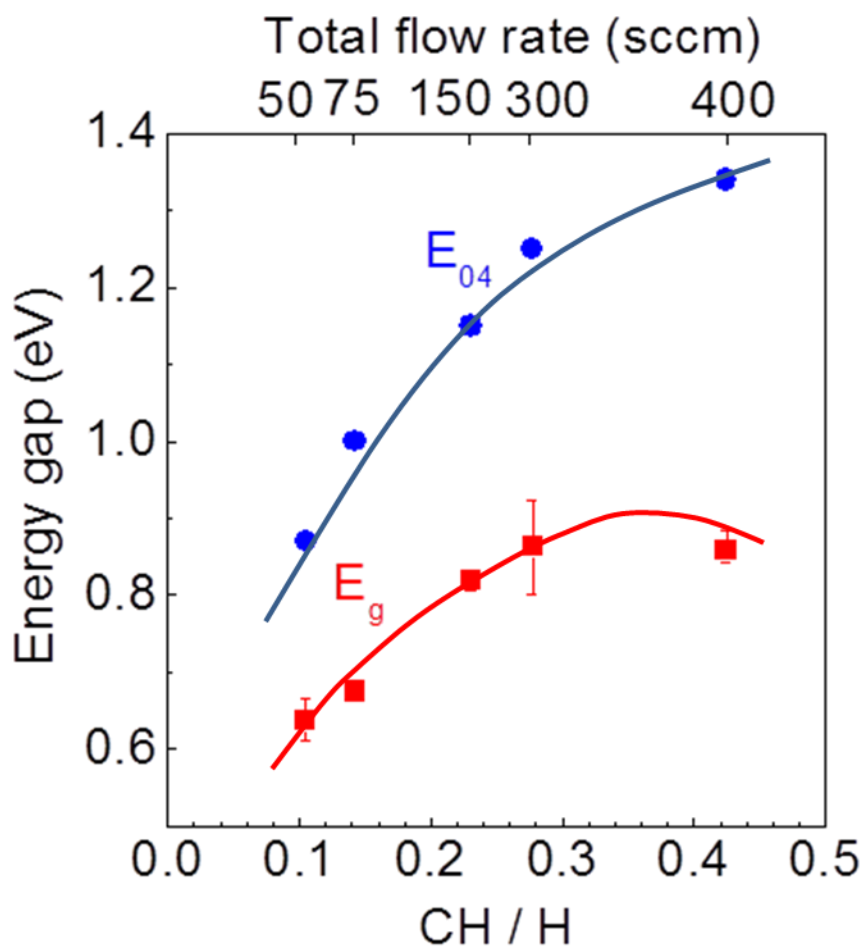

Fig. 4.5.Correlation between energy gap and the radical ratio of CH/H.

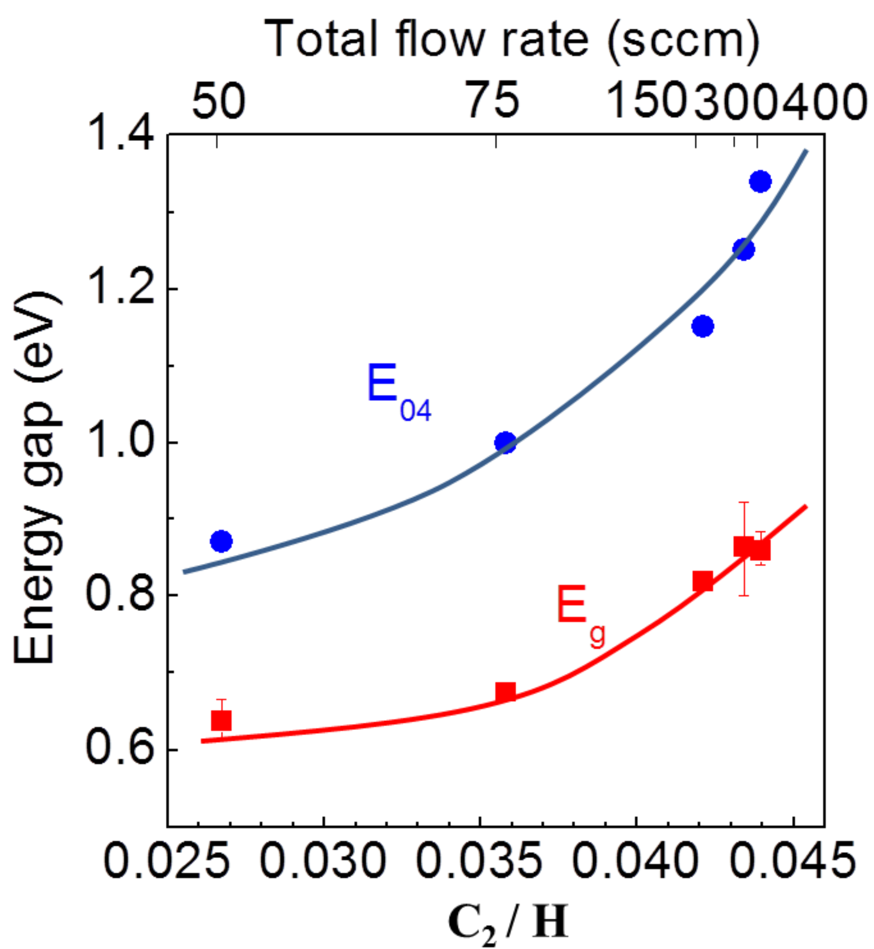

Fig. 4.6. Correlation between energy gap and the radical ratio of C_2/H.

4.3 H concentration

4.3.1 Qualitative analysis of H content by FT-IR

In Chapter 3, it is confirmed that with the change of residence time, equivalent to a reduction in the residence time of radicals in the reaction chamber, the deposition rate reached its maximum value at a residence time of 6 ms. In addition, the optical emission spectral data also displayed a change in the relative intensity of the CH emission with variations in residence time. These two results indicate a transition in the dominant radical species with changing residence time. On the other hand, the Tauc gap E_g and optical gap E_{04} value increased as the residence time increased. These results demonstrate that the electronic structure of a-C can be controlled via the optimization of radical species and their densities throughout the deposition process.

But there still remain a problem that the change in the radical species only can be an inducement rather than the essential reason responsible for the variation in the electronic structure. It is generally accepted that H atoms play an important role in determining the physical and electrical properties of a-C.[1] So in these section we have confirmed the variation in the H content with decreasing the residence time. In addition, we also have checked whether the change in electronic structure are related with the crystallographic properties of resulting a-C:H film.

It is generally accepted that H atoms play an important role in determining the physical and electrical properties of a-C.[1] FT-IR spectra of the a-C films are presented in Figure 4.7a), in which the intensities of all of the spectra have been normalized to the film thickness. In each of these spectra, both the sp2 and sp3 C-H stretching mode peaks are found in the regions of 3085-2955 cm^{-1} and 2950-2855 cm^{-1}, respectively. However,

the intensities of the sp^3C-H stretching mode peaks are obviously greater than those of the sp^2 peaks, demonstrating that the H atoms preferentially terminated sp^2-C dangling bonds. Figure 4.7(b) shows the area values of sp^2 and sp^3 C-H stretching mode peaks as functions of residence time. Here it can be seen that both intensities changed very little with the variations in residence time, hence there was almost no change in H content.

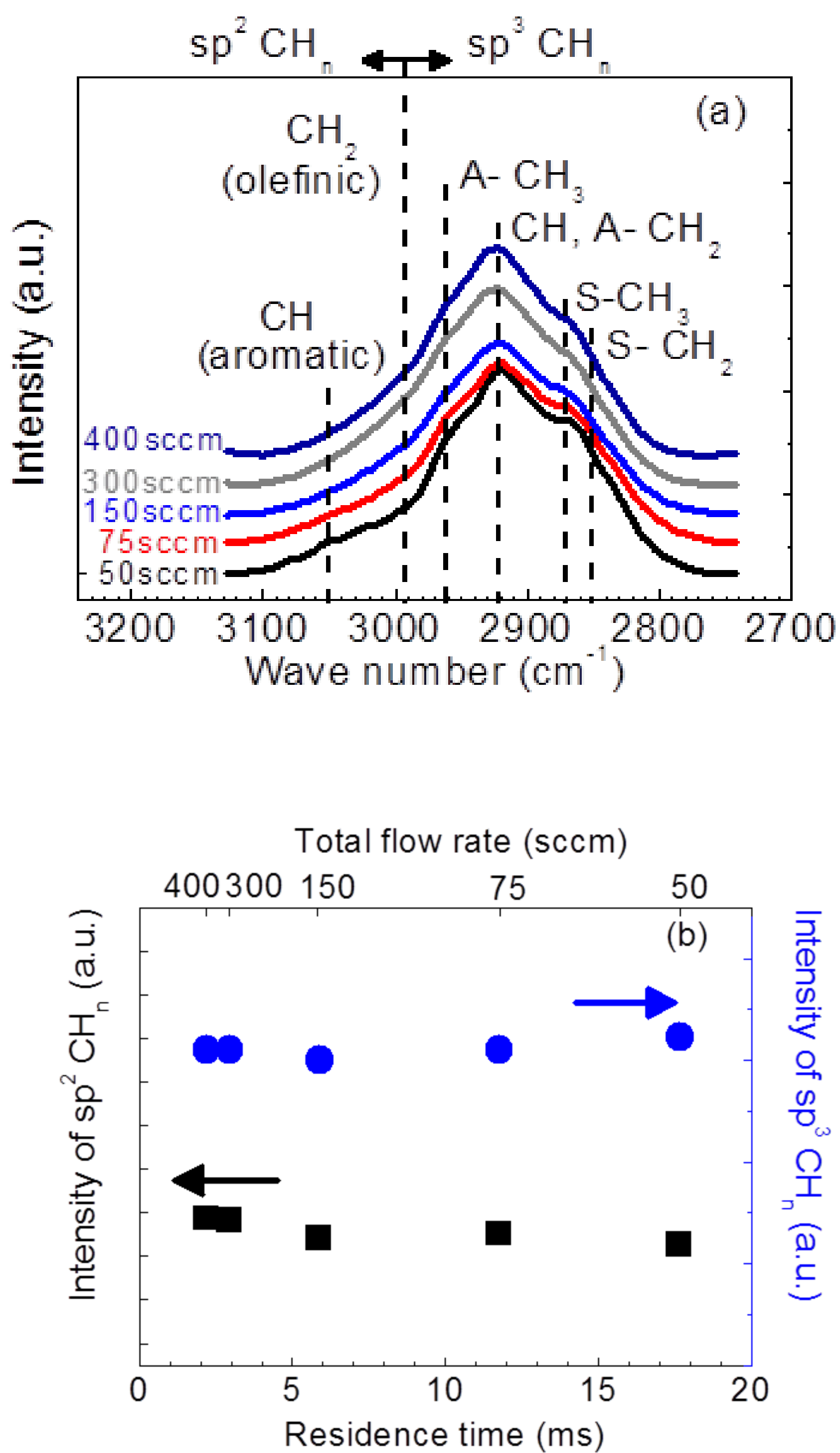

Figure 4.7(a) FT-IR spectra of a-C films deposited at total flow rates from 50 to 400 sccm, and (b) the intensities of sp3- CH_n and sp^3- CH_n peaks as functions of residence time.

4.3.2 Quantitative analysis of H concentration by SIMS

Figure 4.8 provides the H concentration in the deposited films derived from the SIMS analysis as a function of residence time. It was quantified by using a diamond film as a reference. This result shows that relatively high H concentration of approximately 10^{22} atoms/cm3 existed in the films deposited using RI-PECVD employing CH_4/ H_2 mixtures. The H concentration of the films hardly changed in the case of deposition under the different gas flow rates in spite of the variation of composition of dominant species, suggesting that the H concentration of the film was not determined solely by the radicals produced in the plasma. Since there are many other factors, such as growth temperature and, ion energy and flux, which would affect film properties, the H concentration of the film was determined as a result of their synergetic effects.

Figure 4.9 shows the H concentration along the depth direction.. And we can see that no matter with different residence time, it hardly change at different depth. That indicates that hydrogen is even-distributed with the film.

Figure 4.10 shows the secondary ion concentration of C and H atoms. And we can find that the concentration of C is about 10 times more than that of H. That indicates a relatively low H fraction with the resulting a-C:H films in this research.

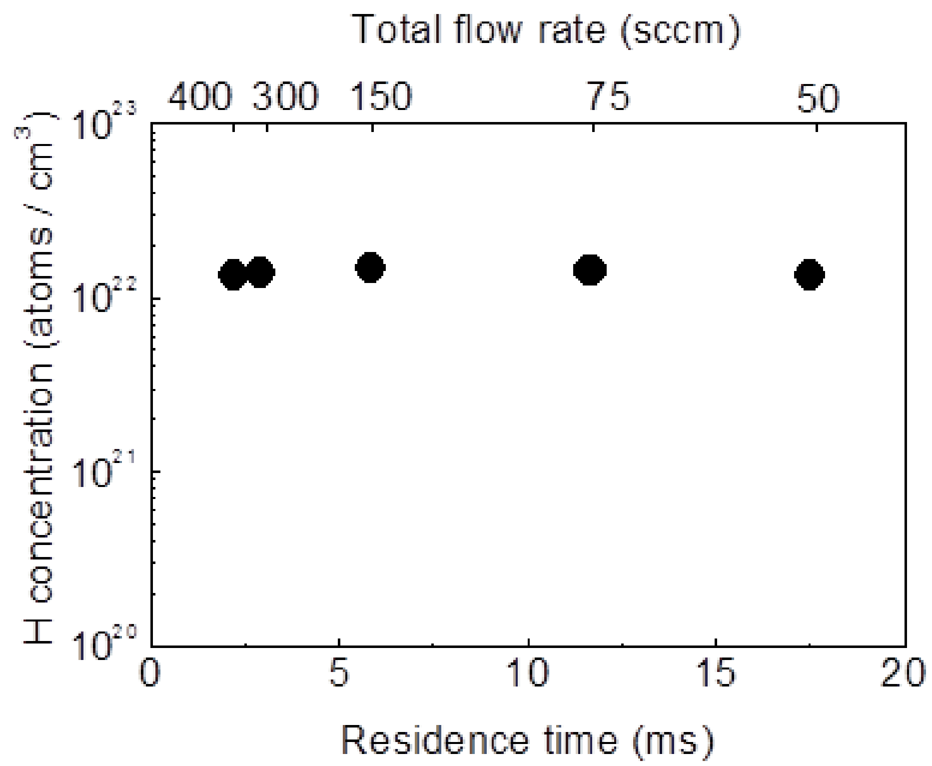

Fig.4.8. H concentration derived from the SIMS analysis as a function of residence time.

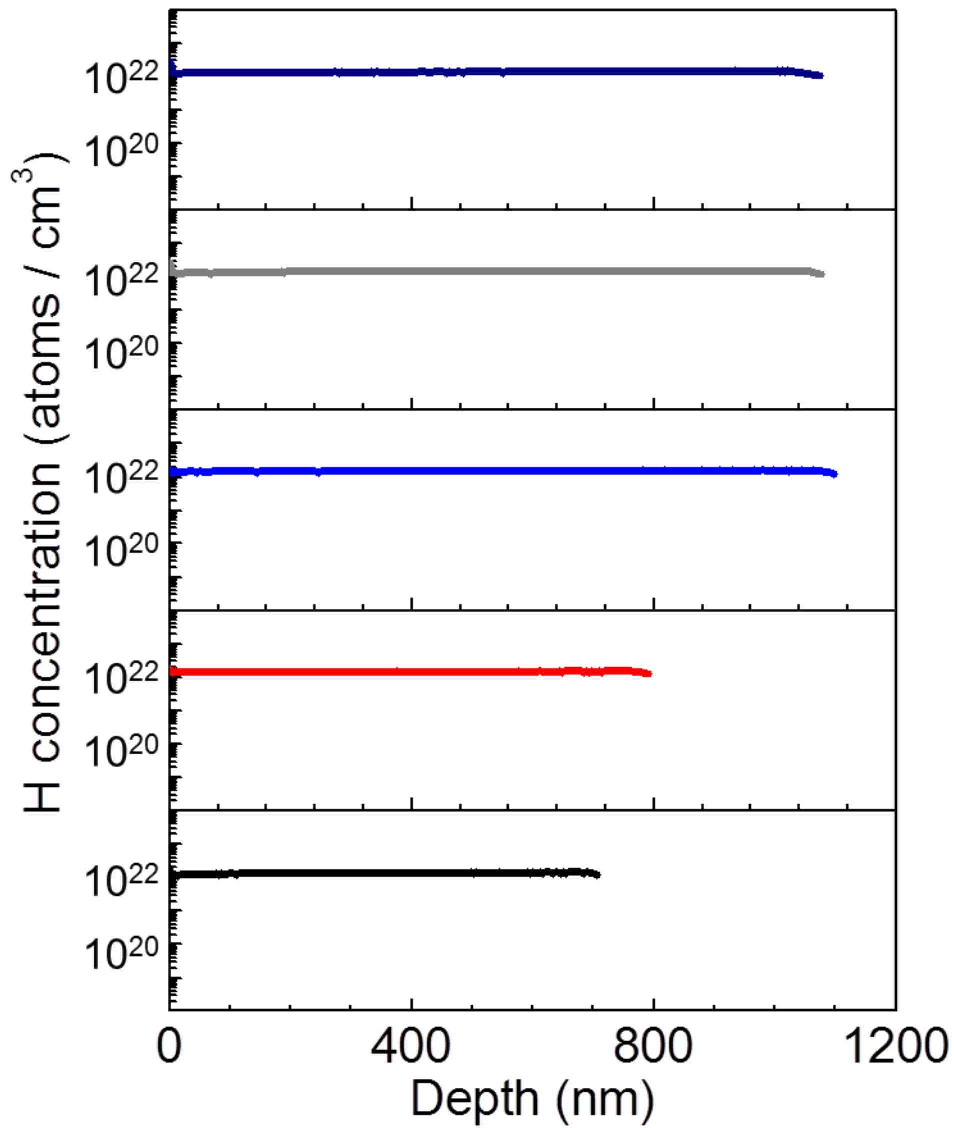

Fig.4.9. H concentration derived from the SIMS analysis as a function of depth of films deposited at different residence time.

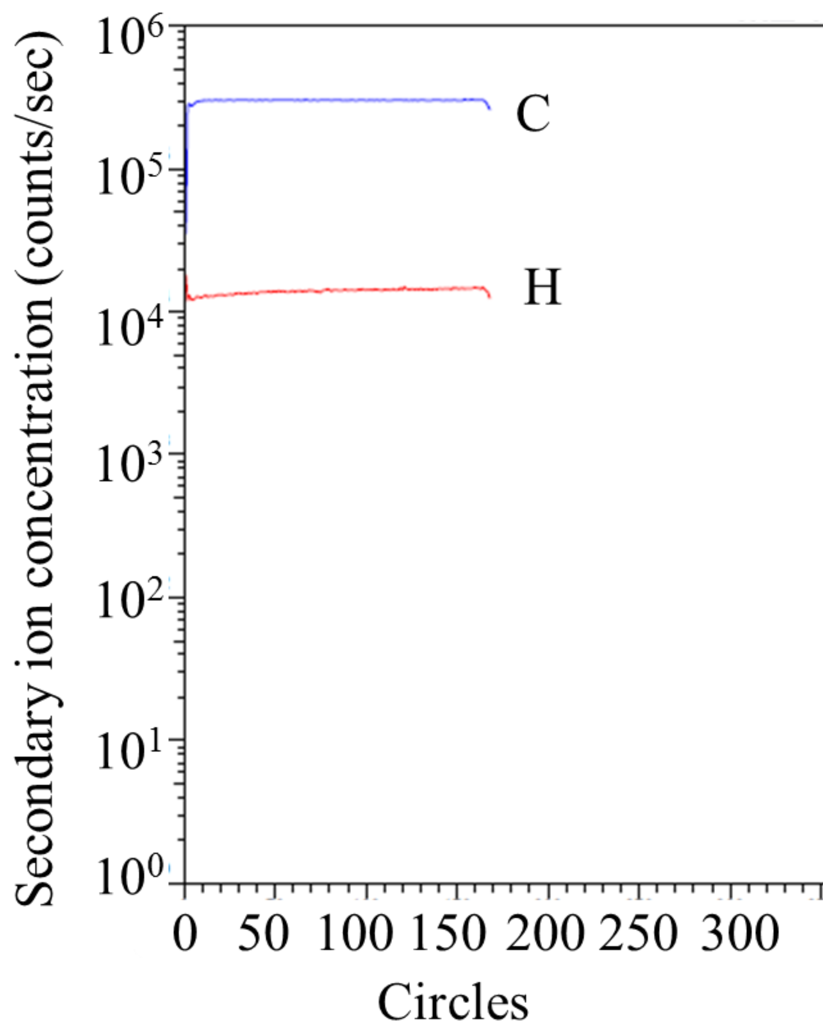

Fig.4.10. Secondary ion concentration of C and H atoms in resulting a-C:H films deposited at 50 sccm.

4.3.3 Correlation between variation in H concentration and optical bandgap

According to both the H content data derived from FT-IR, and the H concentration data derived from SIMS, we can get a conclusion that H content did not change a lot with decrease in residence time. So It also means increase in bandgap at shorter residence time have no relation with variation of H content with the film. In another word, it is some other factor that affected the bandgap.

4.4 Crystallographic properties

4.4.1 Raman scattering

Figure. 4.11 (a) shows the Raman spectra of a-C films deposited under different residence times (flow rates), with a deposition time of 20 min. In all of the spectra, G and D band peaks are clearly seen at approximately 1350 and 1580 cm^{-1}, respectively.

It is well known that the G band peak is attributed to the in-plane bond stretching motion of sp^3-C atom pairs. It should be noted that this mode is found in both six-membered aromatic rings and olefinic chains. In contrast, the D band peak originates from imperfections or disordered structures in six-membered carbon rings. Since this peak corresponds to a breathing mode of aromatic rings, its intensity is strictly related to the presence of six-membered rings. Therefore, a decrease in the I_D / I_G ratio is generally associated with the amorphization of a-C and DLC films.[2] The slope of the photoluminescence (PL) background superimposed on the spectrum slightly increased with increasing total flow rate (or decreasing residence time), suggesting a slight increase in the polymeric components in the a-C film and thus a marginal elevation in the H content.

It should be noted that, since 532 nm visible light was used for the Raman spectroscopy in this study, the sp^2 components would have been 50 to 230 times more sensitive than the sp^3 units,[3-4] and π states would have been preferentially excited. Therefore, as described below, sp^3 components were also present in the a-C films deposited in this experiment.

The intensity ratios of the D and G band peaks (I_D /I_G), the full-width-at-half-maximum (FWHM) values of these peaks and their positions are all summarized in Figure.4.11(b), (c), and (d), respectively. The intensity and FWHM values were obtained by fitting the data with Gaussian shaped peaks.[2] It is evident that the I_D/ I_G ratio decreased with decreasing residence time while, at the same time, the FWHM of the G band increased and that of the D band hardly changed. The decrease in the I_D/I_G ratios and increase in the G band peak width are associated with a decrease in the amount of six-membered carbon rings and the development of amorphization in the a-C films with decreasing residence time. The shifts in the G and D band peak positions also indicate the development of amorphization associated with reduced residence times.

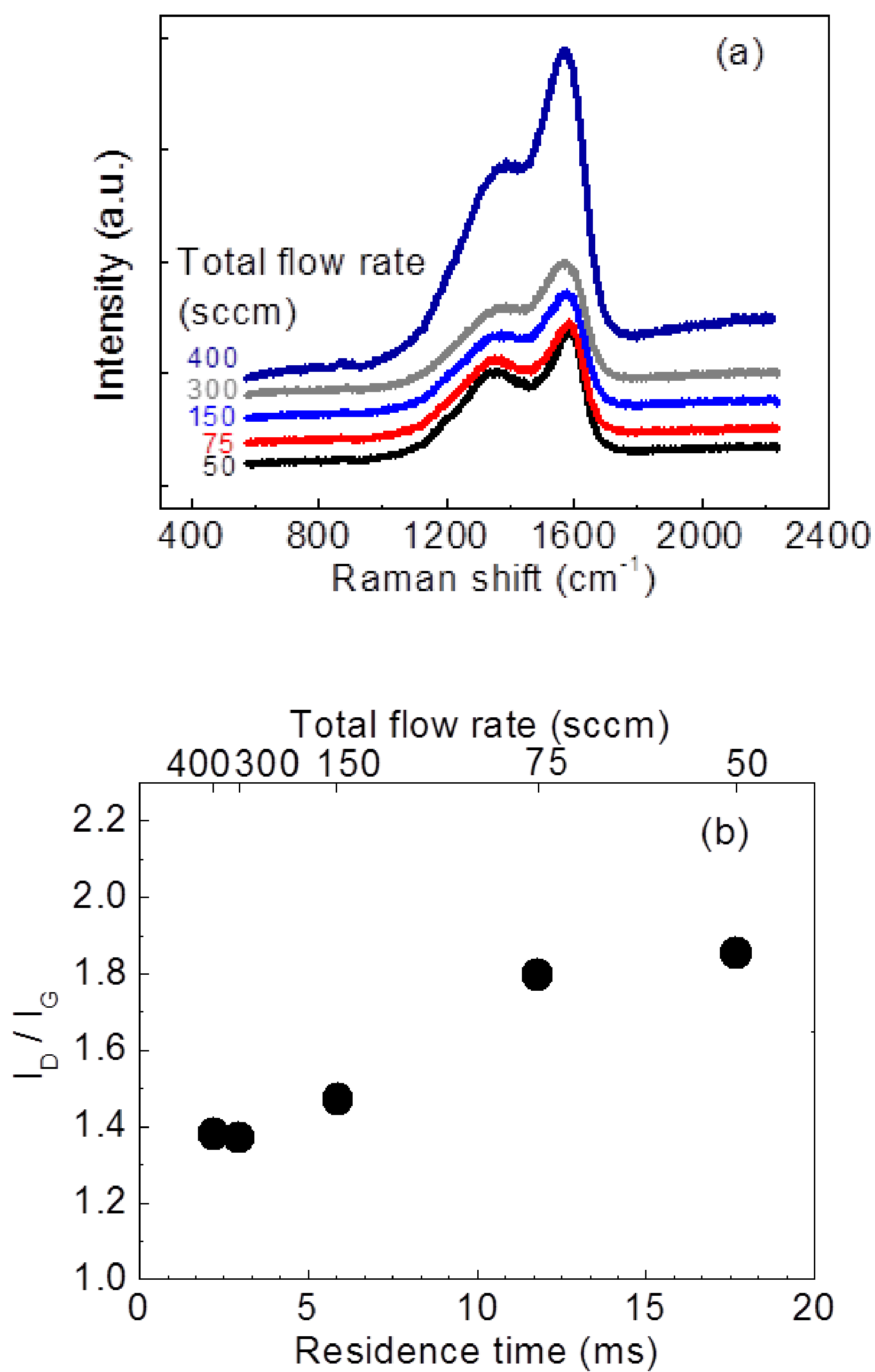

Fig. 4.11.(a) Raman spectra of a-C films deposited at total flow rates from 50 to 400 sccm, (b) D band to G band intensity ratios (I_D / I_G).

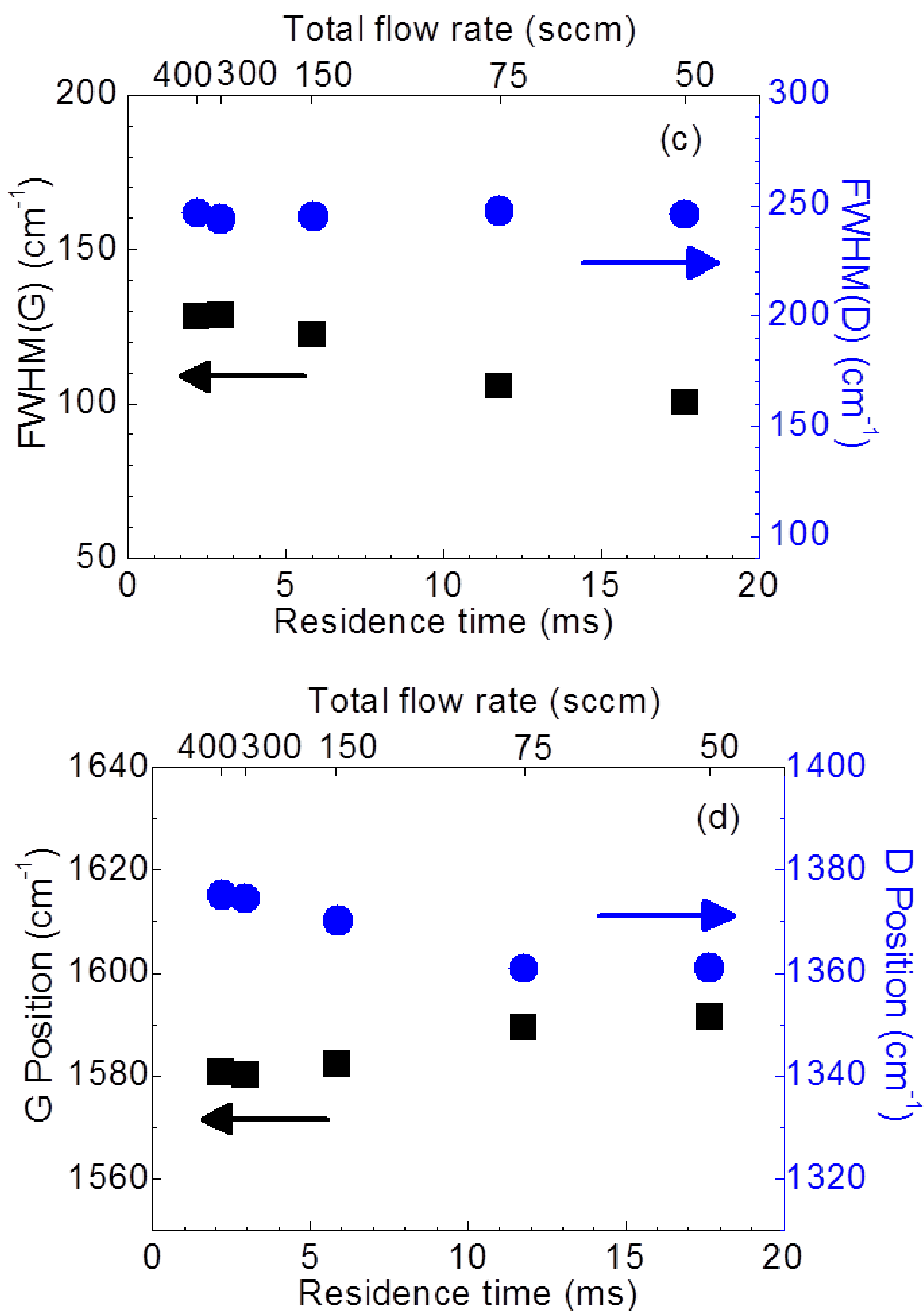

Fig. 4.11. (c) G and D band FWHM values, and (d) G and D band positions, all as functions of residence time.

4.4.2 Effect of crystallographic properties on optical bandgap

From Figure.4.12, it can be seen that with the increase in the optical bandgap, G band position shifts to lower position, and I_D/I_G will decrease.

As mentioned above, both the shift of G band to lower position, and decrease in I_D / I_G, indicates more disorder structure of graphite component within the film. To some extent, it also could be considered as an indication of decrease in the fraction of π bond with the film. Therefore, there would be a corresponding variation in the ratio of sp^2-C/sp^3-C.

In the literatures, [5-7] a lot of information about the correlation between the sp^2-C, sp^3-C fraction and the optical bandgap was reported. Generally optical bandgap shows an inversely proportional relation with the sp^2-C fraction.

Therefore, it is speculated that the increase of optical bandgap of resulting a-C:H samples maybe attributed to the decline of sp^2-C fraction caused by the disorder of graphite component with films.

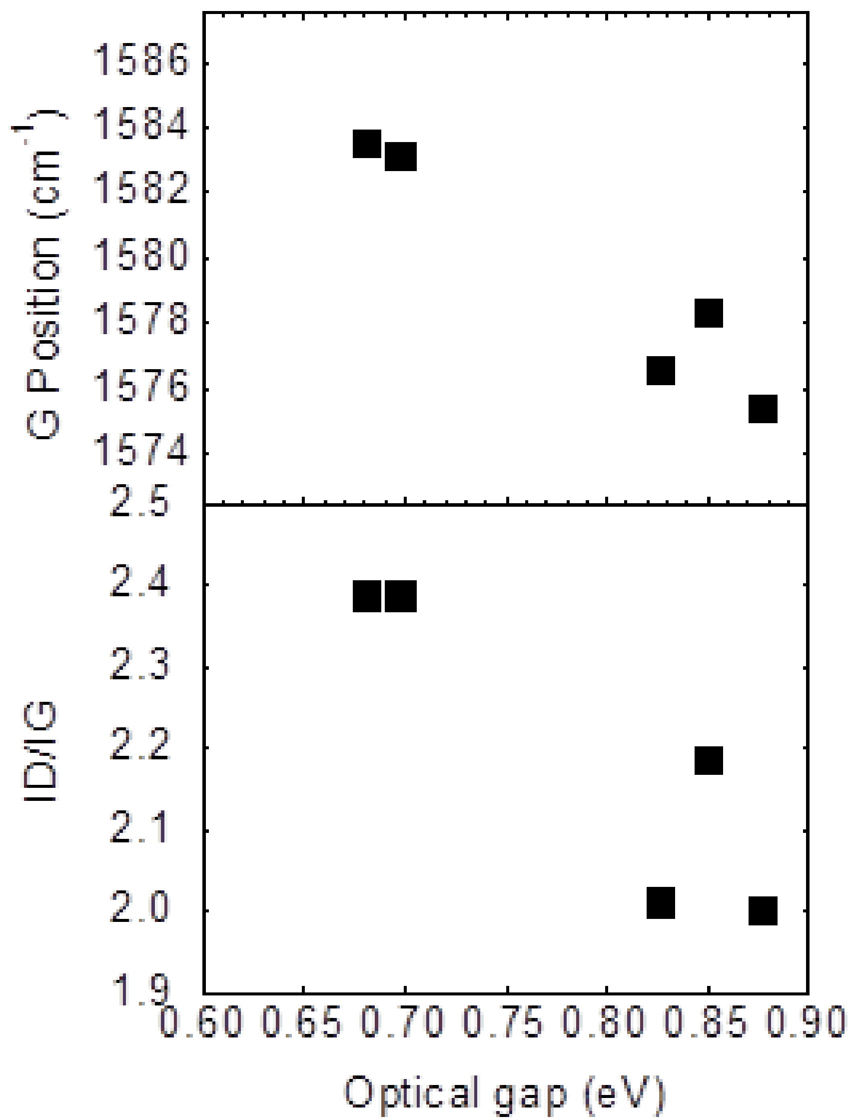

Figure 4.6 Correlation between optical gap and G band positions, I_D/I_G.

4.5 Summary

Amorphous carbon (a-C) films were deposited by radical-injection plasma-enhanced chemical vapor deposition (RI-PECVD) using a CH_4/ H_2 gas mixture, and the dependencies of the electrical properties and electronic structure on the residence time of various species were investigated by changing the total flow rate. With increasing total gas flow rates, equivalent to a reduction in the residence time of radicals in the reaction chamber, both the Tauc gap E_g and optical gap E_{04} value increased as the residence time increased. On the other hand, H content and crystallographic properties of resulting samples were also evaluated in this chapter. And the results turned out that there was only a slight change in H content. However, with the decrease in residence time, we found an obvious variation in crystalline structure of resulting samples. After combination of the variation in optical gap and G position and I_D / I_G, it is speculated that variation in crystalline structure maybe a factor resulting to the change in electronic and electrical properties.

References

[1] A.Pastol, Y. Catherine: J. Phys. D. **23**(1990) 799.

[2] A. C. Ferrari, J. Robertson: Phys. Rev. B., **61**(2000)14095.

[3] M. Rybachuk, J. M. Bell: Carbon., **47**(2009) 2481.

[4] D.L. Wood, J. Tauc: Phys. Rev. B. **5**(1972) 3144.

[5] P. Koidl, C. Wagner, B. Dischler, J. Wagner, and M. Ramsteiner: Mater. Sci. Forum. **52**(1990)41

[6] J.W. Zou, K. Schmidt, K. Reichelt, D. Dischler: J. Appl. Phys., 67(1989) 487.

[7] M.A. Tamor, W.C. Vassell, K.R. Carduner: Appl. Phys. Lett. **58**(1991) 592.

Chapter 5

Effect of radical species on bonding configuration

5.1 Introduction

From the content above, it can be concluded that with the change of residence time, equivalent to a reduction in the residence time of radicals in the reaction chamber, the deposition rate reached its maximum value at a residence time of 6 ms. In addition, the optical emission spectral data also displayed a change in the relative intensity of the CH emission with variations in residence time. These two results indicate a transition in the dominant radical species with changing residence time. On the other hand, the Tauc gap E_g and optical gap E_{04} value increased as the residence time increased. These results demonstrate that the electronic structure of a-C can be controlled via the optimization of radical species and their densities throughout the deposition process.

In Chapter 4, to figure out the essential reason responsible for the variation in the electronic structure, firstly the variation in the H content with decreasing the residence time has been confirmed. And both the data derived from FT-IR and SIMS showed that H concentration did not change a lot with the decreasing residence time. This results

indicate that H content is not the dominant reason caused the variation in the optical bandgap of resulting a-C:H films.

On the other hand, In the Raman spectra, the D band to G band intensity ratio decreased while the width of the G band peak increased as the residence time was reduced. These findings suggest a decrease in sp^2 components and the development of amorphization in the a-C films. So generally we also can concluded the correlation between change in crystalline structure and the optical bandgap of resulting a-C:H films.

So after confirming of the effect of structural properties on the optical bandgap, the next mission in this chapter 5 is that (1) quantifying the variation in the structure. (2) better insight of the variation of bonding configuration with the decreasing residence time.

5.2 Variation in sp^2-C fraction

5.2.1 Qualitative analysis of π bond fraction

Figure 5.1 shows the cross-sectional scanning transmission electron microscopy (STEM) image of a-C:H film deposited at the total gas flow rate of 150 sccm. The homogeneous film appeared on the quartz substrate without any local contrast indicating inclusions such as crystalline grains. It should be noted that the top layer was a thermally-evaporated carbon film used as a protective coating for the preparation of TEM specimen using a focused ion beam system.

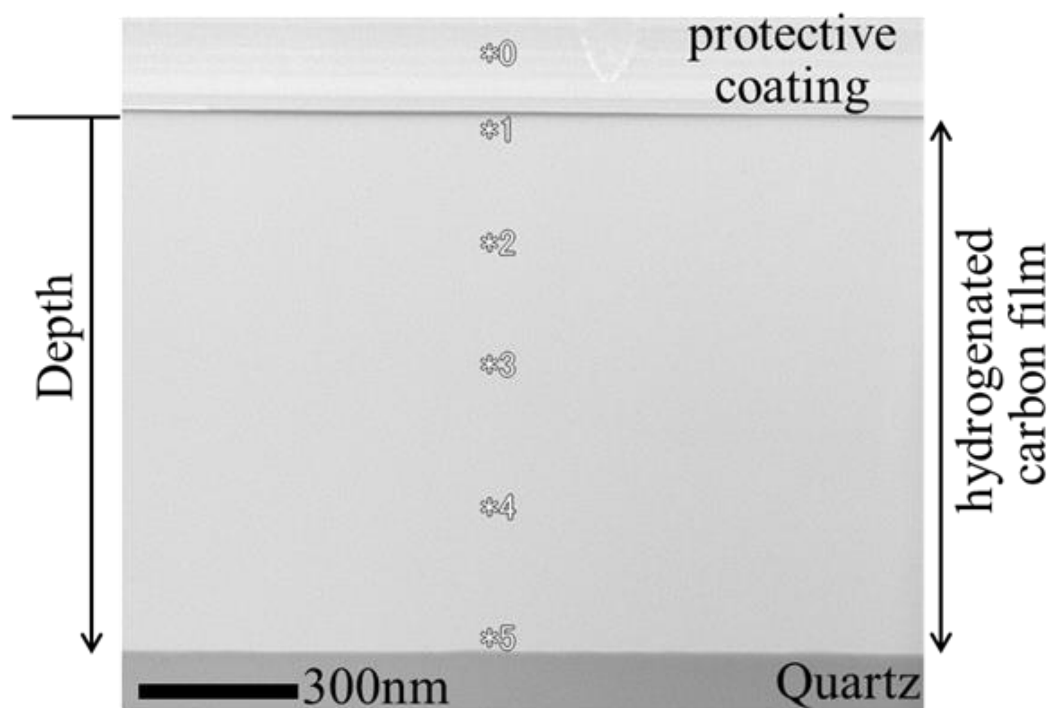

Fig.5.1. Cross-sectional TEM image of a-C:H film under a total flow rate of 150 sccm.

The EELS spectra of a-C:H films in the vicinity of K edge were measured at five different points marked as 1-5 along the depth orientation in Figure.5.1. Figure 5.2 shows the depth variations of π* fraction derived from EELS spectra of a-C:H films. It can be seen that long the depth direction, there is almost no change in the π* fraction. That indicates uniformity in bonding configuration along the depth direction.

By comparing this data with that in Figure 4.4, it can be concluded that both Hydrogen and π bond carbon atom are even-distributed within the resulting a-C:H film in these research.

Besides, since the optical gap data we derived from spectrophotometer are based on the transmittance of light, so the uniformity in H content and π bond will indicate that the E_g value we got represent a mean value not that from a localized structure..

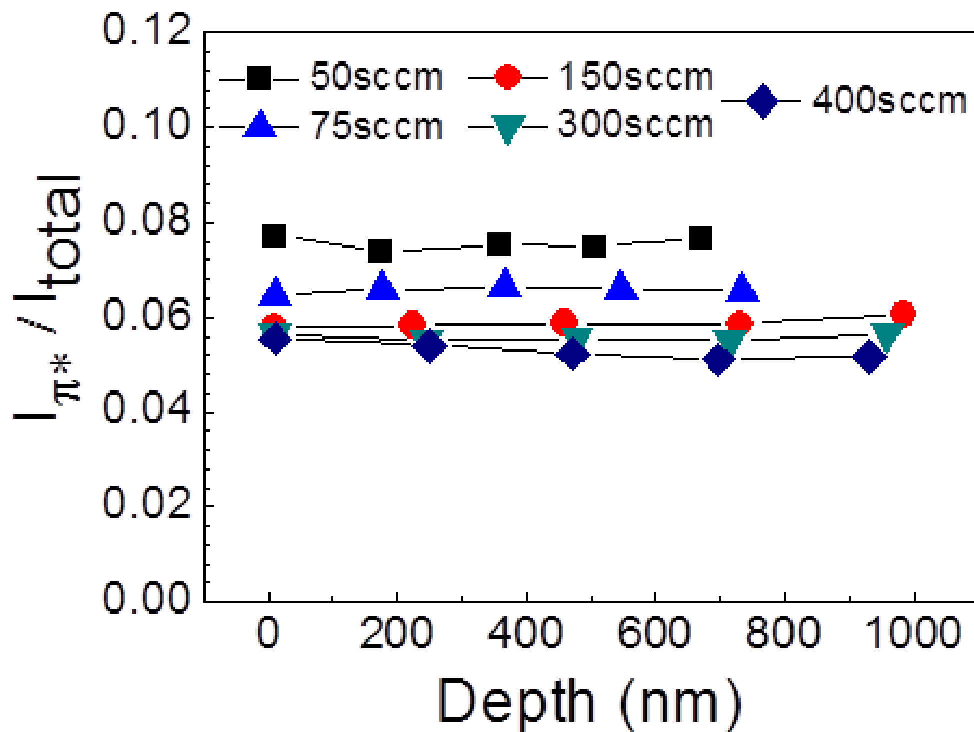

Fig.5.2. Depth variations of π^* fraction derived from EELS spectra derived at different depths corresponding to the points shown in the STEM image in Figure 5.1.

The EELS spectrum measured at the point 1 in the C:H film grown at 50 sccm is shown in the Figure.5.3. Two broad peaks were clearly observed at the position around 283 and 292 eV corresponding to 1s→π* and σ*, respectively.[1] They indicate the presence of unoccupied electron levels in the films. In this study, the deconvolution of the spectra was carried out by fitting several Gaussian peaks. It can be well fitted by introducing a peak located around 287 eV, which may originate from C-H* resonance.[2] Peak intensity ratios of π* spectra (I_{π^*}/I_{total}) were estimated ranging from 280-315 eV. As shown in Figure.5.2, π* fraction hardly changed with different depths.

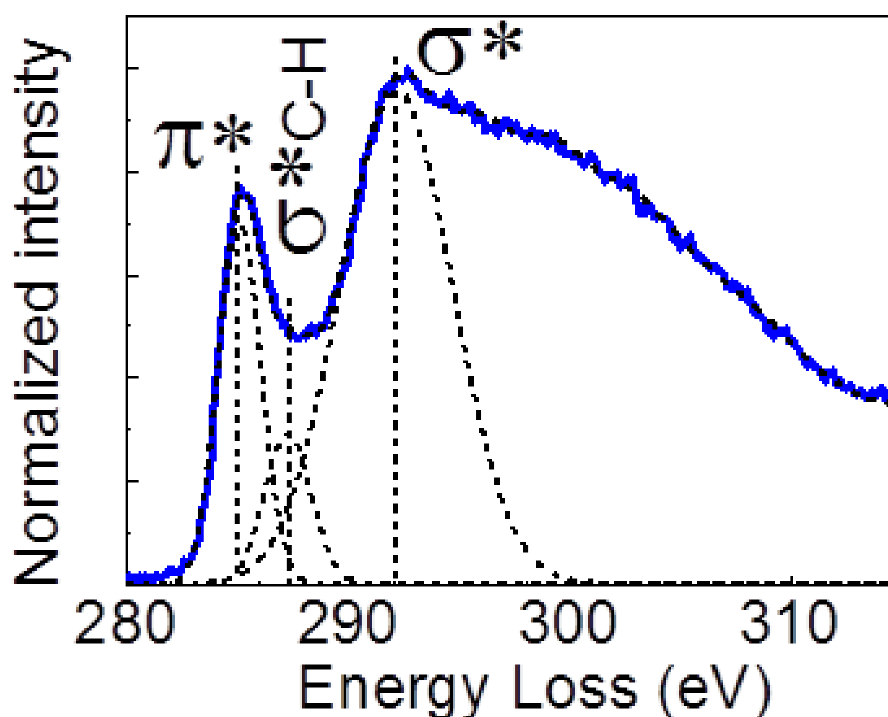

Fig.5.3. Peak fitting of the EELS spectrum measured at the point 1 of TEM image of the C:H film deposited at 50 sccm.

Figure 5.5 shows EELS spectra of resulting a-C:H films deposited at different total flow rate, in another word, residence time. Two broad peaks at the position around 283 and 292 eV, can be clearly observed no matter with the change of residence time. And we can find that with the increase of total flow rate, a shoulder-like area appeared, which is considered to be correlated with the σ*C-H.

After peak fitting of these spectra as shown in Figure.5.3, π* fractions as a function of residence time can be derived as shown in Figure.5.4. The π* fractions decreased with increasing the total gas flow rate. From these results, it is evident that variation in the radical species would affect the bonding configuration.

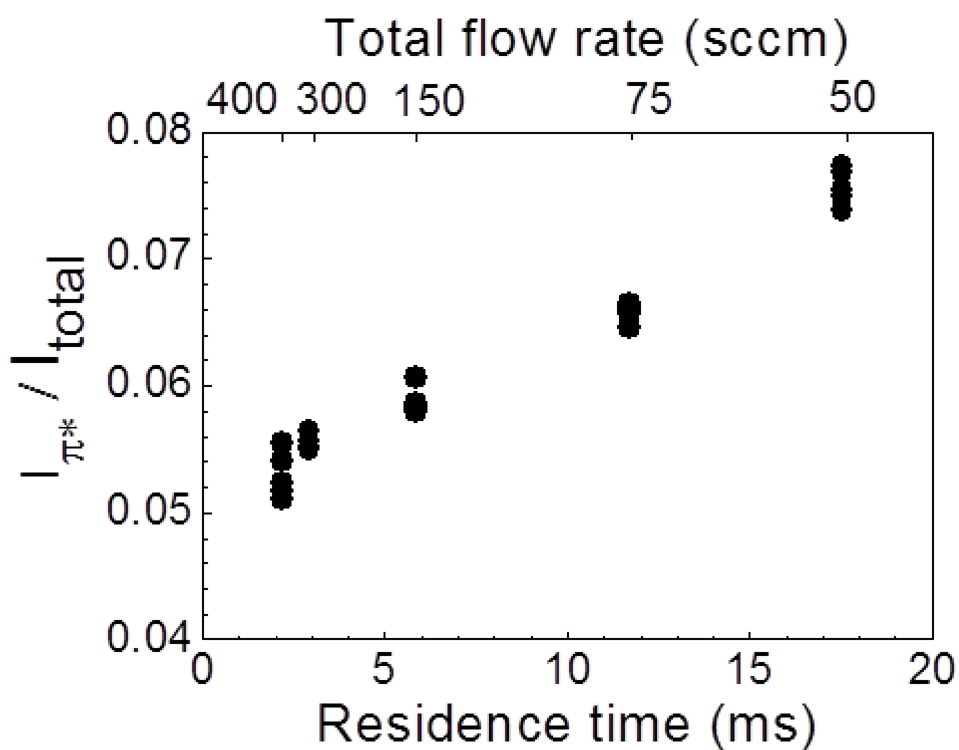

Fig.5.4 π* fractions as a function of residence time derived from the EELS analyses.

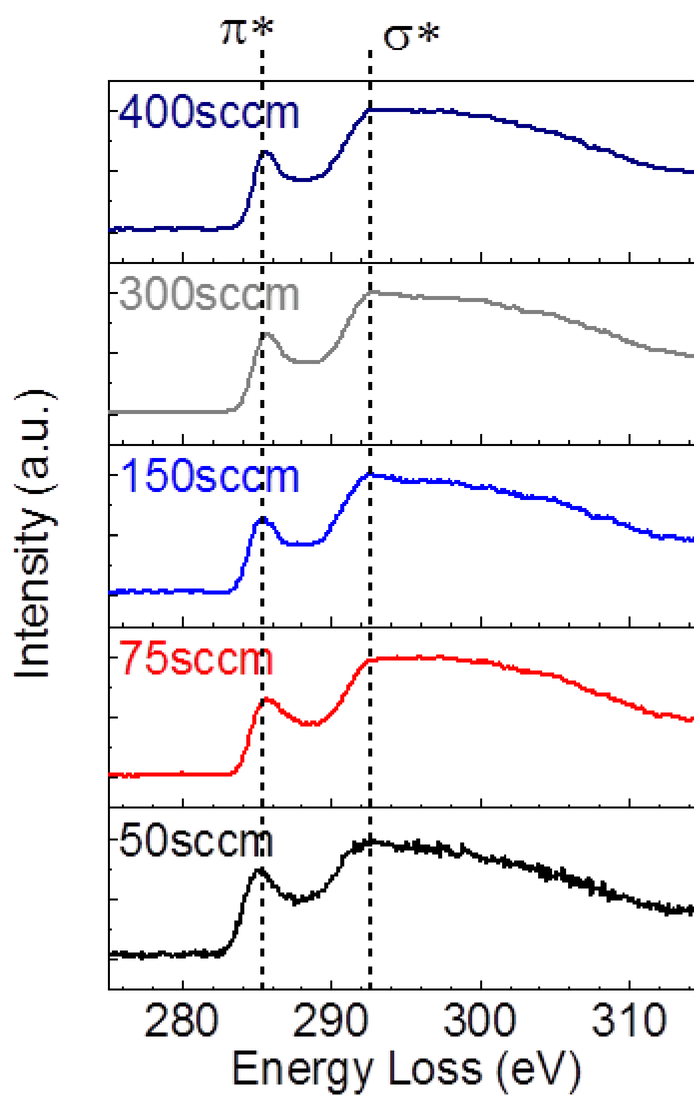

Fig.5.5 EELS spectra of resulting a-C:H films under different total flow rate.

5.2.2 Quantifying of sp^2-C fraction

Ion bombardments, called as sub-plantation model, have been proved to be effective in affecting the bonding configuration and thus the resulting properties of the carbon films.[3-5] It is not effective enough for modifying the bonding configuration solely by control of the ion bombardment energy. In the case of plasma-enhanced chemical vapor deposition (PECVD), not only the ion bombardment energy, but also the radical species act as an important factor. However, the radical species present in the plasma and their reactions are very complicated especially for the deposition process of carbon films. This is because the composition of the radical species is very sensitive to the plasma parameters, and they are source of the carbon film. In previous publications, the dissociation of source gas molecules and the generation of various types of C-containing radicals such as C_2, CHx and CFx in the plasma have been reported.[6-8] Gordillo-Vazquez et al. pointed out that atomic hydrogen was generated from the dissociation of H_2 and CH_4, by calculation of the model to estimate concentrations for H atom in a mixture of CH_4 and H_2 plasma.[9] Barni and Riccardi reviewed chemical kinetics of CH_4 plasmas and the dissociation kinetics of CH_4 plasmas included the dissociation products of CH_3, C H_2, CH and C.[10] Accordingly, the plasma parameters, such as a gas residence time, would certainly determine the amounts and compositions of the radical species for controlling the bonding configuration of the deposited films. The formation characteristics of bonding configuration of sp^2-C and sp^3-C, and their fluctuation in the a-C:H films is required to study comprehensively.

Raman spectroscopy is one of most common tools for the characterization of carbon based materials.[11] Raman spectra indicate crystallinity of six-membered ring structures of sp^2-C. In the case of widely used 532 nm visible light Raman

spectroscopy, the sp^2 components provide 50 to 230 times stronger intensities than the sp^3 units,[12-13] and also π states excite preferentially. Therefore, Raman spectroscopy is generally applied only for qualitative analysis of crystallographic properties of graphitic components in the a-C:H films. X-ray diffraction (XRD) is another available technology for analyzing crystalline structures in the film, having a certain size of crystalline grains. However, amorphous materials cannot be efficiently characterized. Recently, a near edge X-ray absorption fine structure (NEXAFS) spectroscopy has also been used for investigating the bonding configuration and fraction of sp^2-C and sp^3-C in the a-C:H films.[14] X-ray absorption can occur at K-edges of both sp^2-C and sp^3-C atoms. Furthermore, transitions of $1s \rightarrow \pi^*$ and $1s \rightarrow \sigma^*$ in sp^2-C, and $1s \rightarrow \sigma^*$ in sp^3-C have sufficiently different absorption energies, which can provide a possible distinguish of the signal originated from sp^2-C and sp^3-C of amorphous carbon materials.[15]

In this study, we have clarified the correlation between the gas residence time and the bonding configuration in the resulting a-C:H films. As the total gas flow rate was changed from 50 to 400 sccm, the different residence time of source gasses resulted to obtain different variation of radical species on the corollary of dissociation kinetics. The relation between the residence time and the bonding configuration in the a-C:H films are shown at the first time.

The NEXAFS experiments were operated at Aichi Synchrotron Radiation Center, Japan, on the BL7U beamline with an energy resolution of 0.1 eV at the carbon K edge. The NEXAFS spectra were derived in the mode of total electron yield (TEY), with an energy step of 0.5 eV. The intensity of the incident photon beam I0 was measured using a Si photo detector. The absorption signal was given by the ratio of I_s/I_0, where Is was the out-coming electron intensity from the sample. Highly oriented pyrolytic graphite

(HOPG) was used as a reference sample. All the spectra were measured at an incident angle of 54.7^{o} from the sample surface, which is known as a magic angle suitable for quantitative estimation of sp^2 fractions in the a-C:H films.

Figure 5.6 shows the NEXAFS spectra of the a-C:H films deposited under different total flow rates, in which the intensities were normalized by the intensity at 320 eV in energy above edge jump.[14] All spectra were decomposed and two major spectral components were extracted. One is a sharp peak located at 285 eV, due to the π* C=C bond. The other is so-call "σ* region" between 290 and 320 eV, in which two broad peaks related to σ* C=C centered at 292 eV and σ* C≡C bonds at 302 eV. There are also appeared in the spectrum for graphite. This result indicates a lack of the short- or long-range order.[16] In addition of the two major components, three small peaks related to σ* C-H, π* C≡C and σ* C-C bonds at about 286, 287 and 288 eV were taken into consideration in the spectral decomposition. These components are corresponded with those reported by Yoshitake et al.[17-18] The edge jump of the C K-edge at the ionization potential was fitted with an error-function step as expressed as

$$I_{\text{step}}(E) = H\left[\frac{1}{2} + \frac{1}{2}\text{erf}\left(\frac{E-P}{W/c1}\right)\right], \quad (1)$$

The spectral decomposition carried out with assuming symmetrical Gaussian peaks for π* line, and asymmetrical Gaussian peaks for σ* line, respectively. [17-18] The function for asymmetrical Gaussian line is given by [14]

$$I(E) = H\exp\left[\frac{-1}{2}\left(\frac{E-P}{W/c2}\right)^2\right], \quad (2)$$

where H is the height, P is the position, W is the full width at half maximum (FWHM) of peak, c1 is a constant of $2\sqrt{\ln(2)}$, c2 is $2\sqrt{\ln(4)}$, and W depends on E, such that W=E×m+b, m and b are constants.

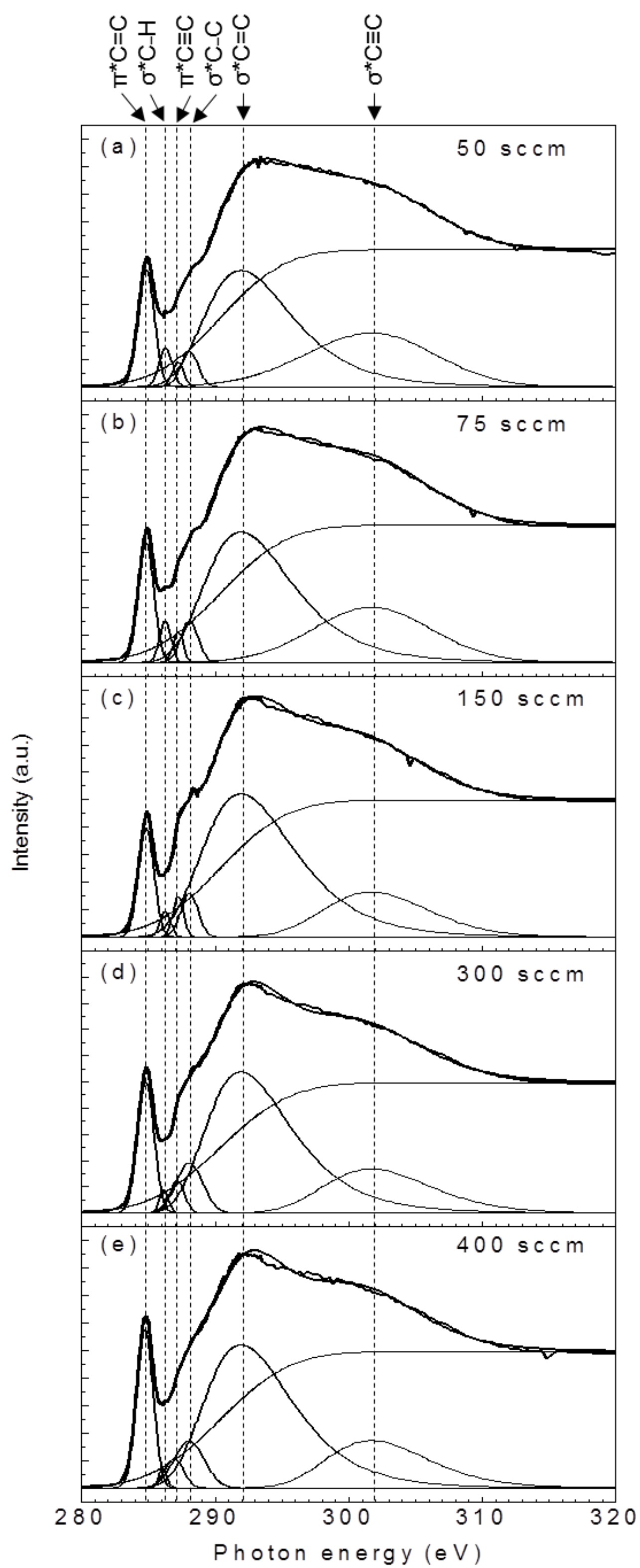

Fig. 5.6. C K-shell NEXAFS spectra of a-C:H films at different total flow rates.

Table 1 lists the parameters of peak position and FWHM for the spectral components due to π* C=C, σ* C-H, π* C≡C, σ* C-C, σ* C=C, and σ* C≡C.[14,19] The peak assignments restricted only the region below 290 eV, since the peaks between 290 and 320 eV were very broad in the case of amorphous carbon.

Table I. Peak position and FWHM of the decomposed component spectra of a-C:H films at different total flow rates.

Flow rate (sccm) Residence time (ms)		π*C=C (eV) 284.86	σ*C–H (eV) 286.31	π*C≡C (eV) 287.23	σ*C–C (eV) 288.09	sp^2 fraction (%)
50 sccm (17.67 ms)	FWHM	1.42	1.13	0.96	1.50	52.5
	Intensity	1.28	0.34	0.18	0.41	
75 sccm (11.78 ms)	FWHM	1.36	0.98	0.88	1.50	50.4
	Intensity	1.25	0.25	0.19	0.29	
150 sccm (5.89 ms)	FWHM	1.36	0.91	0.92	1.50	46.1
	Intensity	1.15	0.18	0.29	0.50	
300 sccm (2.89 ms)	FWHM	1.45	0.78	1.29	2.33	61.1
	Intensity	1.54	0.14	0.34	0.95	
400 sccm (2.21 ms)	FWHM	1.44	0.73	1.66	2.66	70.1
	Intensity	1.76	0.11	0.37	0.96	

In analyses of the bonding configuration, sp^2-C fraction values of the a-C:H films were estimated using a following formula,[20]

$$f_{sp^2} = \left. \frac{I_{a-C:H}^{\pi^*}}{I_{a-C:H}^{total}} \middle/ \frac{I_{grap}^{\pi^*}}{I_{grap}^{total}} \right. , \tag{3}$$

where the superscript of "π*" means peak intensities of π* C=C bonds at about 285eV, and the superscript of "total" is integrate over the energy window (280-320 eV)[16]. Subscripts of "a-C:H" and "grap" mean the areal intensities of peaks within the deposited a-C:H films and HOPG as a reference, respectively.

Figure 5.7 shows sp^2-C fraction values of the a-C:H films as a function of residence time. The sp^2-C fraction of 52% for the residence time of 18 ms decreased slightly to 46% for 6 ms. Then, it increased again from 46% for 6 ms to 70% for the shortest residence time. This result means that the sp2 fraction is not determined simply by a single mechanism, involving that more than two factors exist in this phenomenon. A dependence of the FWHM values of π* C=C and σ* C-C peaks were shown in Figure 5.8. As the residence time decreased, it is apparent that significant increases in the FWHM values of the peaks. The peak broadening indicates a large variance or an increase of fluctuation in the configuration of corresponding bonds. Therefore, it can be interpreted that further amorphization in the bonding configuration on the a-C:H films resulted with decreasing the residence time.

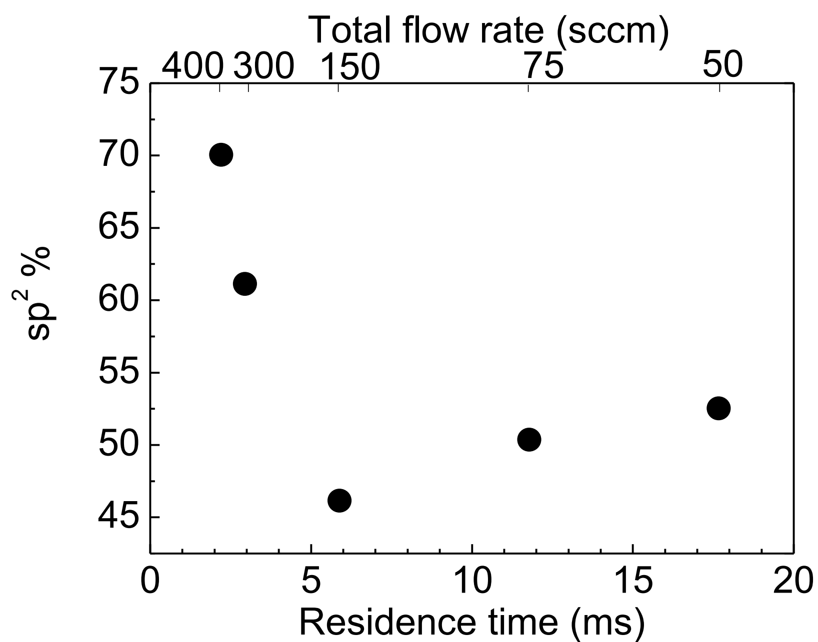

Fig. 5.7. Sp^2 bond fraction in C:H films as a function of residence time.

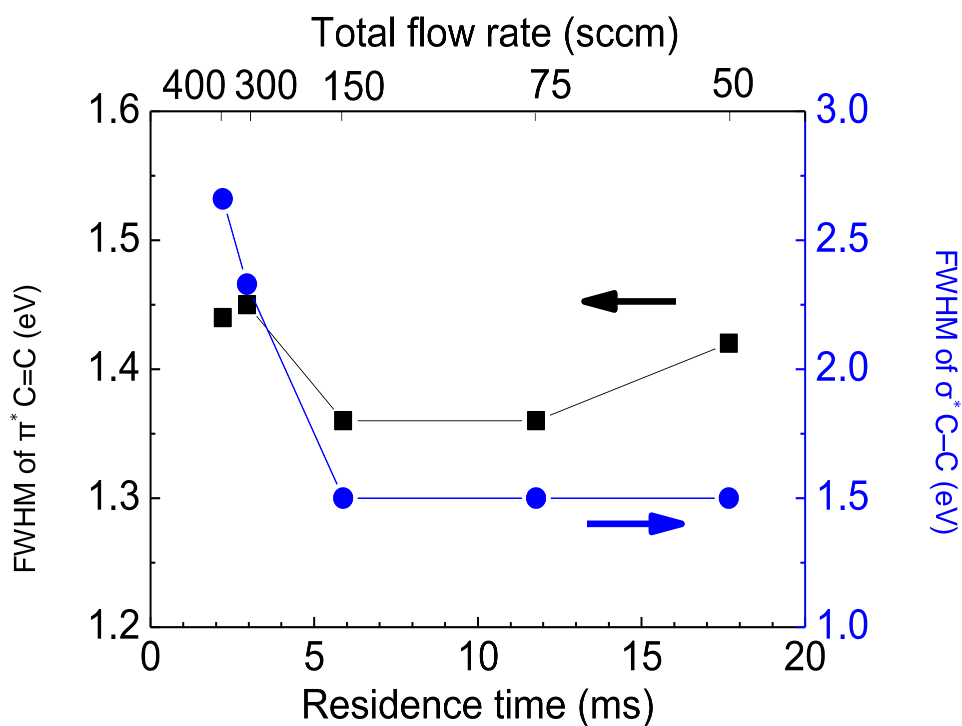

Fig.5.8. Revolution of FWHM of π* C=C and σ*C-C bond peaks as a function of residence time.

From the NEXAFS results, it is evident that variation in the residence time affected the sp^2-C fraction. The dissociation of source gases occurs with a series of chain reactions, such as $CH_4 \rightarrow CH_3 + H$, $CH_4 \rightarrow CH_2 + 2H$, $CH_2 \rightarrow CH + H$, and so forth. Decrease in the residence time would suppress the dissociations, e.g., the radicals at low degree of dissociation would be formed at the shorter residence time. Following knowledge of the conventional dissociation kinetics, excess dissociation would enhance the recombination of them to generate the second-order radicals such as C_2, according with a sort of reactions, $CH_2 + CH \rightarrow C_2H + H$ and $CH_2 + CH_2 \rightarrow C_2H_4$, observed at higher residence time.[21] These radicals as depositing precursors could determine a variety of the bonding configuration, such as sp^2 fraction. The C_2 radicals in gas phase has sp-hybridized bonding configuration and the higher radicals such as C_2H_5 formed resulting from $CH_3 + CH_2 \rightarrow C_2H_5$ has a source of sp^2-hybridized bonds.[22] Murakami et al. and Voevodin et al. suggested that highly-dissociated species, such as C_2, tended to induce sp^2 bonds[23] while CH_3 radicals with H atoms induced sp^3-C bonds.[8] The observed dependence on residence time showed the local minimum in sp^2 fraction. It can be understandable that higher residence time results in higher sp^2 fraction and more inhomogeneous in the structural variations. On the other hand, it is noticeable that the sp^2 fraction increased with decreasing the residence time below 6 ms. At the shorter residence time, the low degree dissociated species of sp^3-hybridized carbons would dominate to deposition precursor and form large content of the sp3-hybridized hydrogenated carbons. These sp^3-C-H bonds may be abstracted by reaction with H atoms. The secondary reactions related with the radicals or ion bombardments on the surface supported that surface sticking probabilities tends to be the order of sp-, sp^2-, and sp^3-hybridized carbons.[22] Namely, the H abstraction on

surface reactions may result to form a large amount of the sp^2-hybridized carbons and the inhomogeneous structure. Therefore, the decrease in sp^2-C with decreasing residence time longer than 6 ms may be attributed to the decrease in the dissociation of CH_4. The complicated reactions on gas phase and surface and their link are needed to be further investigated.

5.3 Variation in C-H bond

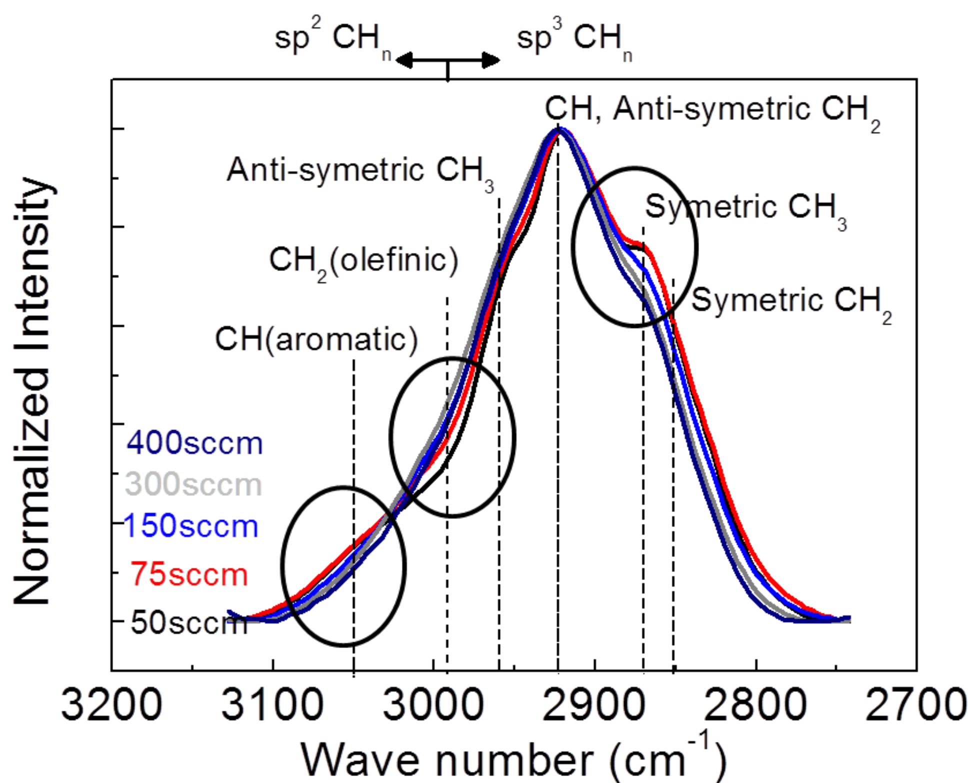

Fig.5.9. C-H vibration as a function of residence time.

Figure.5.9, shows that with the decrease in residence time, an obvious decrease in sp^2 CH (aromatic), sp^3 CH_3, on the other hand, sp^2 CH (olefinic) increased. This indicates that with the change in residence time, aromatic structure have transformed into olefinic structure. This is consistent with the speculation derived from the Raman results, that decrease of residence time caused the disorder of graphite component with the resulting a-C:H film.

5.4 Discussion model

Figure 5.10 shows a discussion model for interpretation of the results derived from this research. When the total flow rate of H_2 and CH_4 was increased from 50 sccm to 400sccm, at a fixed pressure 1Pa, correspondingly the residence time of molecules and radical species existing in the reactor decreased from about 18ms to 2ms. From 18ms to 6ms, growth rate increased due to the increasing supply of source gas, and then from 6ms to 2ms, it decreased caused by the lower dissociation rate of CH_4. And with decrease in the residence time, optical bandgap increased while H content did not change a lot. Besides, similar with growth rate, sp^2-C fraction reached a minimum value at 6ms. It is suggested that From 18ms to 6ms, optical bandgap increased duo to less C_2 in plasma caused by decreasing dissociation. And From 6ms to 2ms, optical bandgap changed in a reverse trend with that of sp^2-C fraction. It indicates that optical bandgap of amorphous carbon material may hardly depend solely on the sp^2-C/sp^3-C ratio. Some other factors, like clustering in the film, bonding fluctuation maybe also act as important roles.

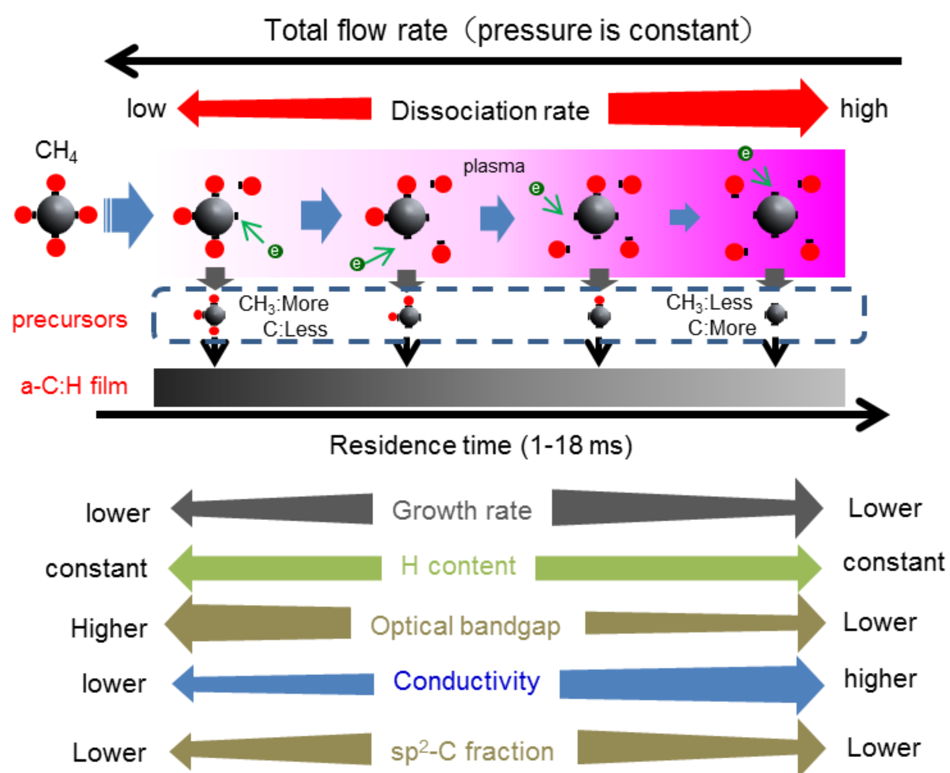

Fig.5.10. A schematic of the evolution of radical species and film properties with variation in the decomposition of CH_4.

5.5 Summary

In summary, the a-C:H films were deposited by the radical-injection plasma-enhanced chemical vapor deposition (RI-PECVD) using a CH_4/H_2 gas mixture. With increasing total gas flow rates, equivalent to the reduction in residence time of radicals or molecules in the reaction chamber, the bonding configurations of a-C:H films were analyzed using the NEXAFS. As the residence time increased, the sp^2-C fraction once decreased and appeared the minimum value at a residence time of 6 ms, then it increased. At the residence time less than 6 ms, the peak widths ofπ^* C=C and σ^*C-C peaks broadened at the shorter residence time, which means increase in fluctuation of bonding structures. We interpret that the variety of radicals species affect the bonding configuration in the a-C:H films via unresolved complicate reactions occurred both in gas-phase and on surface.

According to the EELS spectra, π^* fraction decreased as the residence time was reduced. These findings suggest a decrease in sp^2 components within the resulting films, which is consistent with the quantifying of sp^2-C fraction derived from the NEXAFS spectra. In addition, the H concentration changed only slightly with variations in the residence time.

These experimental results show that the bonding configuration of a-C:H films depended on the residence time in the PECVD process. It should be a useful knowledge for understanding of a-C:H formation mechanism, and will open the way to precise control of their crystallographic, physical and chemical properties.

References

[1] S. D. Berger, D. R. McKenzie, and P. J. Martin: Philos. Mag. **6** (1988).

[2] A. J. Papworth, C. J. Kiely, A. P. Burden, S. R. P. Silva, and G. A. J. Amaratunga: Phys. Rev. B. **62** (2000) 12628.

[3] J. W. Zou, K. Schmidt, K. Reichelt, and D. Dischler: J. Appl. Phys. **67**(1989)487.

[4] M. A. Tamor, W. C. Vassell, and K. R. Carduner: Appl. Phys. Lett. **58**(1991) 592

[5] J. Ristein, R.T. Stief, L. Ley, and W. Beyer: J. Appl. Phys. **84**(1998)3836.

[6] N. Mutsukura, S. Inoue, and Y. Machi: J. Appl. Phys. **72**(1992) 43.

[7] J. R. Rabeau, P. John, J. I. B. Wilson, and Y. Fan: J. Appl. Phys. **96**(2004) 6724.

[8] A. A. Voevodin, J. G. Jones, and J. S. Zabinski: J. Appl. Phys. **92**(2002) 724.

[9] F. J. Gordillo-Vazquez, C. Gomez-Aleixandre, and J. M. Albella, Plasma SourcSci. Technol. **10**(2001) 99.

[10] R. Barni and C. Riccardi, in Chemical Kinetics, ed. V. Patel, (InTech, Croatia, 2012).

[11] Y. Hirose, and Y. Terasawa: Jpn. J. Appl. Phys. **25**(1986) 519.

[12] M. Rybachuk and J. M. Bell: Carbon. **47** (2009) 2481.

[13] D.L. Wood and J. Tauc: Phys. Rev. B. **5**(1972) 3144.

[14] J. Stohr: NEXAFS Spectroscopy (Springer-Verlag, New York, 1992), p. 212.

[15] J. Diaz, O. R. Monteiro, and Z. Hussain: Phys. Rev. B. **76**(2007) 12.

[16] G. Comelli, J. Stohr, C. J. Robinson, and W. Jark: Phys. Rev. B. **38**(1988) 7511.

[17] T. Yoshitake, Y.Nakagawa, A. Nagano, R. Ohtani, H. Setoyama, E. Kobayashi, K. Sumitani, Y. Agawa, and K. Nagayama: Jpn. J. Appl. Phys. **49**(2010) 015503.

[18] T. Yoshitake, A. Nagano, S. Ohmagari, M. Itakura, N. Kuwano, R. Ohtani, H. Setoyama, E. Kobayashi, and K. Nagayama: Jpn. J. Appl. Phys. **48**(2009) 020222.

[19] D. A. Outka and J. Stohr: J. Chem. Phys. **88**(1988)3539.

[20] S. D. Berger, D. R. McKenzie, and P. J. Martin: Philos. Mag. **6** (1988) 285.

[21] L. Jia, H. Sugiura, H. Kondo, K. Takeda, K. Ishikawa, O. Oda, M. Sekine, M. Hiramatsu and M. Hori, in preparation for publication.

[22] A. von Keudell, M. Meier, and C. Hopf: Diamond Relat. Mater. **11**(2002) 969.

[23] Y. Murakami, S. Horiguchi, and S. Hamaguchi: Phys. Rev. E, **81**(2010)041602-1

Chapter 6

Conclusions

6.1 Summary of this thesis

Amorphous carbon (a-C) films are synthesized using a radical-injection plasma-enhanced chemical vapor deposition (RI-PECVD) system employing a mixture of H_2 and CH_4 gases. Variations in the crystallographic and electronic structure of the resulting films with changes in the residence times of radical species and molecules are investigated by varying the total gas flow rate from 50 to 400 sccm. With decreasing residence time, the deposition rate was found to gradually increase, reaching a maximum value at a residence time of 6 ms, after which a decrease was observed. Optical emission spectra showed that the relative intensity of the CH emission increased with decreasing residence time. These results indicate a change in the dominant radical species resulting from suppression of the dissociation of radicals and molecules. Increasing amorphization and an obvious increase in the Tauc gap from 0.6 to 0.9 eV are found with decreasing residence time, while there is little change in the hydrogen content of the films. From these data it is evident that control over the crystallographic and electronic structure of a-C films can be realized by optimizing the distribution of radical species. Finally, the bonding configurations of a-C:H films were analyzed using the NEXAFS and EELS. It provides a between radical species and structural properties of a-C:H films.

In Chapter 1, it is an introduction of the background of this thesis, carbon material. The structures and properties of carbon nanomaterials are described in Section 1.1. A detailed description of a-C materials was given, which are composed of a hybridization configuration of sp^2-C and sp^3-C. This kind of materials has characteristic structural features and exhibit unique macro and micro properties. In Section 1.2, previous studies on growth methods of a-C films are concluded. Especially, we focused on the growth mechanism under plasma enhanced chemical vapor deposition (PECVD), which is the most popular synthesis method of a-C films for laboratory research. Section 1.3 refers to various applications of a-C films, including mechanical application, such as protective coatings, and medical application, and so on. And also we bridged a correlation between the application and the corresponding desirable properties of a-C films.

In Chapter 2, experimental setup and characterization of a-C films was described for details. In section 2.1, the synthesis system of a-C:H films used in this research are described, which is called radical injection plasma-enhanced chemical vapor deposition system. The design concept, difference with conventional PECVD and many details of this custom system are all stated. Besides, to improve the reproducibility and stability of deposition process, growth procedure of a-C:H films are strictly operated. Many details of the growth procedure for deposition of a-C:H films were also described in details in this section. Section 2.2 is mainly about the characterization of a-C films, including thickness derived from stylus profiler, crystallographic properties by Raman spectroscopy, C-H vibration by Fourier Transform Infrared Spectroscopy (FT-IR), Bonding configuration by Electron energy loss spectroscopy (EELS) and Near edge X-ray absorption fine structure (NEXAFS), Tauc gap E_g and optical gap E_{04} by Spectrophotometer, and H concentration by Secondary ion mass spectrometry (SIMS).

In this section, it was introduced not only the basic measurement mechanism of these characterization approaches but also some practical details and important points during measurement in this research.

In Chapter 3, firstly the author did an investigation of the plasma condition and basic film properties. With increasing total gas flow rates, equivalent to a reduction in the residence time of radicals in the reaction chamber, the deposition rate reached its maximum value at a residence time of 6 ms. In addition, the optical emission spectral data also displayed a change in the relative intensity of the CH emission with variations in residence time. These two results indicate a transition in the dominant radical species with changing residence time. On the other hand, the nano-indenter measurement shows that the resulting a-C:H films deposited under the plasma condition mentioned above possess a relative high degree of hardness. And it increased with the decreasing residence time, with a maximum about 18 GPa. The purpose of this chapter is to provide a description of the plasma condition and basic image of the film property. It acts as a fundament for the analysis of the effect from radical species variation in the rest chapters.

In Chapter 4, effects of radical species on the film properties were investigated in details. With the change of the residence time of radicals in the chamber, the variation in optical bandgap, conductivity, crystallographic structure and H content was investigated. And we also tried to bridge a correlation between the variation in crystallographic structure and optical bandgap.

In Chapter 5, effects of radical species on bonding configuration are investigated. With the change of the residence time of radicals in the chamber, both qualitative and quantitative analysis of the variation in π bond fraction, and sp^2-C fraction was operated.

Besides, some other bonding configuration information was also clarified by FT-IR. Similarly, we tried to find the correlation between the variation in bonding configuration and optical bandgap.

In Chapter 6, firstly all the results in the present study are summarized, and a discussion about the effect of radical species on the electronic structure and bonding configuration is stated. According to this, we proposed that electronic structure of a-C:H can be controlled through modification of the bonding configuration via the optimization of radical species and their densities throughout the deposition process. In addition, prospect of application of resulting a-C:H films was also described in this section. The last part of this thesis is the future scopes.

6.2 Scopes for future works

Firstly it is necessary to have a deeper sight into the radical species in the plasma, which could be investigated by QMASS.

From the result in Chapter 5, we interpret that the variety of radicals species affect the bonding configuration in the a-C:H films via unresolved complicate reactions occurred both in gas-phase and on surface. And these experimental results show that the bonding configuration of a-C:H films depended on the residence time in the PECVD process.

To tell the details, we found that with the decreasing residence time, the sp^2-C fraction once decreased and appeared the minimum value at a residence time of 6 ms, then it increased. At the residence time less than 6 ms, the peak widths of σ* C-C peaks broadened at the shorter residence time, which means increase in fluctuation of bonding structures.

Therefore, the complicated reactions on gas phase and surface and their link are needed to be further investigated.

The second one is to bridge the film properties and the application. As mentioned in Chapter 3, the resulting a-C:H films possess a relative high degree of hardness, which is bare in the case of PECVD. Therefore, in the next step, we should figure out the reason responsible for that high degree of hardness. Then based on the well control of hardness, we can apply the resulting a-C:H films to the application, for example, the protective films field.

The last one is about the better control of electronic structure and electrical properties of resulting a-C:H films. Since now, we have found another effective factor, residence time that can affect the optical bandgap, in the next step, we should purchase

a better control of them by synthetically adjusting of all the effective factors, like ion energy, residence time, and doping process.

Acknowledgements

The present research was performed in Professor Hori and Professor Sekine Laboratory, Department of Electrical Engineering and Computer Science, Nagoya University. Author would like to appreciate his research supervisor, Professor Masaru Hori, Department of Electrical Engineering and Computer Science, Nagoya University, for his guidance, advices, and encouragements through the course of this research. The author also would like to thank his chief examiner, associate Professor Hiroki Kondo, Department of Electrical Engineering and Computer Science, Nagoya University, for lots of valuable comments. The author also would like to thank his vice examiner, Professor Seiichi Miyazaki, Department of Quantum Engineering, Nagoya University, Professor Noritsugu Umehara, Department of Mechanical Science and Engineering, and Professor Kenji Ishikawa, Plasma Nanotechnology Research Center, Nagoya University, for their guidance and valuable suggestions in preparing this thesis.

The author is enormous grateful to Professor Makoto Sekine, Plasma Nanotechnology Research Center, Nagoya University, and Professor Mineo Hiramatsu, Department of Electrical and Electronic Engineering, Meijo University, Professor Kenji Ishikawa, Plasma Nanotechnology Research Center, Nagoya University, Assistant Professor Keigo Takeda, Department of Electrical Engineering and Computer Science, Nagoya University, for their valuable comments and suggestions. The author would like to appreciate his senior researchers, Dr. Cho, Dr. Shimoeda, Dr. Tsutsumi and Dr. Kondo for their uncountable superior advices and specific suggestions in the author's research. The author would like to acknowledge Dr. Koji Yamakawa at Katagiri

Engineering Co., Ltd. for their helpful advices and discussions.

The author also wants to appreciate the support from his group members, Mr. Kuki, Mr. Yu, Mr. Xu, Mr. Nakamura, Mr. Sugiura, Mr. Sato, Mr. Okimura.

Finally, the author would like to appreciate his family members.

Jia Lingyun
December 2015

List of papers related to this thesis

1. Original Papers

Title	Journal	Authors Related Chapter
1. Effects of Radical Species on Crystallographic and Electronic Properties of Amorphous Carbon Films Deposited by Radical-injection Plasma-enhanced Chemical Vapor Deposition	Plasma Processes and Polymers (submitted)	Lingyun Jia, Hirotsugu Sugiura, Hiroki Kondo, Keigo Takeda, Kenji Ishikawa, Osamu Oda, Makoto Sekine, Mineo Hiramatsu, Masaru Hori
2. Structural modification of hydrogenated carbon films via control of radical species in plasma-enhanced chemical vapor deposition	Japanese Journal of Applied Physics (submitted)	Lingyun Jia, Hirotsugu Sugiura, Hiroki Kondo, Keigo Takeda, Kenji Ishikawa, Osamu Oda, Makoto Sekine, Mineo Hiramatsu, Masaru Hori

2. International Conferences

Title	Conference	Authors

Title	Conference	Authors
1. Atmospheric pressure glow discharge with large spacing condition	The 16th International Workshop of Advanced Plasma Processing and Diagnostics, Okazak, Japan, Jan. 25-27, 2013.	L. Jia, and W. Liu
2. Atmospheric pressure glow discharge in the frequency range based on the mechanism of ion capture	5th International Symposium on Advanced Plasma Science and its Applications for Nitrides and Nanomaterials, Nagoya Univ, Nagoya, Japan, Jan. 28 ~ Feb. 1, 2013.	L. Jia, and W. Liu
3. Effect of boron doping on amorphous carbon films grown by radical-injection plasma-enhanced chemical vapor deposition	17th Korea-Japan Workshop on Advanced Plasma Processes and Diagnostics & 4th Workshop for NU-SKKU Joint Institute for Plasma-Nano Materials, Sung -kyunkwan University, Suwon & Hanhwa Resort Seorak, Sokcho, Korea, May. 23-25, 2013.	L. Jia, J. Kuki, L. Yu, H. Kondo, K. Ishikawa, M. Sekine, M. Hori
4. Effects of residence time on electronic and electrical properties of amorphous carbon films grown by plasma-enhanced chemical vapor deposition	6th International Symposium on Advanced Plasma Science and its Applications for Nitrides and Nanomaterials, Meijo Univ., Aichi, Japan, Mar. 2-6, 2014.	L. Jia, D. Xu, M. Nakamura, K. Ishikawa, H. Kondo, M. Sekine, M. Hori
5. Effects of residence time on crystalline structures and electrical properties of amorphous carbon films grown by plasma-enhanced chemical vapor deposition	The 20th Workshop on Advanced Plasma Processes and Diagnostics & The 7th Workshop for NU-SKKU Joint Institute for Plasma-Nano Materials, Hokkaido University, Jan 27-29, 2015.	Lingyun Jia, Hirotsugu Sugiura, Hiroki Kondo, Kenji Ishikawa, Makoto Sekine, Masaru Hori

6. Effects of Radical Species on Crystallographic Properties of Amorphous Carbon Films Synthesized by Radical Injection Plasma Enhanced Chemical Vapor Deposition	The 10th Asian-European International Conference On Plasma Surface Engineering, Jeju Island, Korea, September 20-24, 2015.	Lingyun Jia, Hirotsugu Sugiura, Hiroki Kondo, Kenji Ishikawa, Makoto Sekine, Masaru Hori
7. Study on crystallographic and electronic properties of amorphous carbon films grown by plasma-enhanced chemical vapor deposition	8th International Symposium on Advanced Plasma Science and its Applications for Nitrides and Nanomaterials, Nagoya Univ., Aichi, Japan, Mar. 6-10, 2016.	Lingyun Jia, Hirotsugu Sugiura, Hiroki Kondo, Keigo Takeda, Kenji Ishikawa, Makoto Sekine, Masaru Hori